

Encapsulating soldered electronic components for electronically functional yarn

M-Nour Nashed

A thesis submitted in partial fulfilment of the requirements of Nottingham Trent University for the degree of Doctor of Philosophy.

May 2021

Copyright Statement

"This work is the intellectual property of the author. You may copy up to 5% of this work for private study or personal, non-commercial research. Any re-use of the information contained within this document should be fully referenced, quoting the author, title, university, degree level and pagination. Queries or requests for any other use, or if a more substantial copy is required, should be directed in the owner of the intellectual property rights."

Abstract

By M-Nour Nashed

E-Textiles are fabrics with embedded electronic functions that can be used in many fields, such as clothing, medicine, furniture, safety and many others. The integration of electronics with textiles requires a flexible structure that keeps the garment flexible to ensure the textile retains its physical characteristics and feel. E-textiles in wearable applications are subject to human activities. The integrated electronic components are vulnerable to these stresses, such as bending, torsion, and tensile. These forces can potentially damage the components or their interconnection.

Electronics can be integrated into textiles in one of three approaches described as generations of E-Textiles. The Thesis will introduce the three generations of E-textiles through a comprehensive literature review in chapter 2. It will then discuss developing the electronically functional yarn (EFY) as a third generation in E-textiles and garments. The production process of this yarn has three main steps: soldering the semi-conductor on the copper wire, encapsulating it within a micro pod of resin, and covering the micro pod within the filament of the yarn.

A detailed study of the encapsulation process and the unit's design is then introduced in the Thesis, where a novel method for packaging electronics using a UV-curable resin was introduced. The design process for the automated encapsulation of soldered semi-conductor has been investigated in Chapter 3 of this Thesis. The novel approach has been evaluated on various electronics and then extended to thin Kapton strips with embedded electronics. The resulting EFY then can be later used in woven or knitted textile.

Finite element analysis (FEA) of the soldered semi-conductor on the wire is presented in chapter 4. FEA simulations are used to evaluate the mechanical performance of different electronics and how stresses are distributed after adding the resin and creating the micro pod.

This FEA investigation of the materials and micro pod dimensions will understand the packaging method's reliability. The final part of the Thesis included further development added to the design of the encapsulation unit and the electronically functional yarn manufacturing. Developing a reliable, repeatable, and automated electronic packaging method for electronics embedded in the electronically functional yarn (EFY) was achieved in this project. The results were promising for further research.

ACKNOWLEDGMENTS

I would like to thank my supervisory team and the director of studies, Professor Tilak Dias and Dr Theodore Hughes-Riley, for their advice on this research. Thank you for encouraging me and allowing me to grow as a research scientist. It would have been impossible to complete this research successful without your excellent supervision.

I wish to give my deepest thanks to Dr Dorothy Hardy for her effort and help in publishing the results of this work in three papers and Dr Arash Shahidi for carrying out some mechanical alterations to the design, and for his advice regarding the finite element analysis and experimental work. Their support is much appreciated and added value to the work presented in this Thesis.

The work presented in chapter.3 was combined with more experiments and data analysis not presented in this thesis. The work was published as “A Novel Method for Embedding Semiconductor Dies within Textile Yarn to Create Electronic Textiles” (Nashed *et al.* 2019). The experiments and data collected in this research were done by M-Nour Nashed with appreciated assistance from Dr Arash Shahidi in training and using the Zwick tester. Dr Arash Shahidi offered support in designing the winding mechanism and the multi-carrier method design. I would like to thank Richard Arm for his support in preparing the silicon mould and 3d printed models needed in this project. The Candidate programmed the Labview Code.

The author acknowledges funding from EPSRC grant EP/M015149/1: Novel manufacturing methods for functional electronic textiles; and Nottingham Trent University. Another support that was essential during this research was from the 'Council for At-Risk Academics'. This research would not have been possible without CARA's support and their fellowship, for which I am incredibly honoured and grateful.

I am extending my thanks to all the members of the Advanced textiles research group. They have offered me incredible support during this study, Carlos Oliveira, Ioannis Anastopoulos, and Dr Varindra Kumar.

Finally, I would like to express the deepest gratitude to my wife and my parents for giving me so much everything to concentrate on my research and successfully complete this Thesis.

Table of Contents

Copyright Statement.....	I
Abstract	II
ACKNOWLEDGMENTS.....	IV
Table of Contents	VI
Chapter .1 Introduction	1
1.1 Brief Background	2
1.2 Research motivation.....	2
1.3 Aims and Objectives	3
1.4 Thesis outline	3
1.5 Published papers.....	4
Chapter .2 Literature review	6
2.1 Introduction	7
2.2 E-Textiles classifications.....	8
2.3 The First Generation of E-Textiles.....	9
2.4 The Second Generation of E-Textiles	16
2.5 The Third Generation: Fibre and yarn-based electronics	20
2.6 Challenges to E-Textiles	23
2.7 Encapsulation of electronics in E-Textiles.....	26
2.8 ATRG previous work	31
2.9 Summary	37
Chapter .3 The design of the encapsulation unit.....	40

3.1 Introduction	41
3.2 Encapsulation Mould Design	42
3.3 Resin dispensing.....	50
3.4 Resin selection.....	54
3.5 UV Light Source	60
3.6 Encapsulation Unit Design.....	63
3.7 The detection system of the Electronic Component.....	70
3.8 Winding mechanism.....	80
3.9 Conclusion.....	86
 Chapter .4 Stress distribution analysis in the core structure of the Electronically Functional Yarn (EFY)	
88	
4.1 Introduction	89
encapsulation	90
4.4 The influence of resin characteristics on the mechanical properties.....	100
4.5 Influence of the Length of the micro-pod on the stress distribution	102
4.6 Carrier yarn influences on stress inside the micro-pod	104
4.7 Conclusion.....	108
 Chapter .5 Conclusion and future work	110
5.1 Summary and Conclusion	111
5.2 Contribution to knowledge.....	112
5.3 Future Work	112
 References	115

Appendixes	127
6.1 Appendix 1: Electrical Wiring of the Encapsulation Unit components	127
6.2 Appendix 2: The LabVIEW Code used for controlling and monitoring the encapsulation unit.	132
6.3 Appendix 3: Calculation of the Internal diameter of circular warp knitted sleeve.	136
6.4 Appendix 4: Tension Sensor Calibration	143
6.5 Appendix 5: Early design of the encapsulation unit	145
6.6 Appendix 6: Buckling of the copper wire inside the knitted sleeve.....	148
6.8 Appendix 8: Ansys Modelling results	153
6.9 Samples encapsulated by the Encapsulation unit	165

Chapter .1 Introduction

1.1 Brief Background

Electronically Functional Yarn is a novel approach to embedding electronics into yarn. Prof. Dias earlier introduced this approach and then developed it by Advanced textiles research Group ATRG at NTU to automate the labour-consuming process. The manufacturing process was divided into three main stages that were developed independently. One of the essential stages is encapsulating the soldered electronic components.

The Thesis demonstrates the study conducted to develop an automated encapsulation unit. The designed unit will create a micro pod that protects the electronic components and enables a high degree of integration of various sensors in E-Textile. This research is being carried out under the EPSRC project "Novel manufacturing methods for functional electronic textiles".

1.2 Research motivation

Electronics technology plays a crucial part in people's lives. E-textiles technology attempt to embed the technology by combining electronics with textiles to provide convenient and comfortable day-to-day garments.

E-textiles production is limited by the reliability and flexibility of the integration method. The failure to withstand regular wash cycles required different methods of integration to be investigated. Moreover, the size of the mounted electronic would add a different level of integration. Thus, smaller components would keep the flexibility of the textiles and add the functionality needed for various applications. Electronically Functional yarn is one approach that was patented earlier and then developed into many prototypes showing promising results for many applications. However, the process was laborious and time-consuming. Skills and training are essential in manufacturing the yarn. Automating these stages of manufacturing would pave the way to scale manufacturing of this yarn for applications.

This thesis focuses on the automated production of reliable electronic packaging for electronics soldered onto a copper wire or thin plastic substrate that contains conductive interconnects to achieve a flexible and reliable e-textiles product.

1.3 Aims and Objectives

This project aims to investigate automating the encapsulation process. The automated process should create a repeatable size of the micro pod to encapsulate soldered components delivered continuously from a package. To achieve the necessary outcomes, the aim was broken down into the following objectives:

- Design and construct the encapsulation unit as a standalone unit fed with soldered semiconductors onto copper wire.
- Develop the software/program for controlling the unit needed to conduct the steps of encapsulation.
- To design a non-stick mould that can be used for the automated process of encapsulation.
- Find a proper method for soldered components detection system.
- Design a winding mechanism that can store the filaments of the core structure without any damage to the micro pod.
- Find proper working parameters for resin dispensing rate and curing time.
- Understand the distribution of mechanical stresses in the micro pod resin.
- Conduct a small-scale trial using the developed encapsulation unit.

1.4 Thesis outline

The thesis consists of five chapters dealing with Electronically functional yarn (EFY) manufacturing and focusing on one stage of its production: encapsulation. Chapter 2 will outline earlier work in E-Textiles and different attempts to embed electronics in Textiles. This Chapter will classify the previous work on the E-textiles garments into three generations and

discuss each one separately, which outlines the earlier work done by Advanced Textiles Research Group (ATRG) at Nottingham Trent University on the production of Electronically Functional Yarn (EFY). This work would be an extension of the earlier work done by ATRG.

Chapter 3 will introduce the Novel design of the encapsulation unit. The Chapter will discuss each element used in this design and the factors that influence its characteristics in the encapsulation process. Chapter 4 will study the mechanical stress that affect the reliability of the EFY and how adding the resin will change the distribution of the mechanical stress. This study resulted in further development of the micro pod design. The Chapter will introduce improvements added to the manufacturing process of the yarn.

Finally, Chapter 6 will discuss the results of this project and how they can be improved for any future work.

1.5 Published papers

Part of the work of this Thesis was published in journals and conference publications. Here is a list of the published papers:

Hardy, D.A., Anastasopoulos, I., Nashed, MN. et al. Automated insertion of package dies onto wire and into a textile yarn sheath. *Microsyst Technol* (2019).

<https://link.springer.com/article/10.1007/s00542-019-04361-y>

D. Hardy et al., "An automated process for inclusion of package dies and circuitry within a textile yarn," 2018 Symposium on Design, Test, Integration & Packaging of MEMS and MOEMS (DTIP), Roma, 2018, pp. 1-5, doi: 10.1109/DTIP.2018.8394189.

<https://ieeexplore.ieee.org/abstract/document/8394189>

Nashed, M.-N.; Hardy, D.A.; Hughes-Riley, T.; Dias, T. A Novel Method for Embedding Semiconductor Dies within Textile Yarn to Create Electronic Textiles. *Fibers* 2019, 7, 12.

<https://www.mdpi.com/2079-6439/7/2/12>

Hardy, D.A.; Rahemtulla, Z.; Satharasinghe, A.; Shahidi, A.; Oliveira, C.; Anastasopoulos, I.;

Nashed, M.N.; Kgateke, M.; Komolafe, A.; Torah, R.; Tudor, J.; Hughes-Riley, T.; Beeby, S.;
Dias, T. Wash Testing of Electronic Yarn. *Materials* 2020, 13, 1228.

<https://www.mdpi.com/1996-1944/13/5/1228>

Nashed, M.N.; Shahidi, A.M.; Hughes-Riley, T.; Dias, T. Finite-Element Analysis of the
Mechanical Stresses on the Core Structure of Electronically Functional Yarns. *Eng. Proc.* 2022,
15, 2. <https://doi.org/10.3390/engproc2022015002> [https://www.mdpi.com/2673-
4591/15/1/2#cite](https://www.mdpi.com/2673-4591/15/1/2#cite)

Chapter .2 Literature review

2.1 Introduction

Clothing consists of textile fabrics that are either woven or knitted for both protective and aesthetic purposes. Interest in integrating electronics into textiles to create electronic textiles (E-textiles) has increased significantly in recent years, leading to several innovative textiles with integrated computing and sensing capabilities for different applications.

Electronics can be incorporated into textiles at different stages during clothing manufacturing. Clothing manufacture is generally performed in different stages with the industrial process starting with forming the yarn through fibre assembly, followed by the grouping of the yarns to produce a fabric using either knitting or weaving. The next stage is the colouration process; the garment fabric is then cut into patterns and sewn to form the required garment design (McCarthy, 2015).

The clothing manufacturing processes induce different types of stress on the garments, and further stresses will be experienced when the garments are worn, washed, packaged, or stored. This will include physical and mechanical loading due to stretching, bending, and torsion, as well as thermal and ageing effects. Thus, novel technology is needed to develop ETextiles according to the stage that they are incorporated into clothing, and novel approaches are needed to protect these electronics.

The widespread interest in E-Textiles and the growth in the market for E-textile products have encouraged researchers worldwide to discover and innovate different approaches in the field. The market for E-textiles is predicted to reach over \$2 billion by 2029 (Hayward, 2019). This Chapter introduces an intensive review of state of the art in electronic textiles. The Chapter will start by classifying E-textiles into three main generations according to their integration methods and will explore research attempts and market examples for each generation. The challenges encountered by the first couple of generations of E-textiles have led to a new generation being developed. These challenges will be addressed and discussed in this

review. The followed review will then be on encapsulation approaches used to protect electronics in the developed E-Textiles, which will identify the gaps in the existing knowledge in encapsulating embedded electronics.

2.2 E-Textiles classifications

Developments in the electronics industry have led to the development of tiny electronics used in integrated circuits with more efficiency and less cost (H 2013). One remarkable example in the field of small electronic components is the Kinetis KL02, a microcontroller measuring 1.9 mm by 2.2 mm developed by Freescale semi-conductor (Texas, USA). The creation of new, tiny electronic components has led to many new possibilities for the discrete integration of new electronics into textiles.

E-textiles can be classified based on their level of integration into three main categories: Embedded electronics, Textronics, and fibertronics (Langenhove, 2007). Embedded electronics refers to using existing electronic components in a textile, while Textronics refers to the manufacturing of electronic components by textile production techniques and textile material. Fibertronics term refers to electronic building blocks such as transistors into yarns (Langenhove, 2007).

Another classification of E-textiles depends on the integrated electronics level at the different stages in the garment production process (Hughes-Riley et al. 2018; Hughes-Riley & Dias 2017; Dias & Ratnayake 2015). According to this classification of E-Textiles, integrating electronics after the weaving or knitting process (such as through attachment or printing) is classified as the first generation. In contrast, in the second generation, the electronics are embedded during fabric manufacturing, like knitting or weaving. In the third generation, electronics are integrated during the yarn manufacturing process, and the yarns are subsequently used to produce a fabric. The classification is explained in Figure (2.1).

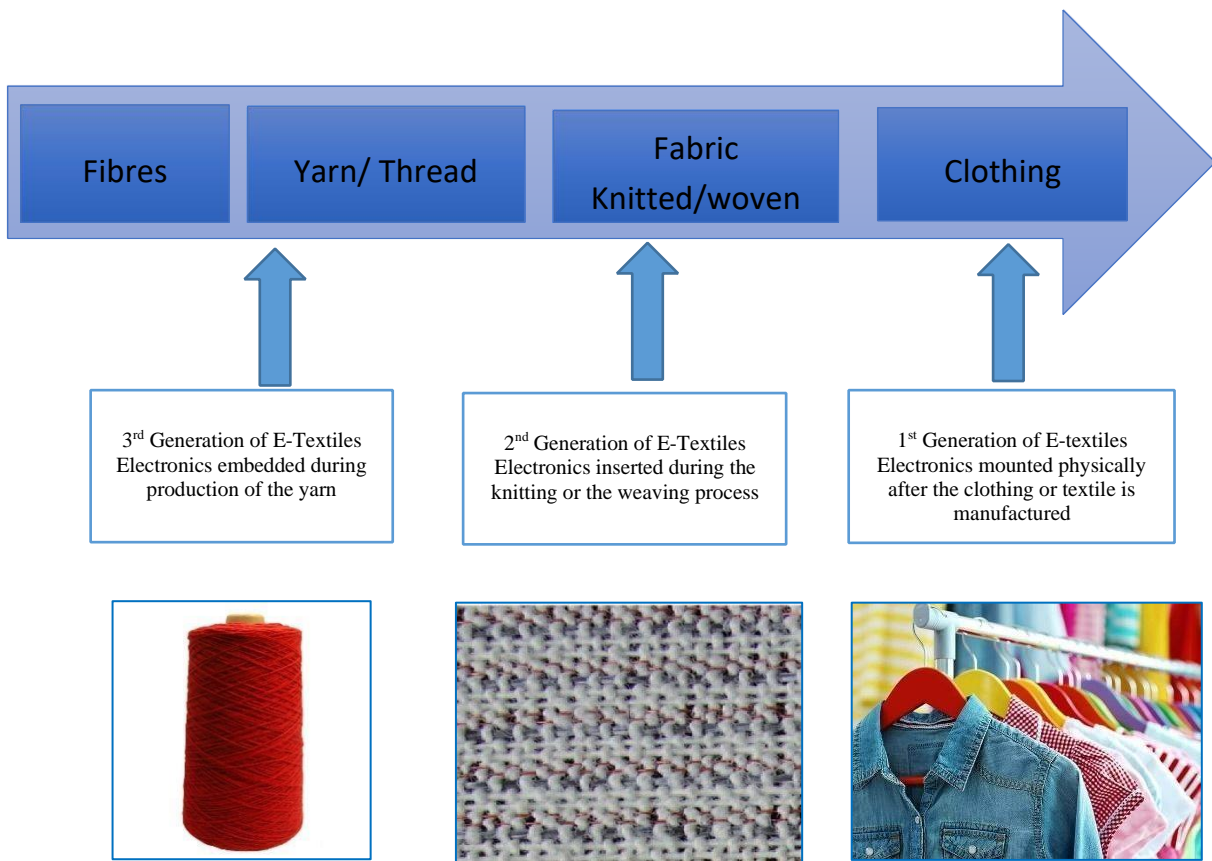


Figure 2-1. The integration of electronics at different stages in the garment manufacturing process and the different generations of E-Textiles.

2.3 The First Generation of E-Textiles

The first generation of E-Textiles is textiles that have electronics attached or mounted directly onto the garments or fabrics. The integration of the electronics in this generation happens after the weaving or knitting of the fabrics and is mainly applied to the textiles' surface (S. Rathnayake, 2015).

One of the early attempts was the ICD+ suit in 2000, which Philips and Levi's developed to be the first commercially available E-garment. The idea of this intelligent garment was to create a wearable and comfortable communication infrastructure including headphones, microphones, small displays and other components (Park, S, & Jayaraman 2003).

Later, different electronics were embedded into jackets like Apple, and Burton's Mp3 jacket (2003) and Infineon's Mp3 jacket (2004); where an electronic board was inserted into a pocket and wires were sewn into the seams of the jacket (Gopalsamy *et al.*, 1999; Park, S, &

Jayaraman, 2003; Stylios, 2013). Additionally, the musical jacket developed at the Massachusetts Institute of Technology (MIT), shown in Figure (2-2), included a conducting fabric sewn onto the surface that offered communication between a keypad and the MIDI Synthesizer

(Park, S, & Jayaraman, 2003). Another example of this generation of E-textiles was the LifeShirt™ System, manufactured by VivoMetrics, which embedded sensors into a garment to collect information on a range of cardiopulmonary parameters (*LifeShirt - Vivonoetics, 2019*).



Figure 2-2. The musical jacket developed by MIT, embroidered keypad on one side and MIDI synthesizer on the other side of the fabric (Stoppa et al., 2014a).

Incorporating sensors into clothing for continuous monitoring of human physiology provides new modes of diagnostics for healthcare delivery. Several attempts have been made to use the first generation of E-textiles for rehabilitation and health monitoring. The bending performance of the body can be monitored using E-Textiles and seated spinal posture has been monitored by the integration of textiles with optical fibres. In the work of (Dunne et al. 2006), where the fibre optics were stitched to the outer surface of the garment using a zig-zag stitch as illustrated in Figure (2-3, a). In a similar concept, fibre optics have also been used to measure hand kinematics using a wearable sensor glove, as shown in Figure (2-3, b). The glove was developed by Simone & Kamper (Simone and Kamper, 2005).

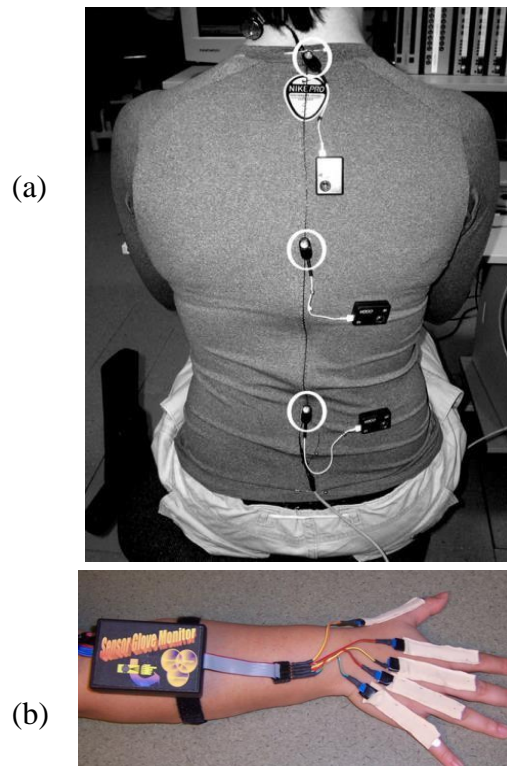


Figure 2-3. (a) Fibre optics have been attached to the outer surface of a garment using a zig. -zag stitch to create a garment capable of monitoring spinal posture. (b) A wearable sensor glove created using fibre optics. (Simone and Kamper, 2005; Dunne et al., 2006)

Embroidered electronics can also be classified as one of the first generations of E-Textiles, where conductive and piezoresistive yarns are embroidered onto the outer surface of a knitted or woven garment (Linz *et al.*, 2005, 2008). This method has been used to create textile electrodes for various applications, including electrocardiogram measurements (Cho et al., 2009) or as an antenna for signal transfer (Wang, Volakis and Kiourti, 2015).

LilyPad, an E-textile technology, is designed to have large connecting pads to allow them to be sewn into clothing. The LilyPad Board is a programmed microcontroller designed to be sewn into wearable projects. Figure (2-4) shows a textile antenna and one LilyPad-based application.

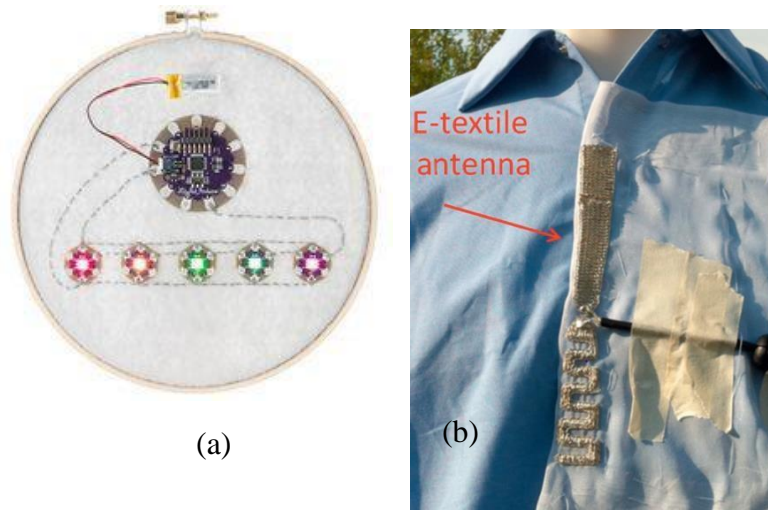


Figure 2-4. (a) Sewn LilyPad circuit with a LED. (b) Embroidered textile antenna.

Flexible substrates like PEEK, Kapton, and Mylar are typically used to mount electronics to achieve flexible embedded circuits, with different adhesives used to get the required flexibility (Komolafe *et al.*, 2019; Li *et al.*, 2019). One recent success in incorporating flexible electronics into textiles was integrating electronics onto flexible plastic strips and attaching these onto garments (Zysset *et al.*, 2013). Printed circuit board (PCBs) were attached to textile substrates to integrate the textiles and electronic components, as illustrated in Figure (2-5). The example of an E-textile shown in the Figure can be used to monitor oxygen saturation (Zysset *et al.*, 2013). A similar approach to develop flexible circuits on Kapton for use in E-textiles has been proposed using three types of metallisation: screen printed silver polymer, evaporation of thin films of gold and aluminium, and using commercially available copper-clad Kapton (Komolafe *et al.*, 2019) illustrated in Figure (2-5).

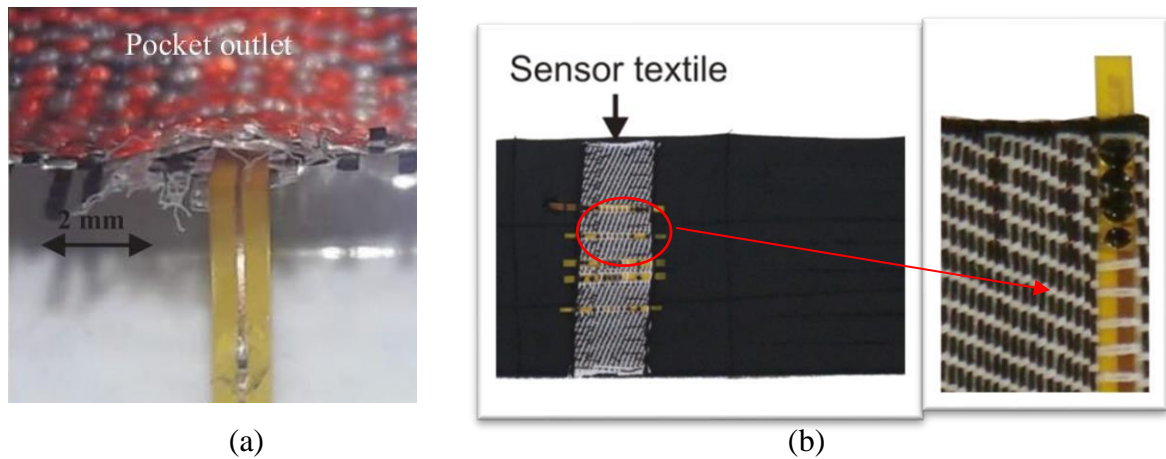


Figure 2-5. Embedded flexible circuit in a textile. The woven structure creates a pocket to insert the flexible circuit into the fabric structure on the left while it is stitched to the fabric on the right. (Zysset, Kinkeldei, et al., 2013; Komolafe et al., 2019).

The fashion industry has shown interest in adding electronic functionality to its designs. "CuteCircuit" is one of the fashion designers who incorporated electronics in their designs of dresses and accessories. Galaxy Dress was one garment that incorporated 24,000 full-colour LEDs. This dress, shown in Figure (2-6), was presented in the Museum of Science and Industry in Chicago, USA, in 2008 (CuteCircuit, 2020).



Figure 2-6. Galaxy LED dress designed by 'CuteCircuit'.

Commercially, LED panels have been integrated into designs in fashion, and some manufacturers have started selling these garments. One example (found on E-retailer) is the LED T-shirt by Gluwy (Leaders, 2020). This shirt, shown in Figure (2-7), can be programmed by a smartphone application to show scrolling messages, animations, or effects. The thin and flexible LED panel integrated into this shirt is attached to the T-Shirt through a Velcro zip. The

LED panel with its wires can be detached from the T-shirt to be washed using a washing machine.

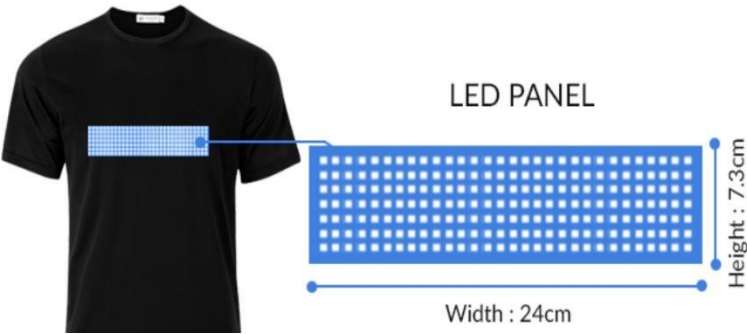


Figure 2-7. LED T-shirt with a programmable display by GLUWY.

Safety garments are another application of E-textiles. Safety vests for children attending schools and nurseries have been developed using an Arduino LilyPad with a global position system tracker, accelerometer, and temperature sensors (Jutila *et al.*, 2014). Another example is the use of LEDs as part of a Hi-Vis vest, as shown in Figure (2-8) (Fuloon, 2020), which can be found on many online retailer websites.



Figure 2-8. LED embedded on HI VIS jacket commercially available on amazon.com

"Radius" is a circular knitted travel backpack with integrated solar panels, shown in Figure (2-9), that was created by a collaboration between Studio Eva X Carola and Santoni Innovation Center in Shanghai (Paulinevandongen, 2020).



Figure 2-9. Travel backpack with integrated solar panels (Amazon, no date).

The 'Mercury' jacket is an E-textile created by the 'Ministry of Supply', a clothing company founded by three MIT students (Ministryofsupply, 2019). The jacket contains heating elements and is voice-controlled. The jacket has an internal and external thermometer to measure the temperature and has an accelerometer sensor that monitors the movement. A micro-controller is embedded to decide how much power to send to the heating elements. The jacket is designed to automatically heat to the right temperature and learn from the wearer's behaviour to predict the correct temperature over time accurately. The jacket is shown in Figure (2-10).

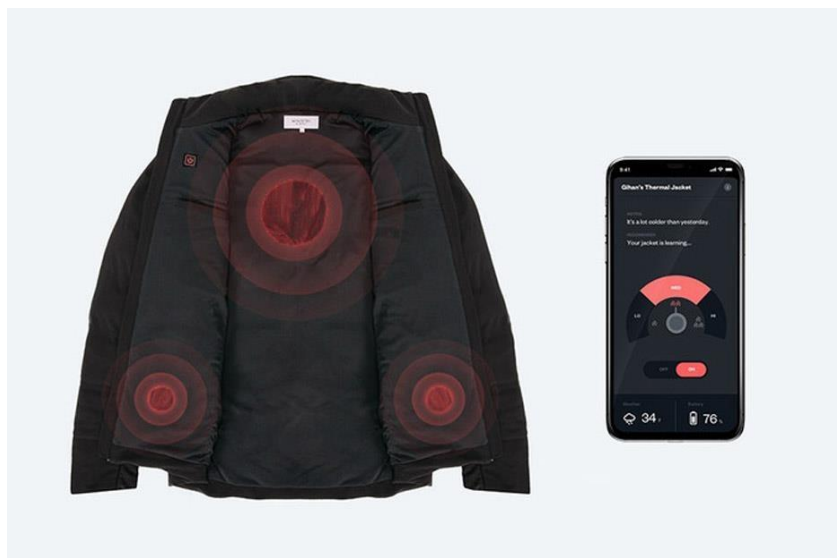


Figure 2-10. 'Mercury' Heating Jacket from 'Ministry of Supply'.

In conclusion, first-generation products were the first attempts to integrate electronics into textiles. Although these products are on the market, they have limitations, which is a

concern for the consumers, limiting their popularity. These limitations have encouraged researchers to develop a new approach to integration.

2.4 The Second Generation of E-Textiles

The next generation of E-textiles used an alternative approach by adding electronic functionality to textiles using conductive fibres made from stainless steel, copper, silver, aluminium, or various alloys. The integration takes place during the knitting or weaving process of the fabric. The resulting fabrics are known as 2nd generation E-textiles.

Several products have been designed and developed using this approach. The idea of using the conductive wires in electrically heated apparel was first proposed in patents in 1910 and 1911 (Hefter, 1910). This technology has also been used for other applications. One of these applications is to create a fully integrated switch (Dias, Hurley and Wijesiriwardana, 2006).

Heeger and colleagues explored the innovation of conductive polymers and published their research in many papers on the chemistry of these polymers (Chiang *et al.*, 1977; Hideki Shirakawa *et al.*, 1977; Wudl, Kobayashi and Heeger, 1987; Cao, Smith; and Heeger, 1993; Heeger, 2010). Conductive polymers are still under development, with the most prominent of these being polyaniline (Pani) and Polypyrrole (Ppy) (Stylios 2013). The importance of these polymer fibres relates to the flexibility of the fibres and their low cost. These fibres may also have applications for textile energy storage devices such as supercapacitors, fuel cells and batteries (Wang, Lin and Shen, 2016). Other conductive polymers used in textile energy storage applications include Poly (3,4-ethylene dioxythiophene), (PEDOT), and polypyrrole (Ppy) (Wang et al. 2016).

Carbon nanotubes can also be used to add electronic functionality to textiles and add heating functionality to cotton fabrics. This has been achieved by coating cotton fibres with single-walled carbon nanotubes through a dip coating method (Ilanchezhiyan *et al.*, 2015) or

direct electrospinning (Weng *et al.*, 2016a). Jeon *et al.* have developed a silk-based electronic textile that can conduct electricity by applying carbon nanotubes onto the silk filaments (Jeon *et al.*, 2018). An exciting aspect of coated conductive yarns is that the final garments preserve their physical and comfort properties.

These innovations have led to many applications where fibres and filaments are used as sensors to use changes in the fibres' resistance when mechanical deformation is applied. Textile electrodes can be made by weaving, knitting, or embroidering conductive yarn into a textile structure. Textile electrodes have uses for health measurements (Pola and Vanhala, 2007) or as an interface for users to interact with capacitively coupled RFID tags (Park, S, & Jayaraman, 2003).

Several projects have been conducted on piezoresistive sensing fabrics, where piezoresistive materials were integrated as fibres and yarns. *ProeTex* was a project funded by the European Community Framework Programme VI between 2002-2006 that developed a garment for emergency disaster intervention personnel. The project outcome was a suit with an integrated sensor that measured heart rate, breathing, and temperature and transferred these data using a textile antenna. Embedded batteries provided the power supply needed for this system. The suit illustrated in Figure (2-11) consists of two components, one part for monitoring the vital signals in close contact with the skin, while another outer part contained sensors to collect data from the wearer's environment (Curone *et al.*, 2007).

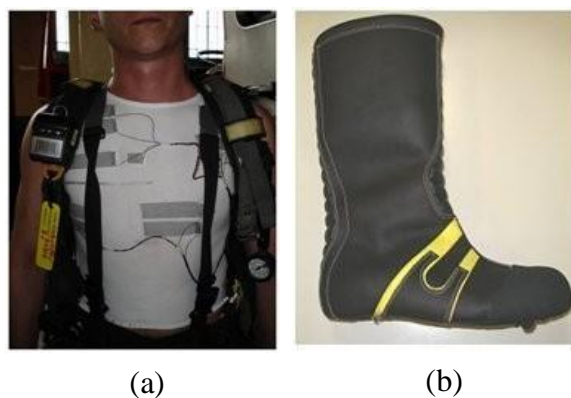


Figure 2-11. Garment developed by ProeTex for emergency workers. (a) A suit with integrated heartrate, breathing pattern, and temperature sensors. (b). Boot with an integrated gas sensor.

One example was the *‘WEALTHY System’* project funded by European Commission in 2002, which created a health monitoring system based on a textile interface for monitoring normal daily activities (Loriga *et al.*, 2005; Paradiso, Loriga and Taccini, 2005). The piezoresistive sensors and their interface bus were knitted and integrated into a textile using a flatbed knitting machine (Loriga *et al.*, 2006). Later this was developed into a cardiopulmonary monitoring system, as shown in Figure (2-12). The monitoring electrodes prepared in this project did not show significant changes in the quality of their signals after washing trials, even though there was no information on how the washing test was performed in their published paper (Loriga *et al.*, 2005, 2006).

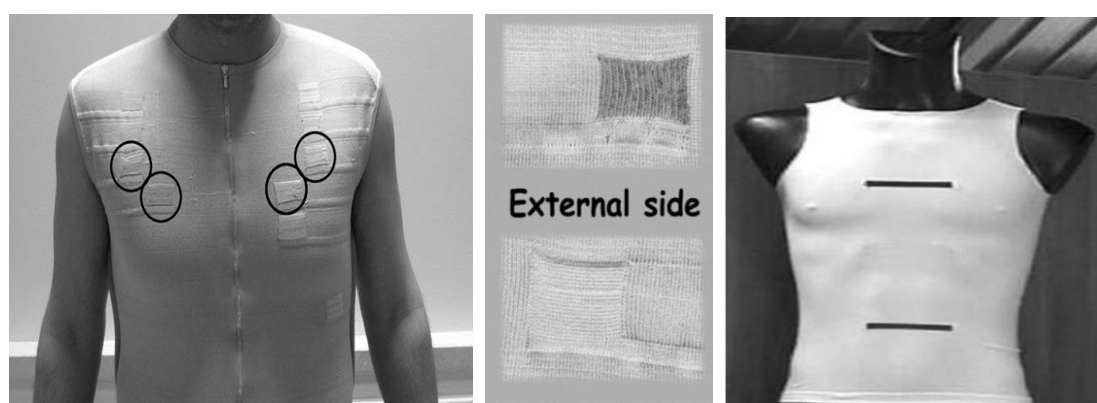


Figure 2-12. Various piezoresistive sensors are embedded into a garment for cardiopulmonary monitoring. (Loriga *et al.*, 2005, 2006).

The work of the European FP7-funded *“INTERACTION”* project was published in 2015. The goal of this project was to design a full-body sensing system to monitor daily life

activities, as seen in Figure (2-13). The system used knitted piezoresistive fabrics like a strain sensor, electrodes for taking EMG measurements, a force sensor and goniometers for the spine and knee (Klaassen *et al.*, 2015). The data was transferred wirelessly to clinicians for monitoring purposes.



Figure 2-13. 'Interaction' system to monitor daily life activities (Klaassen *et al.*, 2015).

Commercial projects have also been developed by knitting or weaving conductive filaments. Nowadays, heated garments are commercially available on many online markets like a heated vest and the USB heated gloves seen in Figure (2-14).



Figure 2-14. Commercially available heated garments. (a) A heated vest with hidden power supply. (b) Heated gloves with USB connection.

The limitation during the manufacturing process and the need for special equipment to insert the electronics during the knitting or weaving process are two challenges for this generation of E-textiles. These types of E-textile sensing/electronic capabilities are limited as they can only be used to make devices that rely on conductive pathways. The use of these conductive fibres can affect the appearance of the garments. There are also, potentially, some durability issues with E-textiles of this type. As a result, a new approach that avoids these restrictions needs to be developed.

2.5 The Third Generation: Fibre and yarn-based electronics

Conductive functionality can be added to fibres that make up a yarn using three different manufacturing methods; coating, blending and integrating electrically conductive materials within the textile fibres (Xue *et al.*, 2004).

Fibre assemblies with electronic and photonic functionality present a promising area for flexible electronics (Zeng *et al.*, 2014) and can be classified as a new generation of Etextiles. The implementation of E-Fibres and yarns have been studied for several applications and have been successful in sensing environmental signals: This includes strain sensors (Mattmann, Clemens and Tröster, 2008; Karim *et al.*, 2017; Afroj *et al.*, 2019), pressure sensors (Rothmaier, Luong and Clemens, 2008), chemical sensors, optical sensors (De Jonckneere *et al.*, 2007), and humidity sensors (Zeng et al. 2014).

Converting solar, thermoelectric, or piezoelectric energy into electrical power is one area of research for applying E-Fibres and yarns that has gained significant interest (Chan *et al.*, 2012; Stoppa *et al.*, 2014). The output power of these fabrics can vary according to the energy source, construction of the fabric, and user response. ‘Fiber-Shaped Solar Cells’ is an example of a fibre-based energy harvesting system, where the photoactive materials were coated onto a fibre electrode and then twisted with another fibre electrode (Zeng *et al.*, 2014; Weng *et al.*, 2016b). A thin layer of electrode material was deposited onto a fibre electrode

coated with a photoactive material, as shown in Figure (2-15). However, commercialising this approach was not feasible as the coated TiO₂ nanoparticles peeled off easily and cracked into patches.

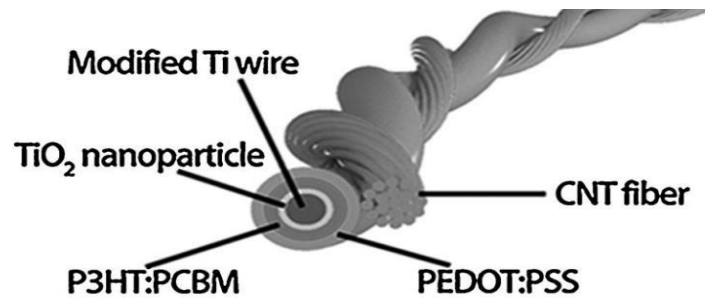


Figure 2-15. This figure shows the structure of the fibre shaped solar cell where Photovoltaic material coated and twisted with textile fibres developed by Weng et al. (Weng et al. 2016; Zeng et al. 2014).

Google announced the ‘Jacquard’ Project at the 2015 I/O conference and reported that they were teaming up with Levi’s to create the first ‘Jacquard’ enabled garment. The ‘Jacquard’ Project used electrically conductive threads with the weight, feel appearance, and performance of standard yarns (Google, 2015). The yarns were created by using thin conductive metal alloys combined with various natural and synthetic fibres. The unique properties of the yarn enabled the technology to be used to develop a wide variety of interactive textiles that are indistinguishable from regular textiles. *Levi’s Jacket with Jacquard by Google*, shown in Figure (2-16), became available for sale in September 2017 (Levi’s, 2019). Connectivity was achieved for this jacket through ‘Jacquard’ Threads and by embedded electronics developed by Google’s research team.



Figure 2-16. Levi's Jacket developed by the 'Google Jacquard' research team.

“*PASTA*” was a project funded by the European Framework Program FP7 in 2010, which combined research on electronic packaging and interconnection with textile research to optimise an innovative approach to E-Textiles (Ericsson and NikeTech, no date). The project introduced a novel concept for electronic packaging and module interconnection, concentrating on a new idea for bare die integration into a yarn. This integration was achieved using three different technologies; micromachining, mechanical crimping as an interconnection technology, and using a stretchable interposer to work as a stress relief interface between the rigid component and the elastic fabric. The outcome of this project led to the development of small electronics embedded within a filament of thread, as can be seen in Figure (2-17).

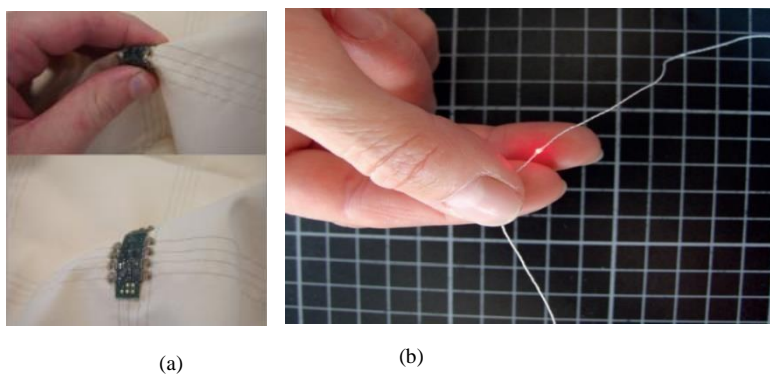


Figure 2-17. (a) Flexible connection for electronic circuit developed by the 'PASTA' project. (b) LED embedded in yarn created using crimp technology (Ericsson and NikeTech, no date).

Another scalable approach for producing E-textiles is to embed electronics within the filament of a yarn which was patented recently by the Massachusetts Institute of Technology (FINK and REIN, 2018). The concept for producing these fibres is shown in Figure (2-18)

(Rein *et al.*, 2018). A thermal drawing process for electrically connected diode fibres was developed by constructing a macroscopic preform in this method. The preform hosts discrete diodes alongside hollow channels through which conducting wires are fed. The conducting wires approach the diodes to make the required electrical contact, resulting in many diodes connected in parallel inside a single fibre (Rein *et al.*, 2018).

An optical micrograph of the resulting fibre cross-section shows two tungsten wires embedded in the fibre cladding without any visible gaps or electrical short-circuiting shown in Figure (2-18) (Rein *et al.*, 2018). However, this process includes drawing of filaments after spinning, which may limit the tenacity of the resulting yarn and reduce its reliability.

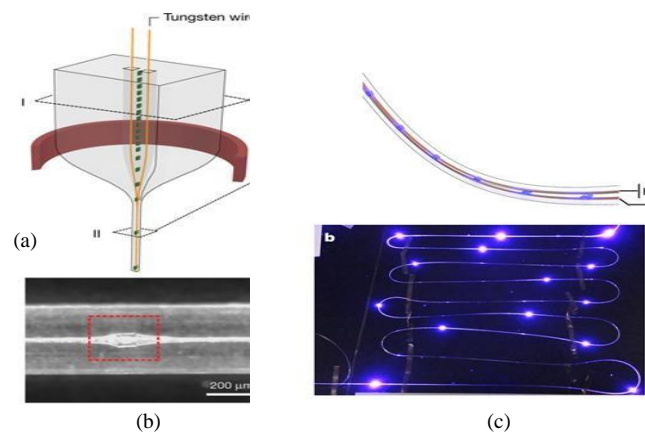


Figure 2-18. (a) Two tungsten wires fed through polymer solution to form contact with LEDs. (b) Microscopic structure of the LED fibre showing the contact between the wire and the LED. (c) Illumination yarn from MIT. (Rein *et al.* 2018).

2.6 Challenges to E-Textiles

The creation of textile-based electrical circuits is an essential infrastructure for smart textile systems. Several properties should exist to make this new platform suitable for commercial production and achieve the required performance expected from electronic textiles. The properties include computing functionality, durability, shape conformability, affordability, flexibility, and the ability to manufacture the textile en masse (Park, S., & Jayaraman 2003). Moreover, the mechanical features of the textiles, such as the ability to conform to body shape due to their shear properties, are essential for the garments and wearable technologies to ensure that they are comfortable to wear (Domskienė and Strazdienė, 2005). The porous structure of the textile adds other vital facts such as breathability, heat transfer, and moisture transfer. These

properties need to be considered in the design of E-textiles. However, the E-textiles design is challenged by many issues summarised in the following points discussed in this section.

A complete combination of the electronics with the textile can be unfavourable from a sustainability point of view as it makes the electronics more challenging to remove at the end of a product's life (Köhler, Hilty and Bakker, 2011). With higher levels of sensors integration and circuits into clothing, the more complex and sensitive these garments have become (Langenhove, 2007). However, most commercially available E-textiles are made either by directly attaching the electronics to the garment that lacks flexibility and washability or external accessories that need to be removed before cleaning.

Electronic circuits that offer elastic mechanical properties against deformations are of growing interest. Stretchability is a requirement of many garments increasing the interest in elastic circuits in E-Textiles. Elastic circuits will be less likely to break when subjected to mechanical loading, which is difficult to satisfy with conventional wafer-based technologies (Kim *et al.*, 2008). These applications need stretchable interconnects that remain intact during stretching and relaxing cycles.

One of the main challenges in the commercialisation of E-textiles is that most research and projects conducted to add electronic functionality to textiles are not suitable for scalable production or mass manufacturing due to the complexity of their preparation or lack of repeatability (Costa *et al.*, 2019). However, designers use different approaches from different generations to achieve a product that can be commercialised in the dynamic market of E-textiles.

The energy source is essential when designing garments that have electronics embedded in them. Most power sources are unsuitable for textile integration due to inflexibility and lack of washability (Cho, Lee and Cho, 2009). The uptake of wearable electronics is expected to

increase when the technology for wearable battery or alternative energy sources become more viable.

The lack of flexibility decreases the reliability of these new products on the market. Flexible substrates for E-textile use are still at the first stage of development compared to solid electronic devices. This lack of reliability is the nature of stresses applied on the interconnection and the substrates by the wearer during the use of E-Textiles (Li, 2018; Costa *et al.*, 2019).

The poor reliability of the interconnection in some E-textiles and their limited wash durability leads to restrictions being applied to the washing and cleaning procedures which limits their popularity (Li, 2018; Li, Tudor, Liu, *et al.*, 2018; Li, Tudor, Torah, *et al.*, 2018). Wash durability is seldom tested, and in a lot of the academic literature, wash durability testing is typically carried out in very mild conditions (Tao *et al.*, 2017; Satharasinghe, Hughes-Riley and Dias, 2020).

All these critical issues play a vital role in limiting the commercialisation of E-textiles. While flexibility is not considered an issue in most printed textiles, their reliability after washing or abrasion still needs to be investigated. On the other hand, the restriction of the first generation of E-textiles, where the electronics are mounted on the surface and removed before they can be washed, is a significant issue with some designs. Fitting the bulky electronics onto the surface also leads to a lack of flexibility due to the encapsulation applied or the rigid components attached, affecting comfort. In terms of 2nd generation E-textiles, they show limitations in their application and thus, a new generation is needed. Table (2.1) compares the different generations of E-textiles and the challenges they face.

Table 2-1. Comparison of the different generations of electronic textiles.

	Firstgeneration	Second generation	Third Generation
Integration into garments at the manufacturing stage	X	X	
Fully automated manufacture	X	X	
Can be produced from yarns on conventional textile machinery	X		
Machine Wash and Tumble Dry	X	Mainly hand wash	
Inconspicuous	X	Visible areas	
Textile-like Characteristics	X	Sometimes stiff and bulky	
Potential for adoption in a vast range of applications	X	Application to niche markets	

This thesis investigates and develops a reliable, scalable packaging method for soldered electronics by applying UV curable resin to the soldered semi-conductor. The designed mechanism should encapsulate and protect a wide range of electronics soldered on copper wire to be inserted into the sleeve of a knitted structure to form a final Functional Electronic Yarn (EFY). This method will give the electronics the flexibility that is lacking in the first-generation E-textiles. The use of encapsulation to protect the soldered semi-conductors will create an Etextile that is washable and reliable.

2.7 Encapsulation of electronics in E-Textiles

Failure of electronics limits the lifetime of E-textile products. In E-Textiles, this is influenced by the flexibility of the garments and the rigours of variable applications. The level of reliability needed in E-Textiles is different from those needed for conventional rigid electronics. Different methods have been applied to embed electronics in textiles, as mentioned earlier in this Chapter. However, the reliability and the failure mode of these prototypes is still one of the main concerns in the design of commercial products (De Kok *et al.*, 2015). Here we will mention the development of encapsulation processes in E-Textiles.

Interconnections between the chip and the substrate provide the path for power and signal. Breakage of the attachment between the electronic component and the conductive fibre is the primary failure in electronic garments (De Vries and Peerlings, 2014). The washability is a barrier in terms of application, reducing the reliability of E-Textiles and making them not robust enough (Tao *et al.*, 2017). Mechanical stresses triggered by the washing cycle destroy the electrical contacts in the electronic wearable garment (Tao *et al.*, 2017).

‘Electronic packaging is the technology that protects electronic components and their interconnections’ (Minges, 1989; Li, 2018; Memis and Goh, 2018; Li *et al.*, 2019). Electronic packaging should be capable of resisting mechanical damage, waterproof and reliable (Minges, 1989; Li, 2018). Flexibility is essential to the E-Textiles. Thus, the packaging of electronics used needs to maintain the flexibility of the garment.

Published papers demonstrated different methods for encapsulating electronic components and maintaining the component's flexibility after the encapsulation (De Vries and Peerlings, 2014). Different materials and approaches that protect the electronic component, maintain flexibility, and add washability features, have been developed for the electronic garment.

One of the early attempts to protect the embedded circuits was demonstrated in a project funded by the Fraunhofer Institute for Reliability and Micro integration and Samsung Electronics. Here an integrating electronic board was combined with textiles by encapsulating the electronic part onto the textile, as illustrated in Figure (2-19) (Linz *et al.*, 2008). The disadvantage of this approach was a lack of flexibility as the components became rigid after the encapsulation.

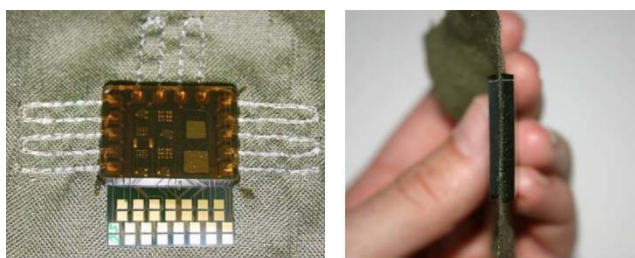


Figure 2-19. An integrated circuit on a fabric encapsulated by rigid resin (Linz *et al.* 2008).

The smart shirt SMASH is designed for rehabilitation and was equipped with an acceleration terminal: which used a similar technique to protect the electronics embedded on the garment's outer surface (Harms *et al.*, 2008). The integration technique used in this prototype attached the system to clothing using silicone gel, as shown in Figure (2-20).

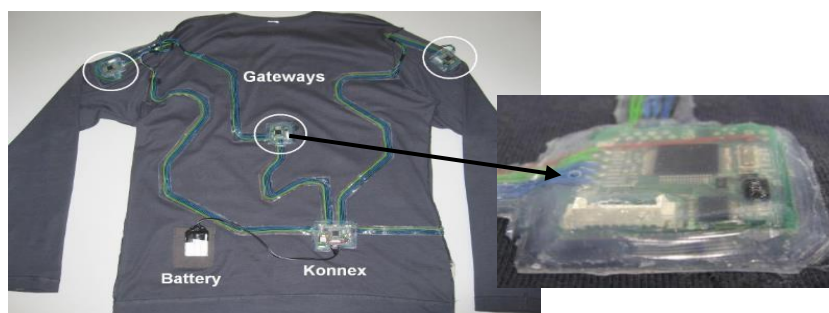


Figure 2-20 Glued system using silicone gel (Harms *et al.* 2008).

Another project that used a similar approach to protect the electronic circuits and their connection was mentioned in a project funded by the European Union's Horizon 2020 research and innovation program. Tao *et al.* used an approach to protect the conductive thread and connect with the flexible PCB by applying a TPU film (thermoplastic polyurethane) to protect the conductive path using a silicon barrier by the press under controlled temperature and pressure parameters. A silicon barrier was then used to protect the whole system, as shown in Figure (221) (Tao *et al.*, 2017).

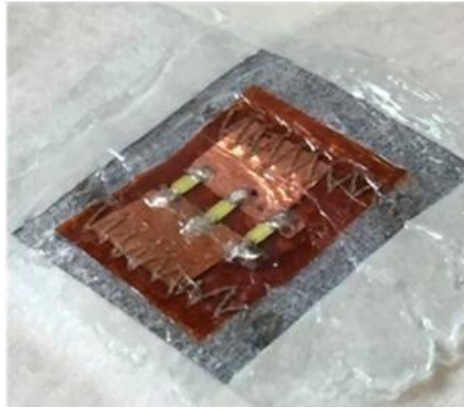


Figure 2-21 Silicon barrier applied on electronic system embedded on the garment's surface (Tao et al., 2017).

Recently, there has been increased interest in embedding electronic chips in a flexible polyimide substrate that achieve low-cost and flexible electronics (Rajoo *et al.*, 2010). The most commonly used substrates are polyimide, polyether ether ketone, or polyester film (Li, 2018). These flexible substrates need further protection to reduce the influence of mechanical stresses on their reliability.

To minimise the mechanical stress on the electronic components and increase reliability, circuits can be protected by a moulded Kapton film (Li, 2018). Flip-chip packaging is a widely used method of bonding an electronic die to a substrate or package carrier. The thin die, shown in Figure (2-22), is located close to the neutral axis of the packaged assembly (Li, 2018).

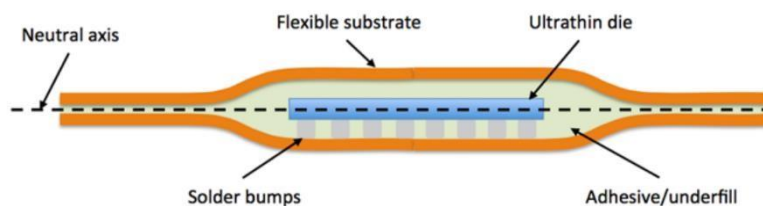


Figure 2-22 moulded Kapton fil protecting flexible substrate at the neutral axis (Komolafe et al., 2019).

Polydimethylsiloxane (PDMS) was investigated as a packaging material for wearable electronics and tailoring its fabrication method specifically for textile integration, as illustrated in Figure (2-23) (Ojuroye *et al.*, 2019).

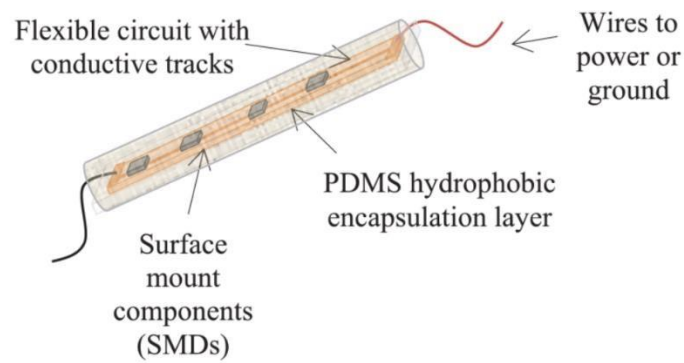


Figure 2-23 PDMS packaging; flexible electronic circuits protected by hydrophobic encapsulation layer (Ojuroye et al., 2019).

The Primo1D E-Thread™, developed at the Grenoble CEA LETI Lab, has led to the creation of an RFID embedded yarn (Andia Vera Gianfranco and Arene, 2017; Gianfranco Andia Vera, 2018; Rolland *et al.*, 2018). The structure of this technology is shown in Fig (224) (Bernard Bancal, 2018), an example of how the integration of electronics into threads can be used in apparel and industrial assets.

The structure of the E-Thread™ from Primo1D integrates the electronics at the filament scale by connecting two conducting wires to the antenna directly to the chip (Emmanuel Arene *et al.*, 2017). The resulting assembly is small and can be incorporated into a textile yarn after applying a resin to reinforce the structure (Bernard Bancal, 2018). However, the concept of encapsulation is not mentioned in the public domain of their publication, and it can be seen from their report that the chip is visible from the yarn structure and therefore subject to wear and abrasion (Bernard Bancal, 2018).

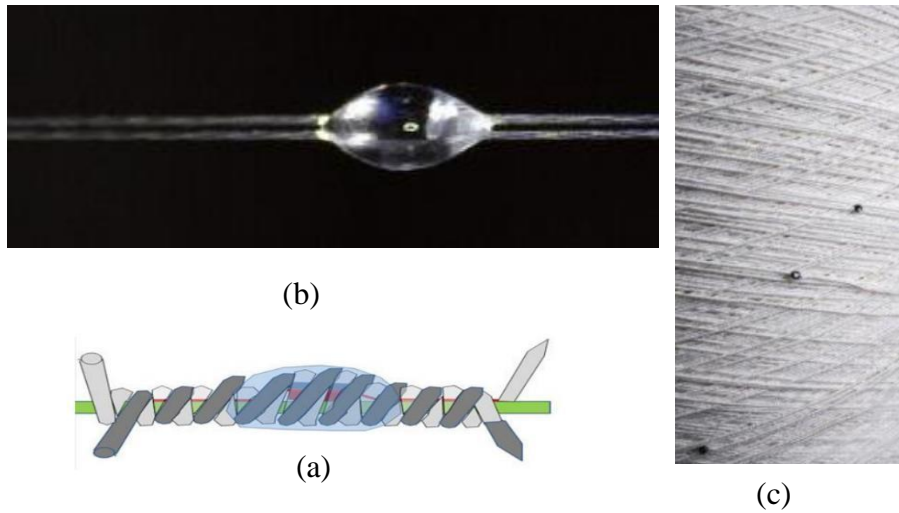


Figure 2-24 The RFID antenna integrated into thread by PrimoID. (a) A schematic concept of the developed yarn. (b) The encapsulation of the electronic component. (c) The electronic components are visible at the surface of the fiber.

In conclusion, protecting the electronic components and the wire interconnection in E-Textiles is critical in developing reliable E-Textiles. Encapsulation of the whole circuits was an early attempt for protecting the embedded electronics. Later, resin and latex were used to cover the wire interconnection to make garments washable. The development of a new generation in E-Textiles requires a new approach to protection. The encapsulation process's objective developed in this project is to protect the soldered electronic component by applying a polymer micro-pod around the components only, which maintains the flexibility of the electronic functional yarn.

2.8 ATRG previous work

Since the work of the Advanced Textile Research Group (ATRG) on electronic yarns is related to the work presented in this Thesis, this part of the literature review will demonstrate the technological solutions developed by the ATRG to prepare the materials and machinery for the EFY.

The manufacturing of the Electronically Functional Yarn (EFY) was a project funded by the Engineering and Physical Sciences Research Council (EPSRC) and awarded to the Advanced Textiles Research Group (ATRG) at Nottingham Trent University and the School of Electronics and Computer Science at the University of Southampton (*Novel manufacturing*

methods for functional electronic textiles – Manufacturing Electronic Yarns, 2020). An essential goal of this project was to scale up the production of electronic yarns, taking it from a handcraft manufacturing process to a semi-automated process. Once the production of this technology can be scaled up, it will lead to industrial commercialisation, which will offer economic and technological benefits in many sectors, such as health monitoring and wearable technology.

EFYs are the 3rd generation of E-textile where the electronics are fully embedded within the filaments of the yarn. Integrating electronic components within a yarn was first proposed in 2010 (Dias and Fernando, 2010). The core structure of the originally proposed EFY comprises a high tenacity carrier fibre attached to a series of electronic components which are mounted onto conductive interconnects, as shown in Figure (2-25). The core was then covered by a group of fibres, called packing yarns, which covered the interconnects and soldered components adding support to the structure.

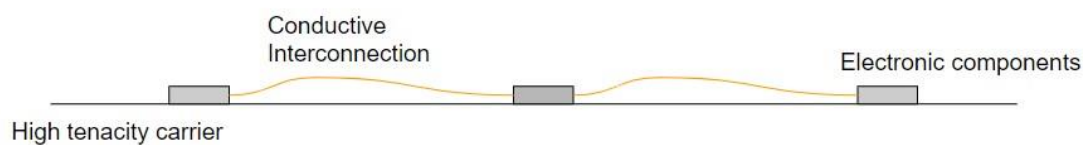


Figure 2-25 The core structure of the Electronically functional yarn (EFY) as originally proposed.

The idea was subsequently developed, and the integrated electronic components are now coated in a resin micro-pod, covered by a group of filaments, and then inserted into a textile sheath to create a final yarn with normal textile characteristics and electronic functionality. The structure of the yarn is illustrated in Figure (2-26). The advantage of this method is keeping the micro pod size minimum and adding the protection needed for the electronics.

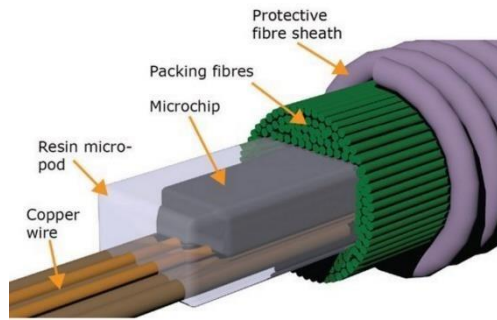


Figure 2-26. The structure of an electronically functional yarn. A microchip is first soldered onto copper wire interconnections, and the electronic component is then protected by a micro-pod. The ensemble is finally surrounded by a group of filaments.

The EFY has been used to pioneer several innovations, including; integrating lighting into clothing for performative art applications (D. Hardy *et al.*, 2018), embedding thermistors into yarns for temperature sensing applications (Lugoda, Dias and Morris, 2015; Hughes-Riley *et al.*, 2017; Lugoda, Hughes-Riley, Morris, *et al.*, 2018; Lugoda, Hughes-Riley, Oliveira, *et al.*, 2018; Lugoda *et al.*, 2020), a yarn with an embedded microphone for use as a noise dosimeter (Hughes-Riley and Dias, 2018), a photodiode embedded yarn (Satharasinghe, HughesRiley and Dias, 2018, 2020) that can be used as part of a pulse rate monitoring system (Satharasinghe, Hughes-Riley and Dias, 2018), and solar cells for energy harvesting (Satharasinghe, Hughes-Riley and Dias, 2020). Figure (2-27) shows some examples of EFY used in prototype products.

To develop a prototype manufacturing process for producing the EFY, the research group at ATRG used machinery and methods from both the textiles and electronics industries. The aim was to develop and automate each of the processes used to manufacture the EFY separately (Hardy *et al.*, 2019). The manual craft process to produce E-yarn required four main stages. The stages of the production process for an EFY with an embedded semi-conductor are described in the flow chart below; see Figure (2-28). This process can be applied to any small electronic components that have two solder pads (like thermistors or LEDs) or circuitry on flexible materials like copper clad Kapton strips (Komolafe *et al.*, 2019).

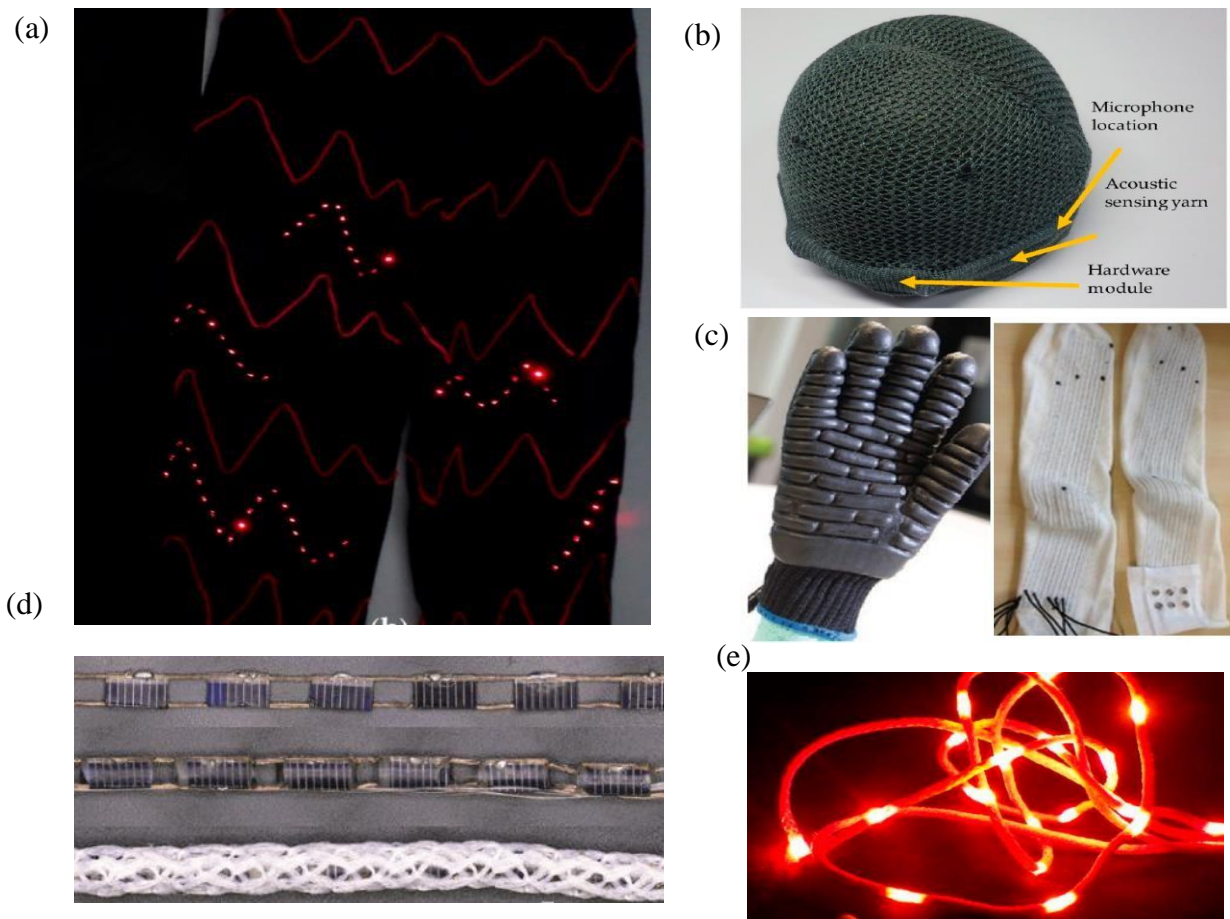


Figure 2-27. Some Electronic textiles developed by ATRG using the technology of the Electronically Functional Yarn (EFY) (Hughes-Riley and Dias, 2017). (b) Acoustic yarn embedded in a military helmet. (c) vibration sensor embedded in protective gloves (d) Temperature sensing socks (e) Fashion application of LED yarn.

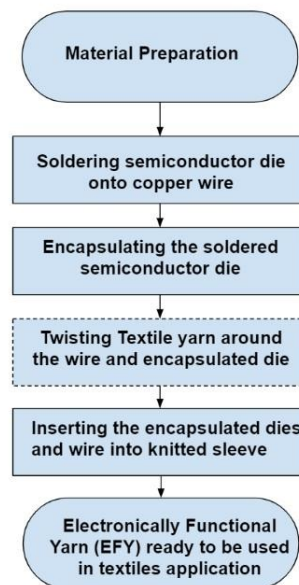


Figure 2-28. The flow chart shows the manufacturing process of an EFY.

The first step in the semi-automated production process was to solder the electronic component onto a conductive wire (D. Hardy *et al.*, 2018). To achieve the accuracy needed,

two stepper motors were used (one to feed the wire and the other motor to draw the soldered components after completing the soldering stage), as well as a robot holding a dispenser to apply the solder paste onto the conductive wire. A pick-and-place device was used to place the electronic components onto the dispensed solder dots. After that, an Infrared source was moved over the component using a robotic arm to apply the heat required to solder the component to the wire. The assembly of the semi-automated soldering prototype is shown in Figure (2-29). Following the soldering process, the short circuit between the two terminals of the electronic component was removed. At this stage, this was conducted manually (usually using a scalpel blade).

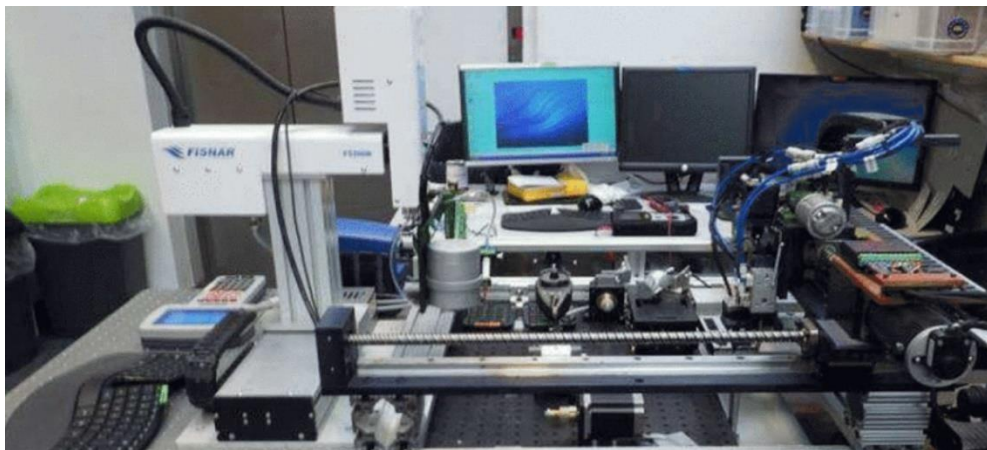


Figure 2-29. The soldering unit was developed by ATRG.

The second step in the production process was to create a micro-pod around the electronic component, shown in Figure (2-30), which is the core of the research demonstrated in later chapters. This process involved adding a carrier yarn, which was a high tenacity fibre (such as Vectran), alongside the copper wire. The carrier yarn, the conductive wire, and the soldered electronic component were positioned using stepper motors into a silicone rubber cylindrical mould to form the resin micro-pod. Once the soldered component was positioned inside the mould at the encapsulation point, a polymer resin was dispensed around the electronic component and then cured by ultra-violet light. The details of this design and the mechanism used are explained in further detail in Chapter .3 of this Thesis.

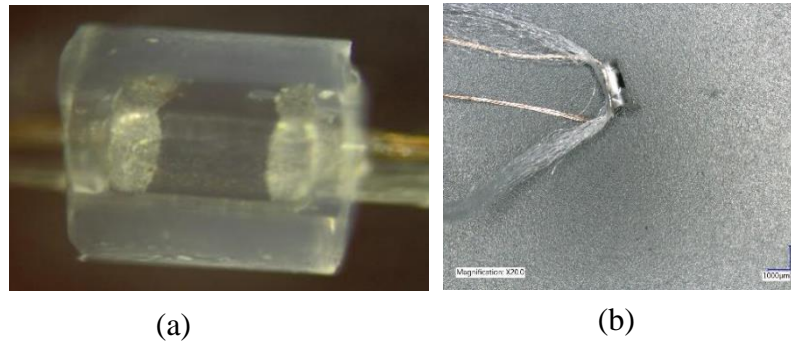


Figure 2-30 (a) Micro-pod resin around thermistor which has been soldered onto copper wire. The copper wire was supported by a carrier yarn (b) the core structure of the EFY after manual encapsulation.

An optional additional stage in the production process was added before inserting the encapsulated component into the knitted sleeve to create the final E-yarn. The carrier yarn and wire with encapsulated die packages were wrapped with multiple strands of cotton yarn using a standard textile yarn twisting machine shown in Figure (2-32). This step was introduced to avoid the phenomena of the copper wire buckling and sticking out of the knitted sheath, as shown in Figure (2-31b). This phenomenon occurred due to the difference in the elasticity between the outer surface fibres of the final structure and the core structure (copper wire). Wrapping the copper wire around a carrier fibre centred the core structure and helped avoid the buckling phenomena, as shown in Figure (2-31a).



Figure 2-31 (a) Twisted core structure provides a control point to avoid bucking the core structure (b) untwisted Core structure of the EFY penetrating through the knitted sheath.

The last stage in the production process was to create a knitted sheath around the encapsulated electronic component and the copper wires. This step was done using a small diameter warp-knitting machine, which knitted a cylindrical tube around the micro-pod/copper wire filament and a set of surrounding packing yarns.

In sum, the manufacturing of the EFY needs different approaches used in both the textiles and electronics industries to achieve the reliability required for textile garments that can be used every day by the wearer.

2.9 Summary

There have been many approaches to embedding electronics into textiles, and these new E-textile products have promising market potential in many fields and for a variety of applications. Embedding electronics within yarns is a novel method that shows encouraging results and can be applied to many applications and different types of electronics.

Although some electronic garments have been offered for public commercialization, the product life cycle is short and many products have been discontinued (Google, 2015; Levis's, 2019). A primary challenge that faces the commercialisation of E-textiles is to protect the electronic components. Many attempts have been tested to protect these components, and this work has been demonstrated in this literature review.

Encapsulating the embedded electronics is a technique that is used in different generations of E-Textiles. This process aims to protect the electronics and increase the reliability of the garment. Resins used in the literature for encapsulation included epoxy, or acrylate-based adhesives (Linz *et al.*, 2008; Harms *et al.*, 2008; Tao *et al.*, 2017; Li, 2018).

The approach of embedding electronics in the structure of a yarn is attracting attention from different researchers in wearable technologies. In the work of (Rein *et al.*, 2018), embedded electronics have two terminals within polymers. However, the mechanical properties of this yarn are not published yet and its reliability is still to be investigated.

The work of the PASTA project (Ericsson and NikeTech, no date), where RFID yarn is developed. However, although Primo1D commercialized the RFID yarn, the integration process is adopted for only one type of electronics to be embedded in.

EFY is a new technology that has improved the flexibility and reliability of E-textile in many applications (Lugoda, Dias and Morris, 2015; Hughes-Riley *et al.*, 2017; Lugoda, Hughes-Riley, Morris, *et al.*, 2018; Lugoda, Hughes-Riley, Oliveira, *et al.*, 2018; Lugoda *et al.*, 2020; Satharasinghe, Hughes-Riley and Dias, 2018, 2020). However, the manufacturing process can be improved for better adoption of the technology with different semiconductors.

The encapsulation process is one stage of manufacturing, and it includes several parameters that can improve the reliability of the resulting electronic yarn. The micro pod protection added washability characteristics to the yarn. These successful applications of the EFY make scalable production an essential stage to progress this technology in the world of E-Textiles and commercialisation.

Published work on EFY (Lugoda, Dias and Morris, 2015; Hughes-Riley *et al.*, 2017; Lugoda, Hughes-Riley, Morris, *et al.*, 2018; Lugoda, Hughes-Riley, Oliveira, *et al.*, 2018; Lugoda *et al.*, 2020; Satharasinghe, Hughes-Riley and Dias, 2018, 2020) have discussed both preparation and materials used for each prototype of Electronically Functional Yarn. They have also focused on each step's influence in the production process on the component's functionality. However, the process of manufacturing is laborious and time-consuming. It does require a lot of time, training and patience. There has been no study on the encapsulation process and how to achieve this protection with scalable repeatability and high reliability.

The work in this Thesis will focus on the encapsulation stage of the manufacturing process, study the design of the core structure of the EFY, design an automated prototype to form the polymer resin micro-pod and discuss the parameters and requirements that influence the operation of the encapsulation unit and the reliability of the resulting micro-pods. The automation of this critical production step will improve the repeatability, and reliability of the EFY and avoid handcraft errors in the production of this yarn.

The mechanical stress in such types of embedded electronics are yet to be studied. Finite element analysis has been applied to study the mechanical stress of different types of electronics embedded in textiles. The work of (Li, 2018; Zysset et al., 2013) integrated small flexible circuits printed on Kapton strips into the structure of the textiles. However, each embedding generation has its limitations. Investigation of such mechanical stresses needs to be investigated for the different layouts of electronics embedded within the yarn.

Chapter .3 The design of the encapsulation unit

3.1 Introduction

The previous chapter shows that integrating electronics within flexible electronic yarns (E-yarns) can create flexible, breathable E-textiles (Dias, 2016). The process for producing E-yarns was discussed in the earlier chapter. This chapter will focus on the encapsulation of the soldered semiconductor.

In this thesis, the term ‘Encapsulation’ refers to the process of applying a curable resin into a pre-defined area around a soldered electronic component to produce a micro-pod. The encapsulated component, and the solder joints that attach it to copper wire, are protected by the resin from environmental effects, such as liquids, humidity, and dust. The resulting E-yarn is, therefore, machine washable.

E-yarns prototypes mentioned in the literature were fabricated using a laborious handcrafting process. The soldering process was done using an Infrared (IR) reflow soldering system where the copper wire was positioned manually on the top of the component to solder it. The short circuit between the solder pads was removed with a staple blade. After this, the encapsulation process was done by inserting the component and a carrier filament into a small non-stick tube. Then, dispensing the resin into the tube from both sides to fully encapsulate the component. The manual encapsulation method was not precise to achieve a uniform micropod.

Moreover, this manual method was time-consuming and introduced repeatability issues into the production process. The quality of the final yarn produced using a hand-craft method was dependent on the crafter's level of professional training and technical skills. Industrial adoption would require automating this production process to allow a larger quantity of yarns to be produced. This part of the thesis will answer *how to create a uniform micro-pod in an automated way with acceptable repeatability*. An automated prototype for the encapsulation stage was developed to prove the scalability of this technology, speed up the manufacturing process, and improve the repeatability of the and reliability of the final yarn. This work outlines

critical design considerations for the automated encapsulation approach: Selecting resin, dispensing method, curing technique, the mould design to achieve the required geometry, and allocating a carrier yarn. The encapsulation unit designed in this chapter has been assembled and built in the Advanced Textiles Research Group lab at Nottingham Trent University (United Kingdom).

3.2 Encapsulation Mould Design

The Glob Top technique protects electronic components from different stresses such as vibrations, temperature fluctuations, moisture, or corrosion. (Press, 1990). This effect is applied by dispensing a fluid resin matrix, mostly an epoxy or acrylate-based resin adhesive, which is then cured. Resin micro-pods can be formed by applying a small amount of resin around a semi-conductor or placing the electronic component within a mould, then injecting resin into the mould.

Applying the resin directly to the soldered components using the glob top method led to a complex geometry of the micro-pod (see Figure (3.2-1)). Moreover, the component's orientation led to cases where the component was not fully protected, as the resin did not cover the other side of the component. However, this can be improved by studying the wettability properties of each electronic component and selecting appropriate resin viscosity to allow the flow of resin to cover and protect the solder joints. These limitations would not suit the automation process where repeatability is required and electronic components are supplied with different surface properties. Thus, an alternative method is needed to do the encapsulation.

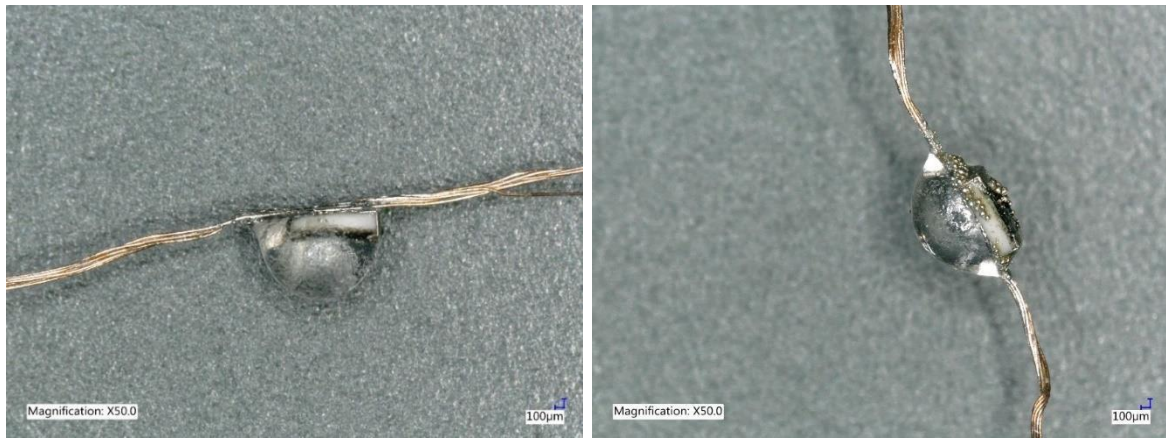


Figure 3-1 Microscopic image of two different components encapsulated in gob top method using Dymax 9001 v3.5. the one to the right shows the components is not covered while the one to the left the solder joints are not protected due to the wettability properties of the components.

Encapsulation using a mould would result in micro-pods with a predictable geometry that protects the soldered components regardless of the physical properties of the outer surface. The design of the encapsulation mould is a crucial part of this process. The material of the mould, the shape, the size, and the orientation need to be designed in a way that allows for a successful and repetitive encapsulation process.

A cylindrical micro-pod shape was chosen for encapsulating the soldered semiconductor, as this shape had minimal edges. This shape is also convenient to pass through the small diameter warp-knitting machine used in the next stage of production of E-yarn. Cylindrical micro-pods are also more likely to be comfortable to the end-users as the circular cross-section of the encapsulation is compatible with the cross-section of traditional textile yarns.

The diameter of the encapsulation should be minimal to keep the yarn fine and suitable for use by ordinary knitting and weaving machines. Simultaneously, the diameter of the mould should allow the resin to flow in a way that fully covers and protects the electronic component.

The selected cylindrical micro-pod shape will be formed within a tubular mould. The internal wall surface tension of the mould arises because of the intermolecular attraction forces that the molecules in a liquid form exert on one another. The properties of the mould material required for this application should be as follows:

- The resin used does not stick to the mould following the curing process.
- The force required to release the micro-pod from the mould needs to be minimised to avoid damage to the semiconductor and its interconnects.
- The wetting properties of the inner mould surfaces are essential for the resin diffusion inside the mould and the final shape of the micro pod.
- The mould walls must be UV-transparent to minimise the absorption of UV by the mould during the curing of the resin.

The two potential materials were examined that fulfilled these criteria and were available in the form of tubes; Silicone (Silicone Tube, part number a16090800ux0404; Sourcingmap, Mountain View, CL, USA), and PTFE (RS PRO Long Coil Tubing Without Connector, Fluoropolymer, Corby, Northants, UK).

A silicon rubber mould was prepared to mount the flexible tube as a mould in the position needed. This mould would guarantee a physical bonding between the PTFE mould and the silicon rubber around it. This rubber mould would form with the flexible tube, one rigid mould that can be mounted physically in the encapsulation system.

The rubber used was Transil 40-1 A&B rubber (Mouldlife, Bury St Edmunds, UK), a two-component platinum silicone rubber that crosslinks at room temperature by a polyaddition reaction. The silicone components were delivered as two-component liquids, which, once mixed, cured to become a transparent, elastic, and resistant material. Transil 40-1 A and Transil 40-1 B were mixed by weight in a fixed ratio (10/100) part A and B respectively, then degassed for 10 minutes and poured slowly into a plastic transparent cylindrical tube while the non-stick tube is held inside of the plastic part.

The advantage of the Transil 40-1 was the outstanding transparency which should decrease UV blocking during the resin curing process. Figure (3-2) shows a PTFE tube and the silicone rubber mould around it, used as a mould unit for encapsulation in a plastic syringe.



Figure 3-2 Silicone mould and the PTFE tube within the Syringe.

The rubber is moulded into a cylindrical plastic tube holding the non-stick tube in the centre of the mould. The cylindrical shape of the rubber mould will give the outer surface of the mould the properties of a lens by focusing the UV- rays on the area where the encapsulation curing takes place, as demonstrated in Figure (3-3).

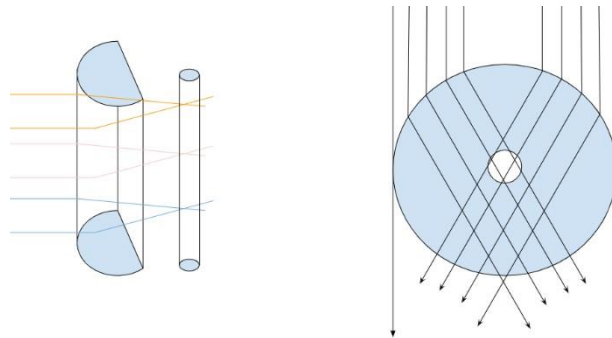


Figure 3-3 UV light refraction and lens focusing the UV intensity on the centre of the mould.

The silicone rubber properties are essential in the mould's design to hold the PTFE tube for the encapsulation process. Although the rubber used was clear, it would affect the UV curing process. The UV is absorbed by the rubber, which will decrease the energy transferred by the UV light to the resin during the curing process. (Group, 2000). To investigate the influence of the silicone rubber on the curing process and how the UV intensity is reduced by absorption from rubber surrounding the tube mould, a sample set of different thicknesses was prepared from the Transil 40 rubber illustrated in Figure (3-4). The yellowish colour of the samples is the age effect of the silicon, as this image was taken after a year of the measurements reading. The UV intensity was measured using a UVA+B meter with a spectrum range between 280nm and 400nm and a maximum measuring range of 200mW/cm².

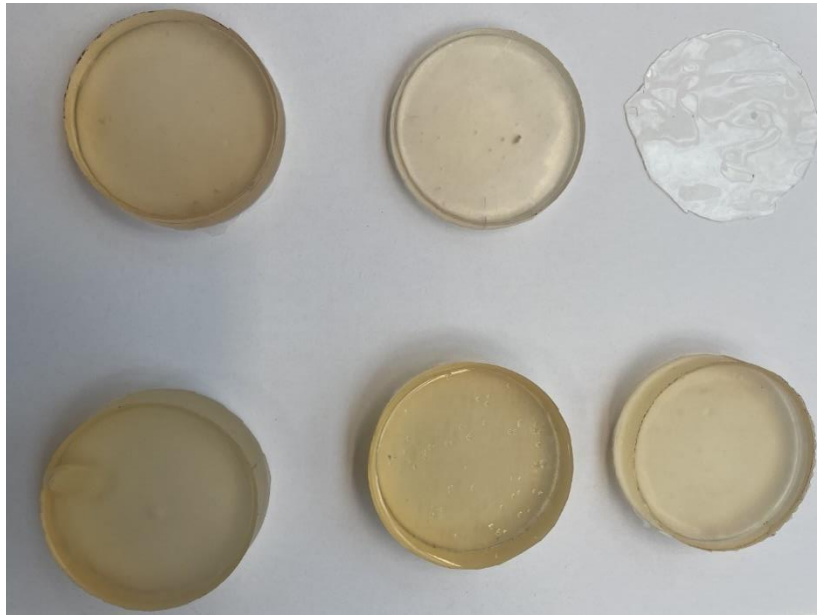


Figure 3-4 Sample of transil 40-1 silicon rubber at different thickness. the colour degradation can be seen on the samples. the image was taken after a year of preparation of the sample.

Absorbance presented in Figure (3-5) proves the decrease of UV energy for different rubber thicknesses when the sample is exposed to a UV source at different distances. These curves show that the UV light intensity absorbed by the mould and lost due to the distance is considerable. Thus, the system's design should guarantee close contact between the UV light source and the point of encapsulation. Moreover, the rubber absorbance used to prepare the mould range between (10-20 mW/cm²) for a rubber thickness of 14mm. This absorbance has a low impact on the curing of the resin inside the mould.

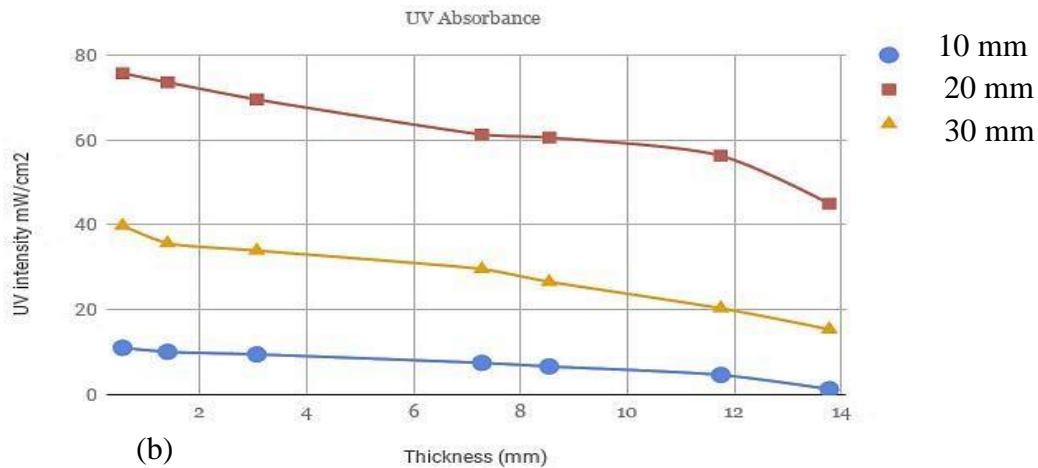
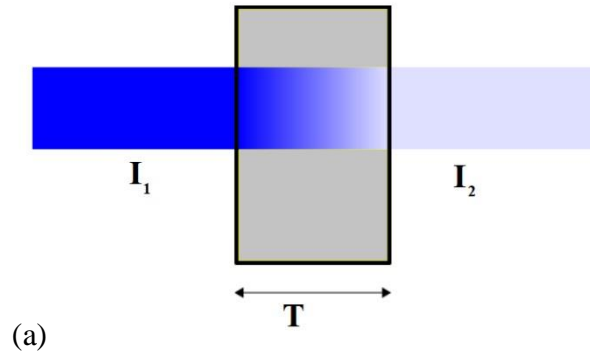


Figure 3-5 (a) shows the principle of UV absorbance by the walls of the mould. (b) UV absorbance vs the thickness of the mould wall. The intensity of light transmitted through an absorbing material as a function of thickness, d , in mm for different distance of the light source from the mould (10mm,20mm,30mm)

Following curing the resin and forming the micro-pod inside the mould, the other point that needed investigation is the force needed to remove the micro-pod from the mould for continuity of the process. Although the mould was chosen from a non-stick material, the micropod showed resistance when removing it from the mould after curing. The force needed may lead to failure of the resulting yarn due to stresses induced during the removal of the micropod. Theoretically, the higher the contact surface between the micro pod and the mould itself, the higher the force needed to eject it.

Experiments were conducted to find the required forces to remove the cured micropods from the mould. Dummy micro pods were created inside the mould tube onto the Vectran as carrier yarn for the dummy pods. Following the resin curing, the dummy micro pods were removed using Zwick tensile tester Z2.5 (Zwick/Roell, Ulm, Germany). The mould was

mounted to the static jaw of the tester while the movable jaw applied the pulling force to remove the micro-pod from the mould.

The results were compared with the tensile forces needed to break the core structure of the yarn. This set up the limitations of the moulding system, showing at which micro-pod length frictional forces would prevent removal from the mould when using the carrier yarn to provide the demoulding force.

Micro-pods were pulled from the mould, as shown in Figure (3-6a). This force is expected to increase in proportion to the contact surface between the cured resin and the mould tube walls. Figure (3-6b) shows this contact area.

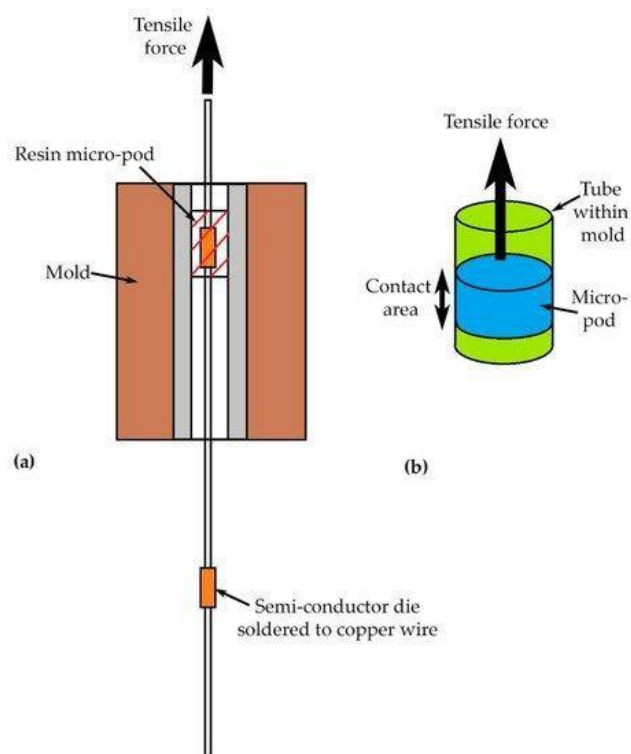


Figure 3-6 (a) Schematic showing an encapsulated die being pulled from the mould. (b) Diagram showing the area over which friction forces will act when pulling a die from the mould. Image reproduced from (Nashed, 2019); this image is licensed under a Creative Commons Attribution 4.0 International License (CC BY 4.0).

Figure (3-7) shows the force required to extract micro-pods from the mould after curing different resin volumes inside a 1.00 mm diameter PTFE tube. The increasing tensile force

needed shows that increasing the volume of resin, which led to increased micro-pod lengths required an increased force to be applied to remove the cured resin from the PTFE tube. The tensile force should not exceed the braking force of the Vectran as carrier yarn (usually between 26.2 and 27.6 N). The results indicate that the force needed to remove the micro-pod from the silicone tube was a less than the force needed for the PTFE tube for the same volume. However, further increases in the volume of resin or the diameter of the tube could lead to the force required to remove the micro-pod from the mould exceeding the carrier yarn strength, which limits the length of the micro-pod.

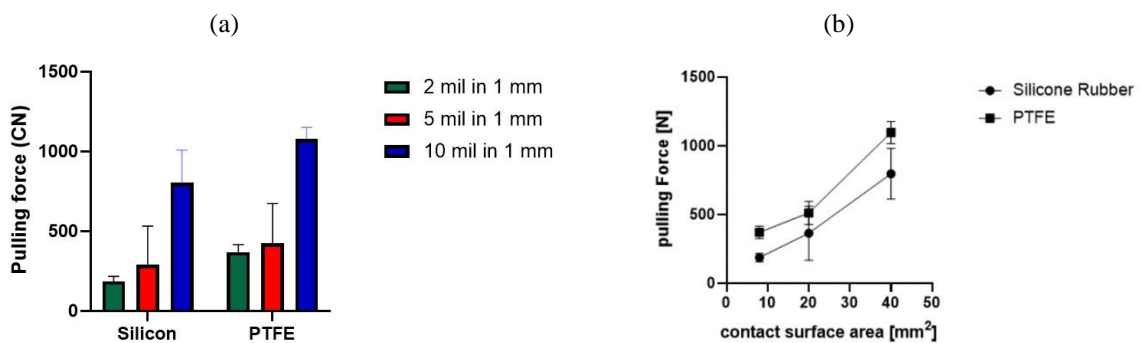


Figure 3-7: (a) Tensile forces required to pull a micro-pod from a mould as a function of the quantity of resin used to encapsulate a semiconductor in a 1.0 mm-diameter PTFE tube. (b) Contact surface area vs pulling force for PTFE and silicone rubber tubes. Image reproduced from (Nashed, 2019); this image is licensed under a Creative Commons Attribution 4.0 International License (CC BY 4.0).

The internal surface of both tubes used in this project was examined and assessed using a scanning electron microscope (Scanning Electron Microscope, JEOL JSM-840A, SEMTech Solutions, Billerica, MA, USA). Figure (3-8) shows the internal surfaces of the tubing made from (a) PTFE and (b) silicone. 10,000 times magnification scale on both surfaces reveals apparent differences in roughness between the two surfaces, with the surface of the PTFE tube appearing much rougher than that of silicone. This can be related to the manufacturing process of each tube.

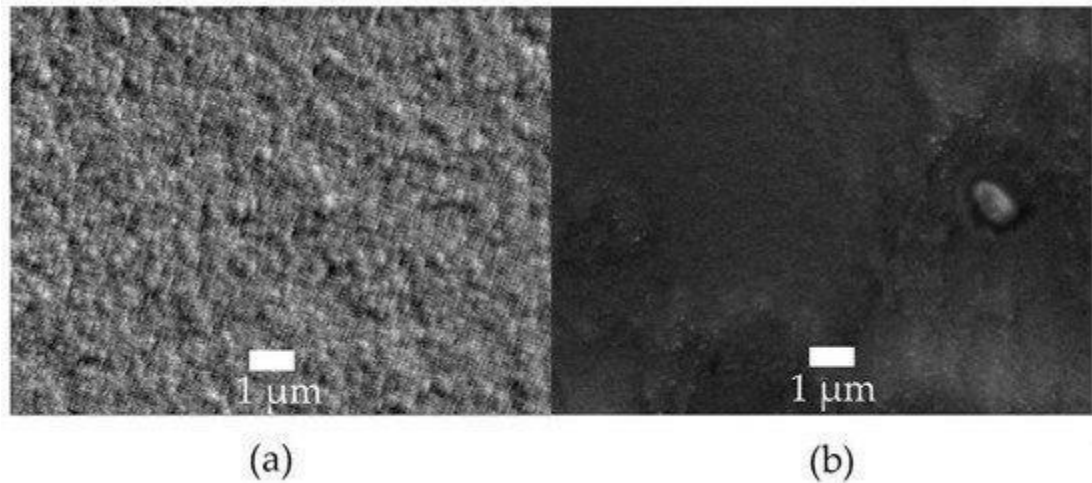


Figure 3-8 SEM images of the inner surface of the encapsulation mould materials at 10,000 times magnification: (a) PTFE (polytetrafluoroethylene) tube. (b) Silicone tube.

3.3 Resin dispensing

Applying the resin onto the electronic component requires injecting a small pre-determined volume of resin into the mould to surround and seal each electronic component held within it. This volume depends on the size of the package die that needs to be encapsulated.

One primary requirement of the dispenser is to minimise the formation of air bubbles within the micro-pod created during the encapsulation. Time/pressure dispensing controllers can be used to control fluids. The disadvantage of these dispensers is their temperature sensitivity and the need to calibrate the dispensed resin volume depending on the temperature. An alternative method is peristaltic pump dispensers, which transfer liquids by pressure displacement applied by turning a rotor against a flexible tube carrying the material. These pumps are preferred because they dispense consistent volumes for the same setting.

Jet dispensing is another alternative that can deliver exact, repeatable deposits. However, this non-contact method of dispensing does not suit the in-mould encapsulation procedure needed in this project.

To apply the resin and create the micro-pod around the electronic components, a Preeflow eco-PEN (Intertronics, Oxfordshire, UK) was chosen. This system uses a progressive cavity pump principle that doses and dispenses a wide range of viscosities with no stress to the

material and provides volume control. This dosing system could dispense small quantities, with a minimum volume of 0.001 ml and with flow speeds of 0.12–1.48 ml/min.

The volume of resin needed to encapsulate the electronic component depends on the size of the components themselves and the geometry of the micro-pod. For cylindrical micro-pods, the diameter needed for the micro-pod to seal the component needs to be defined. The minimum diameter D_m needed to seal the components needs to be larger than the diagonal length of the cross-section of the component.

$$D_m = \sqrt{b^2 + a^2} + 0.1 \quad (3.3.1)$$

Where a and b are the dimensions of the rectangular cross-section of the electronic while H is the length in the direction of the mould axis as shown in Figure (3-9).

Thus, the minimum volume of resin (V_r) needed to create the micro-pod is calculated by deducting the volume of the electronic components (V_c) from the resulting micro-pod volume (V_m).

$$V_r = V_m - V_c \quad (3.3.2)$$

Where:

$$V_m = \frac{\pi \cdot D_m^2 \cdot (H + T)}{4} \quad (3.3.3)$$

T : is the tolerance needed on both sides to fully encapsulate the component Thus:

$$V_r = \frac{\pi \cdot D_m^2 \cdot (H + 2 \cdot T)}{4} - a \cdot b \cdot H \quad (3.3.4)$$

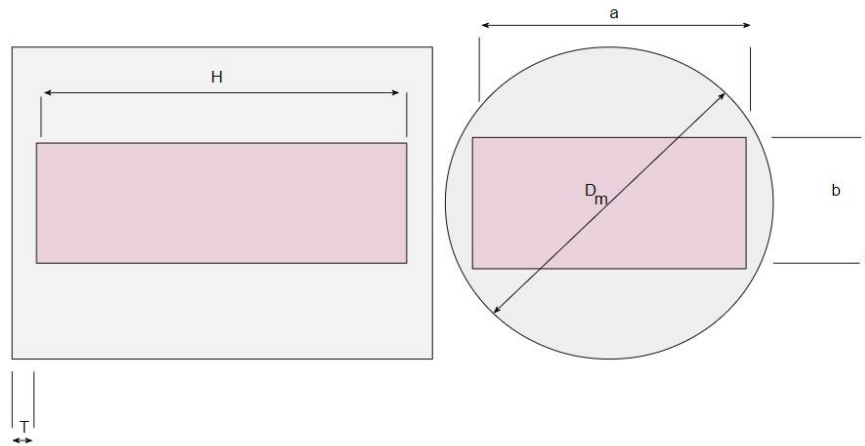


Figure 3-9 The side view and cross-section of the micro-pod and its dimension

The shape and size of surface mount resistors are standardized, and most manufacturers use the JEDEC standards. The size of SMD electronics is indicated by a numerical code, such as 0402. This code contains the width, height, and length of the package. Table (3.1) below shows the minimum resin volume needed for some standard electronic components size encapsulated in this research.

Table (3.1) calculates the minimum needed volume of resin needed based on the minimal diameter of the required micro-pod. Moreover, the quantity of resin dispensed would need to consider the amount of resin sucked back by the needle due to surface tension forces. Thus, the table can guide the quantity of resin that is required to encapsulate the electronic components.

Changing the dispensing rate could lead to changes in the deposit volume of the resin. When the dispense rate is changed, the deposit size could change. For example, 50 forward steps at the high dispense rate produce a smaller deposit than 50 forward steps at the low rate. That is because the faster rate compresses the fluid and restricts the flow path, while a slower rate gives the fluid more time to dispense. For optimum consistency, the changes in the volume observed for the dispense rate needs to be consistent with the deposit settings.

Table 3.1 The volume calculations for standard size electronic components.

Imperial size	0402	0603	0805	1206	1210
Metric size [mm]	1.0X0.5X0.35	1.55X0.85X0.45	2.0X1.2X0.45	3.2X1.6X0.55	3.2X2.5X0.55
Volume of the semiconductor Vc[ml]	0.175	0.6	1.00	2.8	4.4
Minimum Di- ameter of the mould dm[mm]	1.01	1.36	1.68	2.1	2.9
Volume of the micro-pod Vm[ml]	2.4	5.16	8.87	17.86	35.75
Volume of the resin Vr [ml]	2.22	4.57	7.79	15.0	31.35

Dymax 9001 v3.5 was dispensed into a PTFE tube at different flow rates to study whether a change in the volume needs to be considered. The volume dispensed was 0.005ml and 0.015ml at the following rates 0.1 [ml/min], 0.5 [ml/min], 1.0 [ml/min], and 1.5 [ml/min]. the volume was recorded after that by microscope (Keyence, UK) at 100X to compare the volume dispensed at different flow rates. The images presented in Figure (3-10) do not show a noticeable difference in the volume dispensed for different flow rates. This, there were no further steps needed.

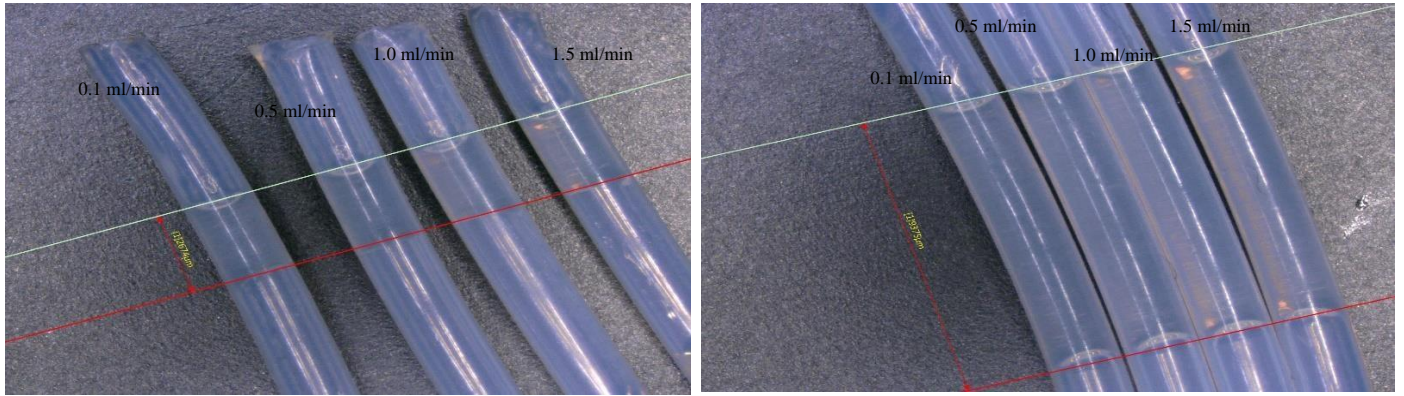


Figure 3 -10 Resin dispensed at different flow rate in clear PTFE tubes. The right one has 0.015ml volume while to the left 0.005ml.

3.4 Resin selection

A conformal coating is a protective coating that can be a non-transparent or transparent varnish applied to parts of a Printed Circuit Board (PCB) (Decker, 2001). The curable materials are dosed onto the PCB forming a thin or a thick film (Li, Tudor, Liu, *et al.*, 2018). Typical materials used for conformable coatings in PCB manufacture include Urethane, Silicone, Acrylic, and Urethane Acrylate (Henkel, 2019).

Selecting the resin for the manufacturing of the EFY is critical to the encapsulation process as it plays a significant role in the functionality of the resulting yarn and affects the fabrication process. The following points need to be considered when selecting the resin:

- The viscosity of the selected resin should allow small quantities of resin to be dispensed accurately.
- The curing parameters are essential for proper resin selection. Curing needs to be conducted without causing damage to the electronic component or the soldered interconnection. Moreover, the speed of the curing process should be suitable for the mass manufacturing of the E-yarns.
- The physical characteristics of the cured resin, which forms the final micro-pod, should fit the application of the E-yarn. For example, the resin used for an LED embedded Eyarn needs to transmit light, while it is essential to use a resin with suitable thermal

properties in thermistor embedded E-yarn to allow heat transfer to the embedded component.

- Post-curing micro-pod should withstand the mechanical and chemical stresses endured during washing and other mechanical stresses due to wearer activity. Thus, a degree of flexibility is needed to make the E-yarn compatible with the surrounding textile materials.

Resin polymerization requires the introduction of energy into the resin to cure it. Depending on the chemical structure of the resin, the curing process can be initiated by either thermal energy or photon energy from light. Encapsulating electronic components using a heat curing method can be undesirable. Heat curing can lead to the mechanical failure of electronic components due to temperature-induced elastic or plastic deformation (Minges, 1989). Thus, a photo-initiated curing method was selected for creating the micro-pod in this research. Advantages of photonic curing include a low operational cost, easy maintenance, and a small footprint for the required machinery. Moreover, an Ultra-Violet (UV)-curable coating reduces solvent emission since most of the formulation comprises oligomers and reactive diluents (Decker, 2001; Srivastava *et al.*, 2008). These advantages led to UV-curable resins being explored for this project.

The formulation of UV curable coatings contains binders (oligomers, resins), diluents (monomers, water, or solvents), photo initiators, and additives (Decker, 2001). Diluents are often necessary to control the viscosity of the formulation to enable application by spraying, jetting, roll-coating, printing, or other techniques. The oligomers determine the material's overall properties, such as hardness and optical properties (Kunwong, Sumanochitraporn and Kaewpirom, 2011a). Monomers and oligomers in UV formulations are generally derivatives of acrylates or methacrylates containing polyurethanes, polyesters, polyethers or acrylic chemistries (Decker, 2001).

Polymerization is a reaction when small molecules react chemically to form large molecules and molecular networks called polymers. This process is also known as hardening as it converts liquid formulations into a hard, solid film or elastomeric solid. Photopolymerization utilizes the photons emitted by a light source to initiate the chemical reactions by exciting photo-initiators. Upon absorption of the light energy, the photo-initiator produces a reactive chemical species that initiates the crosslinking between the resinous components (oligomers, monomers, and others) to cure the adhesive (Boyd and Phillips, 1996) (Boyd and Phillips, 1996; Kunwong, Sumanochitraporn and Kaewpirom, 2011b).

An acrylated urethane was selected for this research: Dymax 9001-E-V3.5 (Dymax, Torrington, UK). This resin is transparent to visible light, making it suitable for the encapsulation of LEDs. Moreover, it is widely used in bonding applications in the electronics industry, meaning that it has been thoroughly tested on various electronic devices (Rajoo *et al.*, 2010). Table (3-2) shows the material properties as advertised by the manufacturer (Dymax Corporation, 2009).

Table 3-2 Dymax 9001v3.5 mechanical and physical properties.

Tensile at break	5 MPa
Elongation at break	150%
Young's modulus of elasticity	17 MPa
Durometer hardness	D45
Viscosity	17000 cp

The correct resin curing can be verified by a physical change in the resin tactility of converting from a liquid to a solid. However, other techniques can be used to study the curing process. A potassium permanganate staining test can provide a qualitative indicator of UV chemical curing (Bretterbauer *et al.*, 2013). Raman Spectroscopy has also been used in some literature and published papers to determine the degree of curing (Osaka *et al.*, 2006; Bretterbauer *et al.*, 2013). Differential scanning calorimetry (DSC) measures the heat produced

by the reaction and can determine the degree of cure as the reaction proceeds (Diz and Spragg, 2011).

Fourier-transform infrared (FTIR) spectroscopy provides more chemical information than DSC because more absorption bands are measured. Curing acrylic resin involves the disappearance of C=CH₂ bonds in the monomer. C=CH₂ twisting shows a peak at 812 cm⁻¹ while the deformation of the C=CH₂ peak is near 1400 cm⁻¹ (Kunwong, Sumanochitraporn and Kaewpirom, 2011a).

An investigation of the optimal curing time was carried out using Fourier Transform Infrared Spectroscopy (FTIR). Resin samples were prepared by dispensing 5 µl Dymax 9001 v3.5 samples onto a non-stick PTFE plate. The samples were cured independently for 10 sec, 20 sec, 30 sec, and 50 sec by exposure to a 385 nm UV light source (light source details). Time has been selected around the values suggested in the datasheet of the resin. The samples were then kept in black bags to avoid any further curing by visible light before their transmission spectra were analysed in an FTIR spectrometer (Perkin Elmer Spectrum Two; Llantrisant, UK).

The purpose of the study was to evaluate the level of curing for optimum treatment. One sample was cured for 50 seconds to evaluate the over-curing effect on the resin. The FTIR analysis of 50 sec samples is shown in Figure (3-12). Figure (3-11) shows transmission spectra for the samples cured for 10 sec, 20 sec, 30 sec, and 50 sec. The curves show similarities in the peak strengths for different duration of curing beyond 10 sec. The peaks of the analysed samples are similar to spectra found in the literature for cured acrylated urethane resins (Kunwong, Sumanochitraporn and Kaewpirom, 2011b), indicating that curing of the resin had occurred.

By extending the time of the curing to 50 sec, no further chemical changes in the resin would happen. Thus, it was acceptable to use a 10 second curing time for a sample of this size.

However, we had to consider the absorbance of the UV energy by the rubber mould when the system is in full operation.

The curing level of the resin can be estimated by the spectroscopy absorbance curve from FTIR. The chemical structure for N-H which appears in the FTIR at peak 3200-3420 cm^{-1} totally disappeared after curing for 10 seconds. This is an indication of proper curing by UV. The 2260 cm^{-1} peak for the NCO chemical structure decreased clearly in the FTIR spectroscopy. The similarity between the spectrum of the sample indicated a very similar level of curing for the treated samples. However, it is worth noting that the slight change in the mass of the samples can change the absorbance of the FTIR slightly.

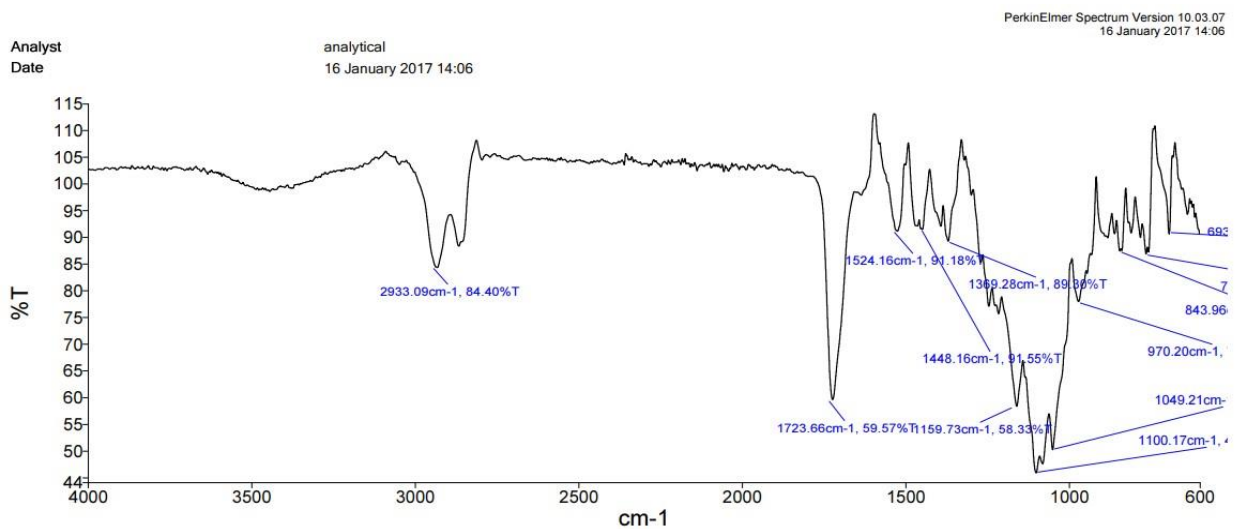
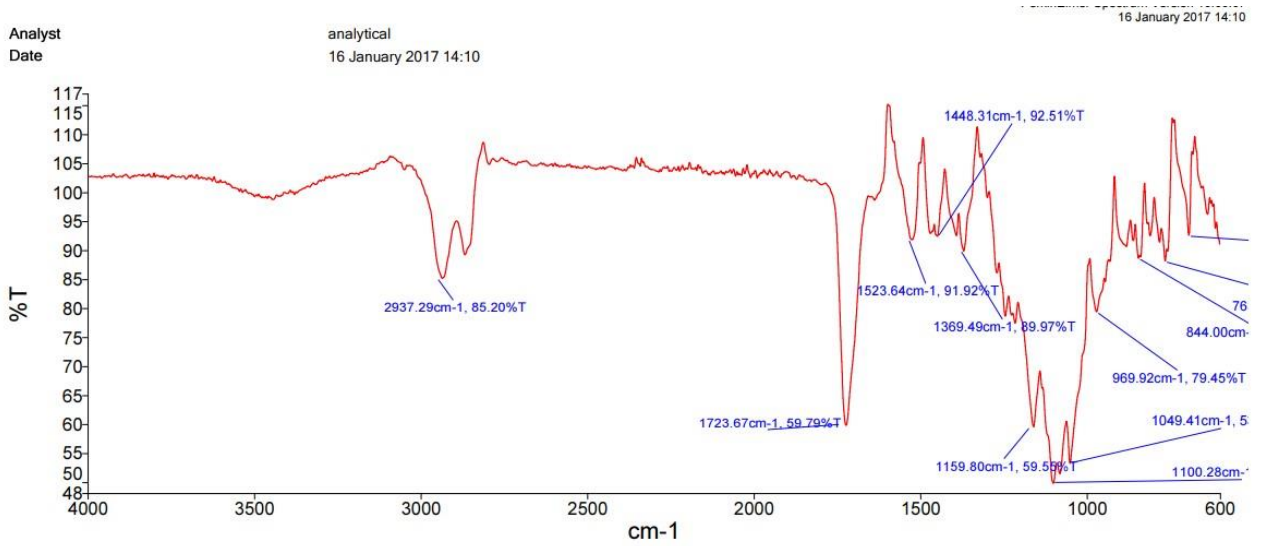
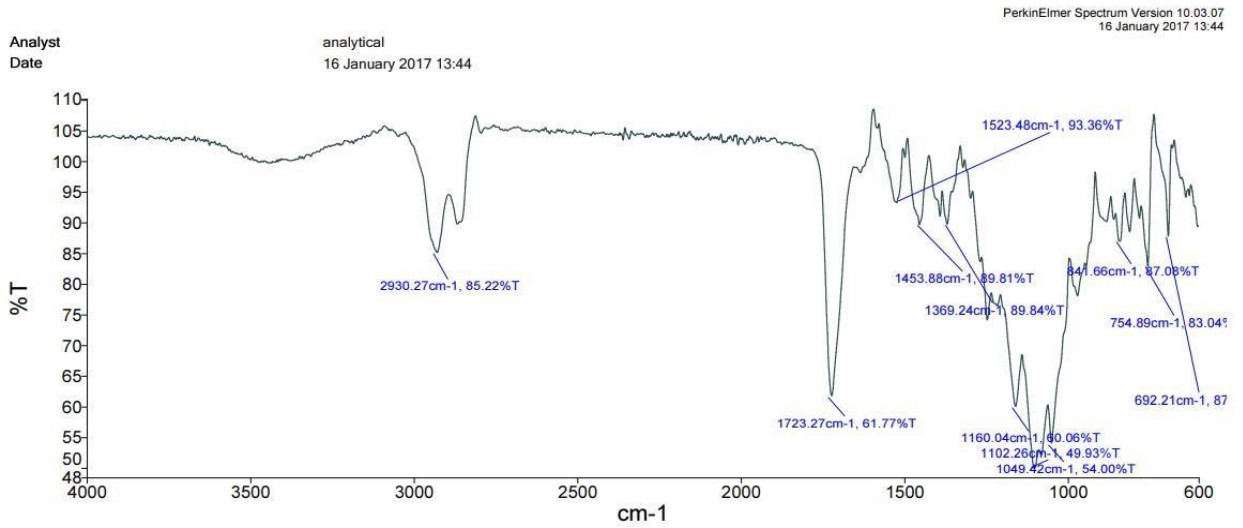


Figure 3-11 FTIR transmission graph for samples cured at 10 seconds (a), 20 seconds (b), and 30 seconds (c). the graph shows the peak and the transmission absorbance as percentage for comparison between different time cured resin chemical changes.

Over-curing should be avoided, as this may change the mechanical properties and optical characteristics of the resin. Minimizing the UV curing time for encapsulation had two advantages: Increased speed of encapsulation and prevention of degradation of the micro-pods (Kunwong, Sumanochitraporn and Kaewpirom, 2011b).

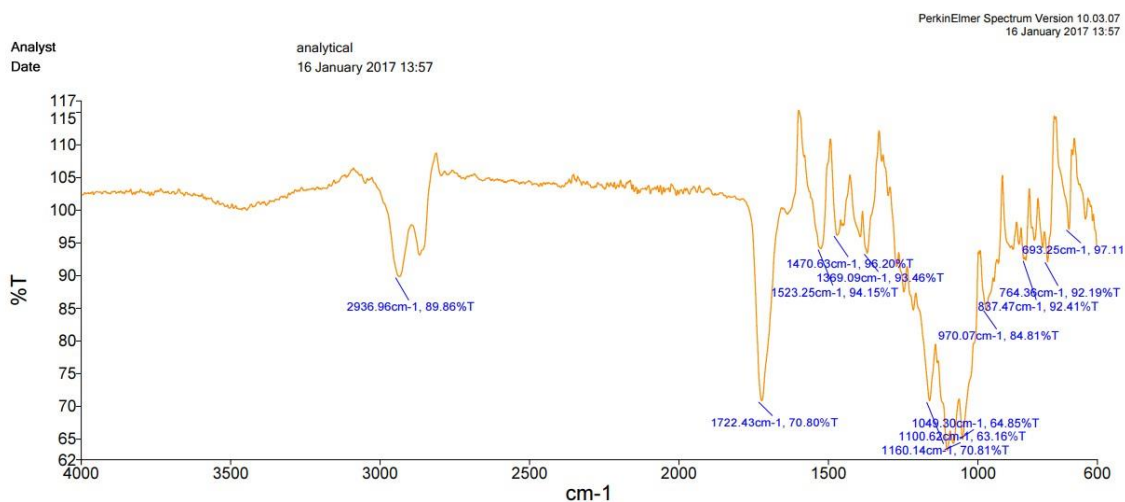


Figure 3-12 FTIR transmission graph for samples cured at 10 sec (a), 20 sec (b), and (30) sec (c). the graph shows the peak and the transmission absorbance as percentage for comparison between different time cured resin chemical changes.

3.5 UV Light Source

The selected resin in the earlier section must be cured using a UV light source. The wavelength of typical light ranges from (100 to 280nm) up to visible light (400 to 700nm) and infrared (700 to 3000nm).

UV-A range (315 to 400nm) emissions from current high-irradiance UV-LED systems penetrate through thick and pigmented materials more efficiently than UV-B or UV-C wavelengths (UV-C: 100 to 280nm; UV-B: 280 to 315nm), producing in-depth cure of the material that typically improves adhesion (Sholtes, Keliher and Linden, 2019). The Dymax 9001 resin is designed to be cured with light at wavelengths from 320–450 nm (Dymax Corporation, 2009). A curing system was selected to be carried out in the middle of this range, with a 385 nm UV light source chosen.

Optical power, measured in (Watt), is a function of both photons and wavelength numbers. The advancements in diodes and lamp technology increased the irradiance (W/cm^2) produced by UV-LED light sources. Today, UV-LED lamp systems are widely used to cure inks, coatings, and adhesives (Higgins, 2016).

The source of UV light reduces intensities at various working distances from the LED lens: This is due to the diffusion of the light. Maintaining optimal distance from the UV source throughout the curing process is an important way in which accumulated radiation exposure can be maximised. Theoretically, this is based on the inverse square law, shown in Figure (313).

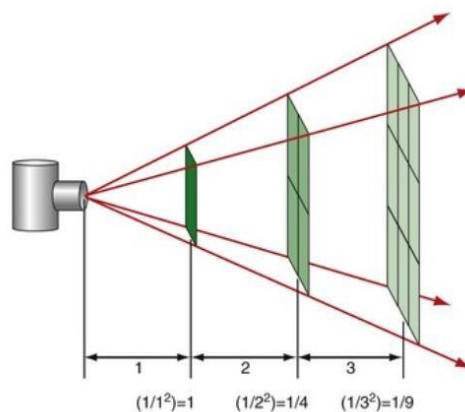


Figure 3-13 the decrease in intensity against the distance from the light source.

The depth of penetration of UV into a coating, ink or adhesive formulation during curing depends on the absorptivity of the formulation at each wavelength (Osaka *et al.*, 2006). Thus, consideration is needed when selecting the wavelength of the UV source to match the absorbance bands of the photo-initiator and consider the absorption characteristics of the other additives in the formulation to avoid competitive absorption that can prevent the UV wavelengths from reaching the photo-initiator.

A BlueWave QX4 LED Multi-Head Spot-Curing System (Intertronics, Kidlington, UK) was chosen for the encapsulation system. One essential factor that needs to be optimised is the amount of energy absorbed by the flexible mould surrounding the soldered

semiconductor. The energy introduced by the UV source to the dispensed resin and the influence of the mould on the curing energy will be illustrated later in this thesis.

The decrease in UV light intensity as a function of distance had to be understood. The ability to cure the resin may have been weakened if the UV LED is located far from the encapsulation area. Thus, it is essential to evaluate the decrease in the UV light intensity due to the location of the LED lens in the design of the encapsulation unit. The intensity of the UV irradiated by the lens is measured by (3-4) at different distances from the lens. The LED source was mounted on an adjustable height bracket, while the reader was mounted on a bracket and adjusted to change the distance between the LED source and the UV meter.

Figure 3-) shows the measured inverse square relationship between the distance from the LED lens and the UV intensity. This needs to be considered later when positioning the UV LED in the encapsulation system to maintain the maximum energy transferred to the resin during the curing. It can be concluded from the graph that beyond 25 mm, there would be a significant decrease in the power transmitted. It is worth mentioning that these measurements were limited to the maximum intensity measured by the device at 200 mW/cm^2 .

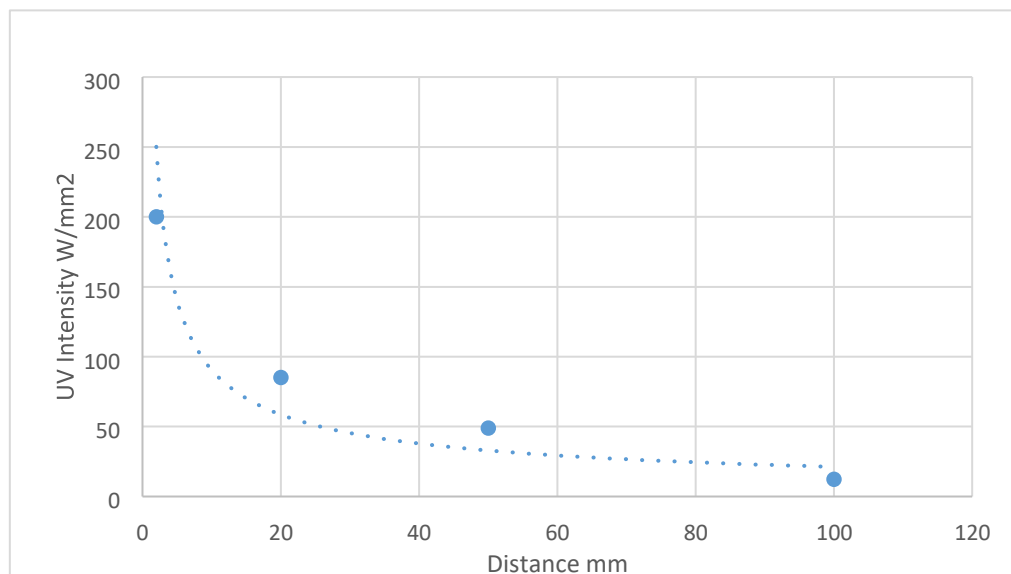


Figure 3-14 The decrease in the intensity against the distance from the UV source for the Bluewave QX4 385nm.

3.6 Encapsulation Unit Design

This part of the thesis demonstrates the automated process of E-yarn production, which will significantly help the manufacturing processes toward scaling up and commercialization. Automating the encapsulation process of soldered electronic components required a method to be developed. This part of the thesis demonstrates that E-yarn production can be automated; thus, manufacturing processes could ultimately be scaled up and commercialized.

This has been achieved by guiding the semiconductor into the cylindrical mould to the encapsulation area and leading the encapsulated semiconductor out of this section using a controlled automated driving system.

The core structure of E-yarn consists of the following elements:

- 7-strand copper wire with a 50 μm strand diameter (Knight Wire, Potters Bar, UK) was used for soldering the electronic component.
- Different size semiconductors of package dies were used as samples to verify the functionality of the mechanism designed. The examples shown in this work are Kingbright LEDs that used a rectangular 0402 package (model: KPHHS-1005SURCK; RS Components, Corby, UK) and a thermistor (Murata 10 k Ω 100 Mw 0402 SMD NTC thermistor; part number NCP15XH103F03RC; Murata, Kyoto, Japan).
- A carrier yarn, 100 Dernier VectranTM (Kururay, Tokyo, Japan), used for its high tensile strength, was included within the encapsulation to increase the tensile strength of the core structure, enabling the removal of the micro-pod from the mould.

The ‘*encapsulation mechanism*’ consists of the following components: A linear translation stage, a resin dispenser, a non-stick mould, a UV source, and a take-off and winding system. The design of this unit was built on the following assumptions.

- The wire and the soldered electronic components are fed into the encapsulation unit on the spool package from the soldering unit.
- The sensing system will detect the existence of the electronic component and activate the encapsulation process. The sensing point is defined as the ‘*detection area*’.
- A mechanical pulling system is needed to drive the electronic component and the carrier yarn to a pre-determined point where the encapsulation process occurs. This point will be defined as the ‘*Encapsulation area*’. Once the soldered component is located at the encapsulation area inside the mould, the *encapsulation mechanism* will be activated, and the system will complete a series of steps according to an algorithm to apply and cure the resin.
- The pulling system needs to apply sufficient force to remove the micro-pod from the mould following the creation of the micro-pod. A schematic of the process is illustrated in Figure (3-15).

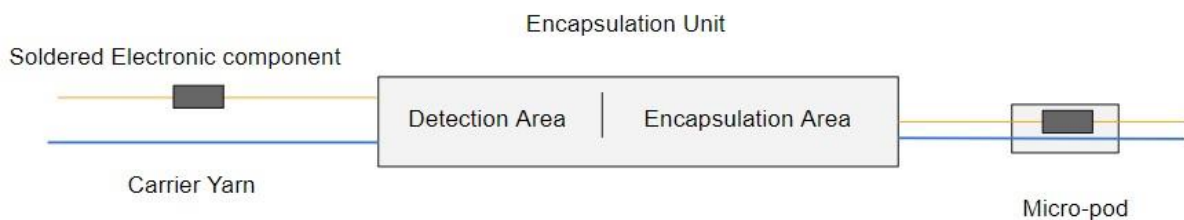


Figure 3-15 Encapsulation unit main three areas. Materials are fed to the system where the detection area is followed by the encapsulation area. The outcome of the process would be both the carrier yarn and the cooper wire encapsulated at the point of soldering the electronic components.

The resin dispenser unit is mounted onto the linear translation stage, enabling the resin dispenser to travel vertically to a specific encapsulation point. Hydraulic and pneumatic actuators were excluded due to the precision required. A linear stage LTS 15 (Thorlabs, ELY, UK) with an integrated controller was selected and mounted to move vertically. Unlike a DC servo motor translation stage, the platform with a stepper motor is designed to remain fixed when no power was supplied, so a brake was not required to keep the stage in its position. The LTS150 stage featured an integrated electronic controller controlled using a computer or

manually via buttons and a velocity potentiometer on the control keypad. The linear stage provided 150 mm of linear travel with a maximum vertical velocity of 3 mm/sec. The accuracy for the stage calibration was calibrated by the manufacturer with an accuracy of 20.0 μm .

It is crucial leading the copper wire precisely until the soldered chip reached the encapsulation point. Thus, a stepper motor, ISM 7411 (National Instrument, Newbury, UK), was introduced to drive the soldered electronic component on the copper wire. The motor is fitted with a micro-step emulator that increases the accuracy of the movement up to 20k steps/rev.

'Check Cycle' is defined as the number of steps that the copper wire would move before the system checks for the existence of a new component to encapsulate it, as shown in Figure (3-16). The motor shaft is equipped with a rubber cylinder that drives the soldered semiconductor a predetermined distance L for each *check cycle*. Motor steps, driving roller diameter, and the friction between the driving rollers are the factors that influence the accuracy of driving the copper wire are.

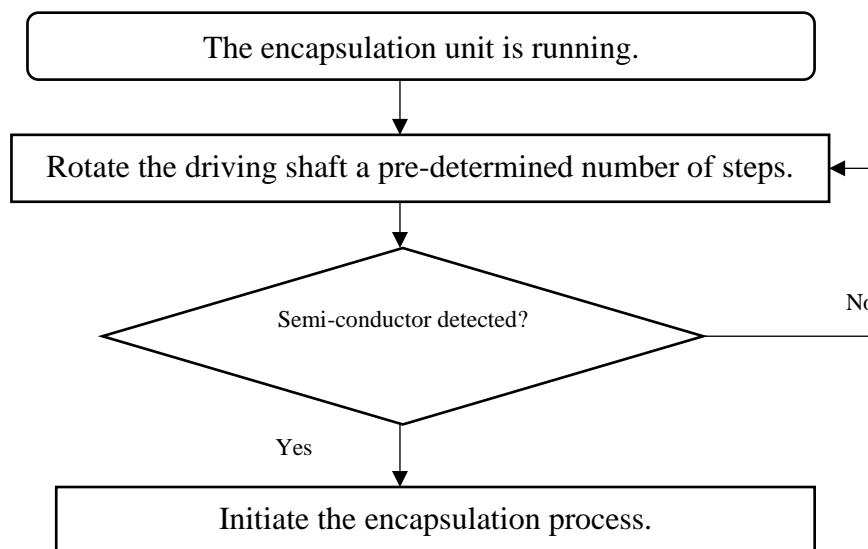


Figure 3-16 The check cycle used in the LabView

The distance L directly relates to the number of steps that the motor rotates for each check cycle. One full cycle is divided into four hundred steps, as micro-steps were not used to control the stepper motor better. A complete cycle will wind at a length equivalent to the circle

circumference ($\pi \cdot D$) as shown in Figure (3-17), where D is the attached roller diameter. Thus, the number of steps $[N]$ needed to wind $X[\text{mm}]$ is:

$$N = X * \frac{400}{\pi * D} \quad (2.7.1)$$

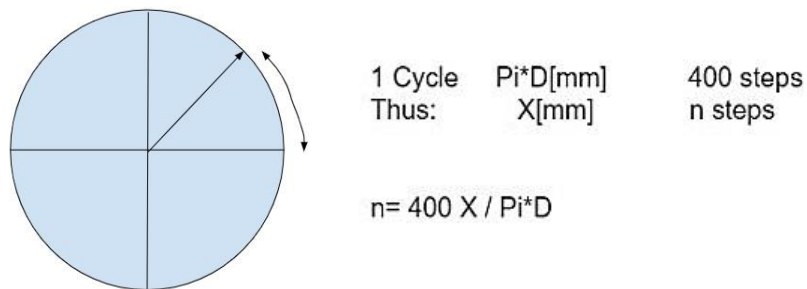


Figure 3-17 Distance calculation when the motor shaft rotates a number of steps n .

LabVIEW code is developed in this project, and the following formula was used in the LabVIEW code to give the operator the option to change the distance moved for each *check cycle*. The Code shown in Figure (3-18) is used on the soldering, which shares the principle of driving the copper wire, while Appendix (2) will show the LabVIEW code used in the encapsulation unit design.

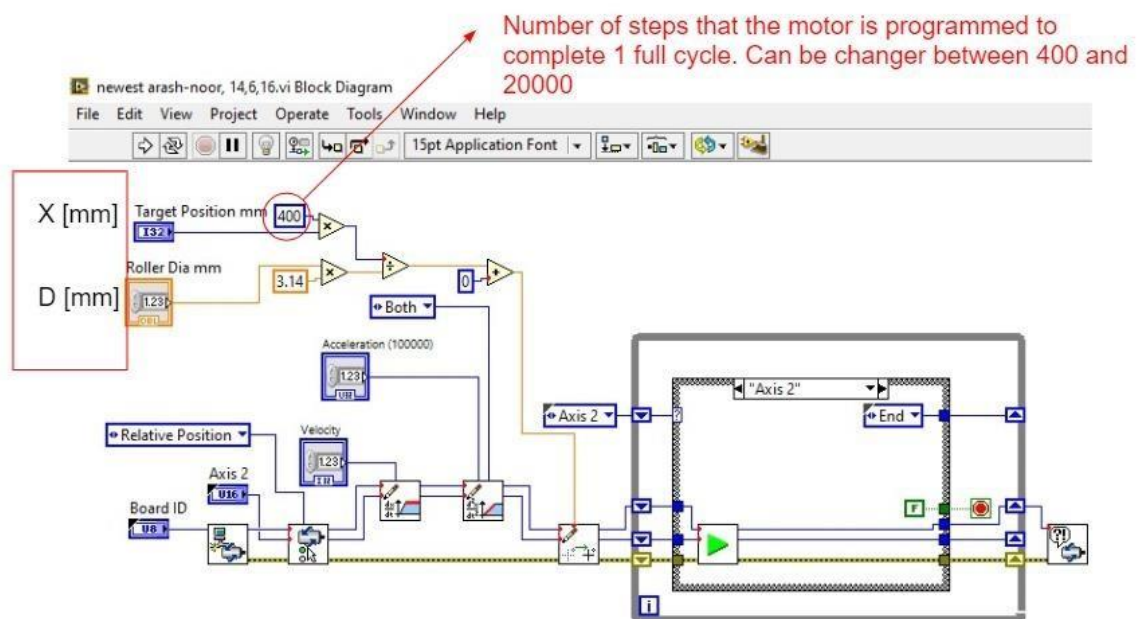
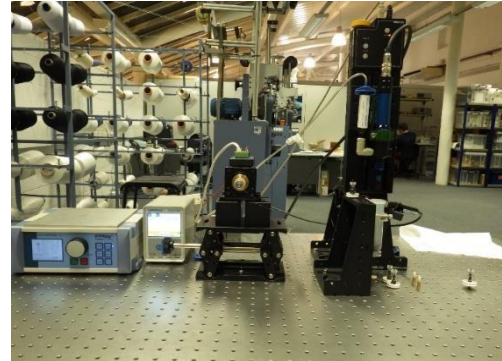
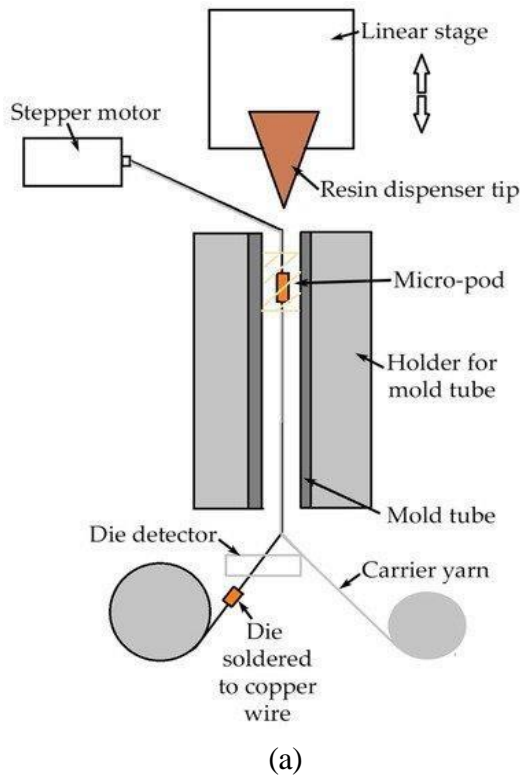


Figure 3-18 The LabVIEW code used for converting distances to several steps needed.

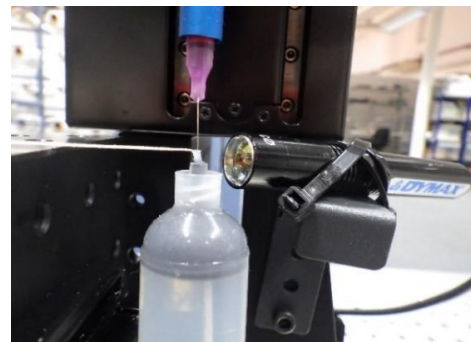
The interface programmed in LabVIEW was designed to switch between two operational modes. The user could switch between them through the program interface. The manual mode will start the encapsulation once the user pressed the encapsulate icon on the interface for a bespoke encapsulation. The system would then wait for the following command from the operator to encapsulate the next component.

The other option is an automatic mode where the motor runs once the user presses the start button. The system will keep running until a chip is detected by the detection system, then move the component to the encapsulation point where it would be encapsulated automatically. This mode would be used for continuous production when a consistent operation.

A schematic of the prototype encapsulation system is shown in Figure (3-19 a). Here the copper is shown passing through the sensing area and entering the encapsulation unit. The semiconductor is encapsulated and then pulled out of the mould by the stepper motor.



(b)



(c)

Figure 3-19 (a) Schematic illustration of the automated encapsulation unit, showing die detection before entering the silicone mould (b) the initial design of the encapsulation unit. (c) the encapsulation area

The encapsulation process consists of the following steps: Once the electronic component arrived at the encapsulation point in the mould, the stepper motor stopped, and the linear stage moved the dispenser until the tip reached the encapsulation point where the soldered chip was located. The resin was then dispensed, and the linear stage moves the dispenser up again to avoid curing the resin in the dispenser's tip. Subsequently, The LED UV light source cures the dispensed resin inside of the transparent mould. The whole process was controlled and monitored by a LabView program, which controlled the sequence of tasks illustrated in the flowchart in Figure (3-20).

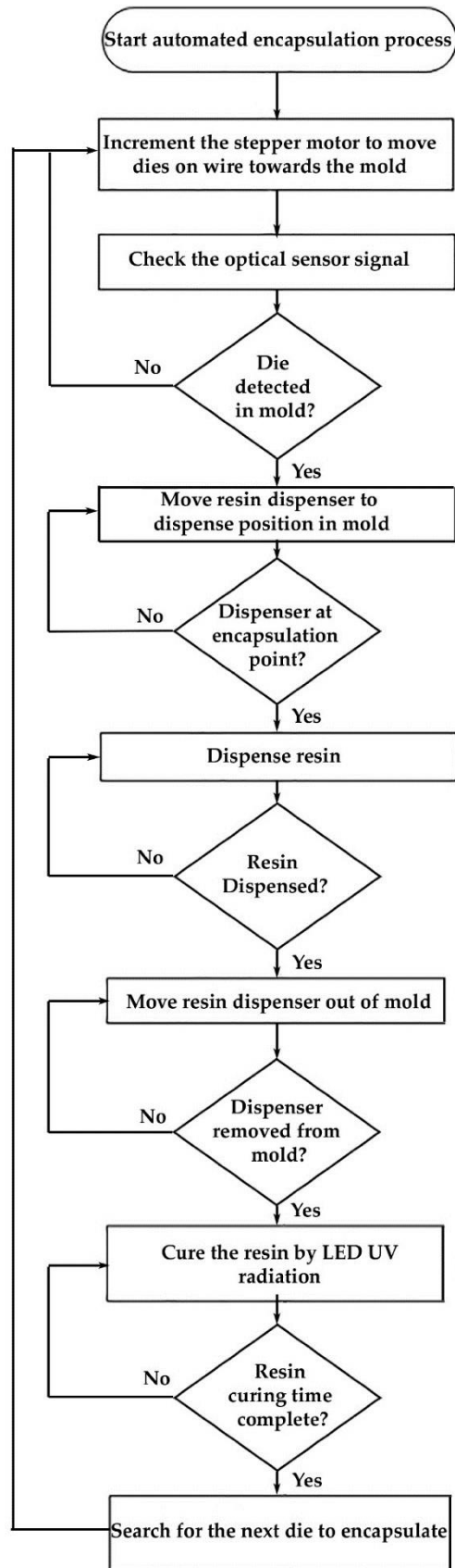


Figure 3-20. A flowchart illustrating the sequence of steps required for encapsulating one semiconductor soldered on copper wire using the encapsulation unit.

3.7 The detection system of the Electronic Component

Applying the resin around the soldered semiconductor requires the electronic components to be precisely positioned inside the mould to fully encapsulate the weak solder joints and avoid partial coverage with resin. The encapsulation process will occur inside the rubber mould holding a non-stick tube, as shown in Figure (3-21). Accurately detecting the soldered semiconductor is one main challenge in the encapsulation automation process.

Theoretically, the detection area can be in the same area as the encapsulation area, with the driving system stopping to apply the resin at the same point. For this process, the soldered components would be detected inside of the mould, the delivery of the wire would be stopped, and the encapsulation process would then be initiated.

Another design is that the detection area and the encapsulation area can be at different locations: This would require the driving system to move the component to the encapsulation area to start encapsulation after detection. Both designs were tested in this work. While the component size and the geometry of the interconnections added a level of complexity to the detection process, different types of sensors were tested to detect the soldered components. Sensor's performance and their reliability were evaluated and presented below.



Figure 3-21 partially encapsulated semiconductor.

3.7.1 Photo micro-sensor

A photo micro-sensor was the first sensor evaluated in the design. The sensor (Transmissive Photo Interrupter, model EESX398; Omron, Kyoto, Japan) detects the light intensity with a wavelength in the IR spectrum (700 nm) and has an aperture of 0.5mm wide.

The reliability of the system depends on the sensor used in the detection process. The photosensor consists of an IR LED on one side and a phototransistor on the other side. Once an obstacle interrupts the infrared beam, the voltage output of the transistor will rise and detect the existence of the component.

To identify the component, the soldered component needs to pass between the transmitter and sensor receiver. However, it was difficult to control the position and orientation of the semiconductor within the detection space. The small aperture size limited the sensor sensitivity to the semiconductor location and the copper wire vibration between the transmitter and the receiver of the photo microsensor. Looking at the side view of the sensor and the various possible locations that the soldered component can take between the two parts of the photosensor, there would be four possible positions, as illustrated in Figure (3-24). The vibration in the wire would lead to the soldered component ending up outside of the detection range.

On the other hand, the twisted wire would change the relative position of the soldered component inside the detection range. Figure (3-22) illustrates the event when the wire is out of detection range and the best position where the soldered component blocks the beam between the two sides of the sensor. If the soldered component were to rotate, then this would lead to either partial detection as shown in Figure (3-22 b) and Figure (3-22 d), or not being detected as demonstrated in Figure (3-22 c).

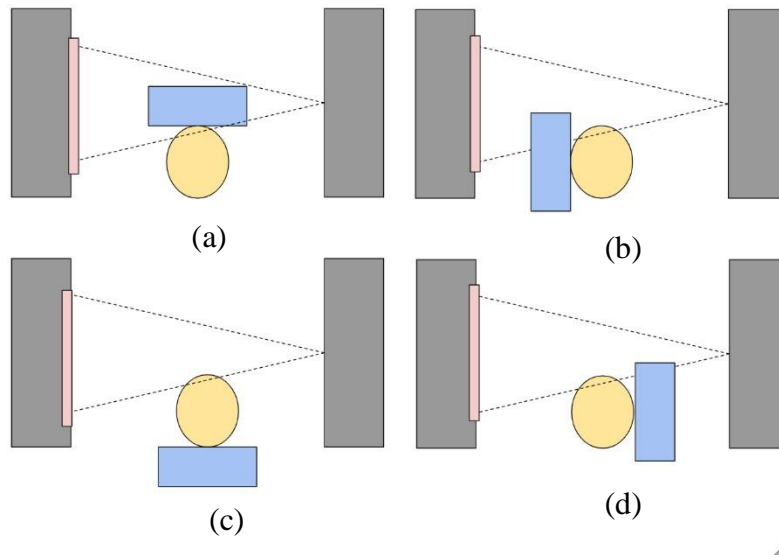


Figure 3-22 The possible relative location of the soldered component within the detection volume of the photo micro-sensor. (a) The detection position. (b) and (d) partially detection. (c) No detection

3.7.2 Laser micrometre

A laser micrometre is a different approach to detecting the existence of the soldered component. Laser micrometres measure the outer diameter of the object that is passing through the detection area Figure (3-23c). The operational principle depends on a charge-coupled device (CCD). It consists of an integrated circuit containing an array of coupled capacitors acting as small pixels. The light falling onto each pixel is converted into a charge pulse processed by electronics and represented by analogue voltage output. The sensor used was a Multi-Purpose CCD Laser Micrometre IG series IG028 (Keyence, Osaka, Japan) shown in Figure (3-23b).

The laser micrometre was used to detect the chip before it entered the PTFE mould. The minimum detectable object was 0.2 mm for a 100 mm setting distance, which could be increased to 0.1 mm when working in the high sensitivity mode. The transmitter and receiver were mounted using a standard bracket supplied by the manufacturer to maintain the distance between them at 100 mm. the laser micrometre was mounted outside the mould due to the size and space limitation of the design.

Once the soldered component passes into the detection region, the external diameter of the wire changes and this change should be captured by the sensor. The sensor outputs this information as an external voltage (0-24V) that could be interrupted using a microcontroller to inform the automation of the process. The signal was processed using LabVIEW, which controls the encapsulation system as described in the earlier section.

Moving the component between the detection area and the encapsulation area required the driving system motor to rotate several steps before the encapsulation process started. This method required the stepper motor to move the component accurately and precisely a distance L between the *detection point* and the *encapsulation point* inside of the mould, as shown in Figure (3-25a). A controlled tension had to be applied between the feeding package and the driving roller to improve the reliability of the driving system.

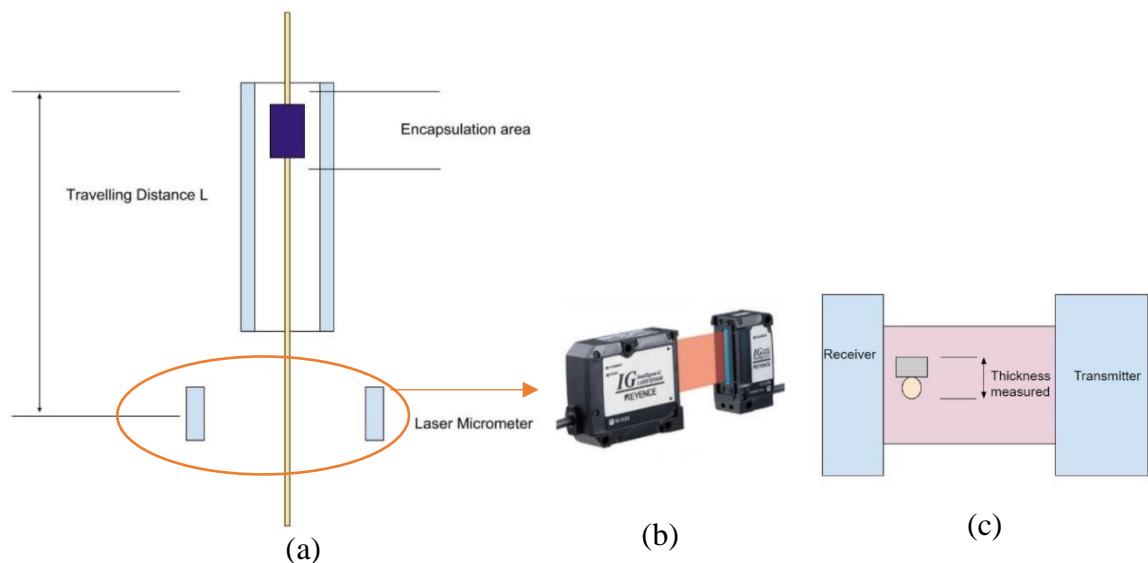


Figure 3-23. (a) The laser micrometre arrangement shows the travelling distance needed to move the electronic component from the detection area to the encapsulation area. (b) A photograph of the laser micrometre from Keyence. (c) The working principle of the laser micrometre used.

Although the laser micrometre sensor showed high detectability results, the driving system did not achieve an acceptable repeatable result due to the motor's tension variation and control limitation. Moreover, false detection was reported due to copper knots that were detected by the sensor. A tension controller feeder (Ultra feeder, BTSR) was added later to the system to avoid tension fluctuation of the copper wire.

3.7.3 Fibre optics

The primary purpose of using this fibre optic was to allow for the detection of the component simultaneously where it was to be encapsulated. This required a sensor with a small diameter to be integrated into the mould design and suitable sensitivity to detect the existence of the small, soldered components.

A transmissive fibre optic FU-58 from (Keyence, Osaka, Japan) was used to detect these components while passing through the PTFE tube, as illustrated in Figure (3-24). The minimum detectable object was 0.005 mm^2 , which was adequate for all chip sizes of interest at this stage of the project. Once the light intensity drops due to a component arriving between the two parts of the fibre optic sensor (transmitter and receiver), the voltage drops (0-12V), and a signal was sent to the encapsulation unit. The signal was interpreted using a LabView program (Version 14; National Instruments, Newbury, UK). The sensor detected the soldered component inside of the transparent mould tube at the point at which encapsulation took place.

Results showed that adding the fibre optic was a promising approach to increase the component's detectability inside the mould. Experiments showed that the FU-58 sensor could detect 94% of eighty-seven soldered thermistor chips tested (0402 packages); however, working with LEDs (0402 package) showed less favourable results, where the sensor could detect only 46% of the fifty-four soldered LEDs tested.

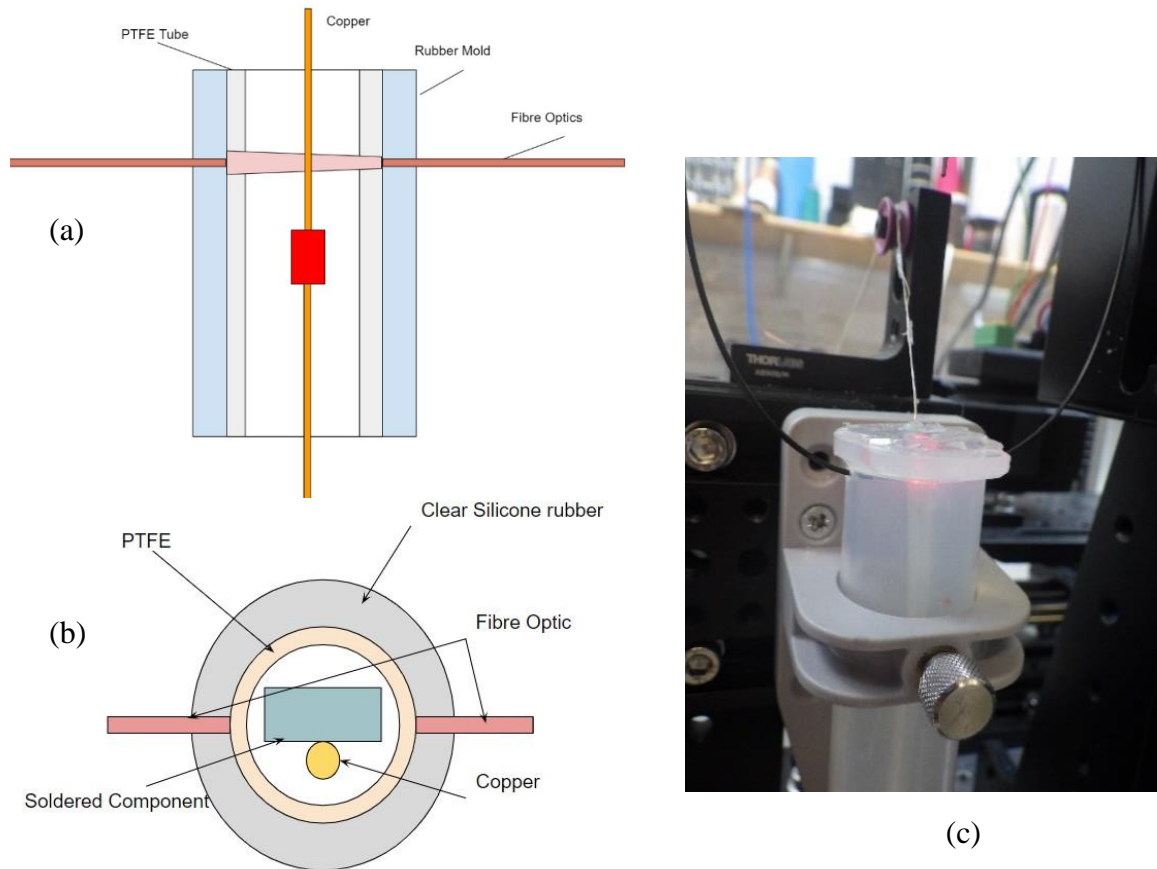


Figure 3-24 (a) The side view diagram of fibre optic arrangement inside the mould. (b) Cross section views of the fibre optic arrangement. (c) A photograph of the assembled design.

This reduction was due to the bright colour of the LEDs and the structure of the LED itself. It was believed that this was due to the semiconductors being a different colour and that the fibre optic was sensitive to different colours. Components with darker surfaces were much easier to detect using the fibre optic than the semi-transparent LEDs. Moreover, the geometry of the components makes them less detectable at certain angles. Under certain circumstances, the component was sitting outside the light beam and could not always be detected, as illustrated in Figure (3-25a). To improve this sensitivity, we added another fibre optic working perpendicular to the first. The new layout of sensors is illustrated in Figure (3-25b). Using this new arrangement, the sensors had a higher detection rate and detected thermistors with an accuracy of 98 % and LEDs with an accuracy of 87 %.

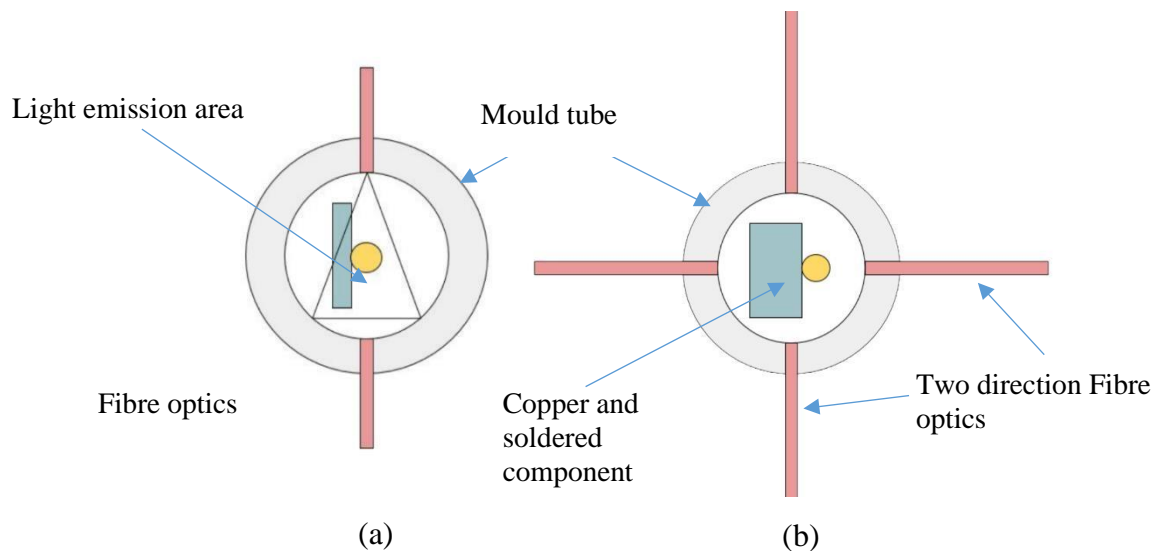


Figure 3-25 Component location in the light beam. (a) Original configuration with one fibre optic sensor. (b) Revised configuration with two fibre optic sensors perpendicular to one another.

It was mentioned earlier when discussing the algorithm of the controlling program Figure (3-26) that after each detection cycle, the motor rotated a specified number of steps before checking the status of the detection sensor. This made it essential to check the number of steps that the stepper motor rotated before checking the sensor signal. The number of steps should lead to a linear movement of the component that is less than the length of the detecting area, as shown in Fig (3-26). Making this number higher would lead to the component moving into the detection area and leaving it before checking the sensor status, which would decrease the system's detectability. To overcome this issue, we had to use a low number of steps for each detection cycle to reduce the possibility of the phenomena described.

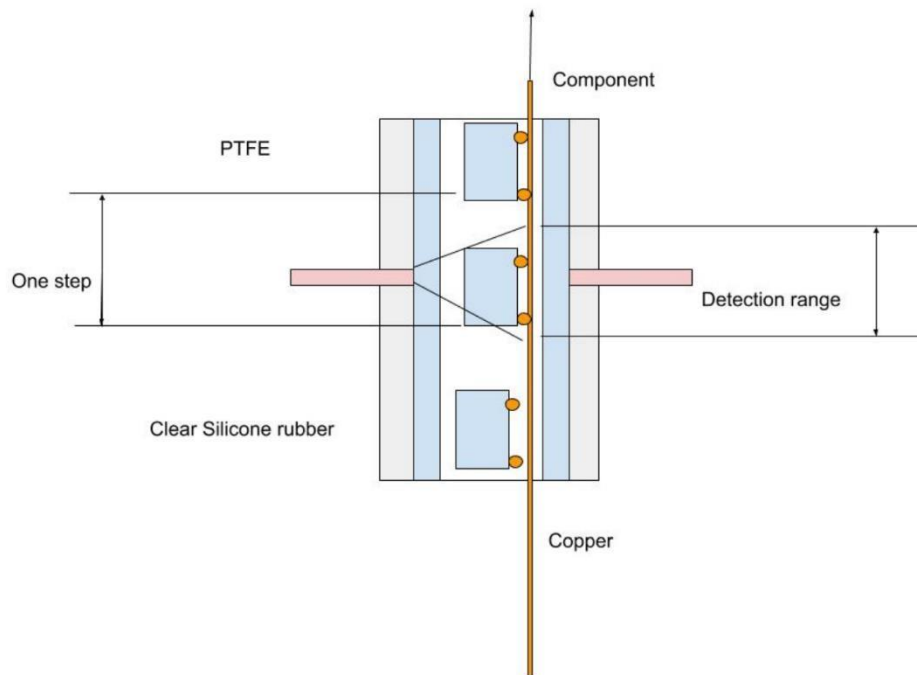


Figure 3-26 The detection area length and the impact of the one-step distance on the possibility of the component passing the sensor without detection.

3.7.4 Vision sensor

The last detection system explored was a digital camera that can focus on the encapsulation area and compare the image of that area with a reference image stored at the system's calibration. The sensor used in this case is (IV-HG150MA Narrow field, Keyence) shown in Figure (3-27). The sensor is mounted in a range between 50mm and 150mm from the encapsulation area. The camera is supplied with a software program to program the detection judgment of the sensor. The program is comparing the images captured by the system with a master image. The master image should teach the system when to trigger the activation signal. The trigger signal from the sensor will initiate the encapsulation process.

The program would compare the instant image with the master images based on one or a combination of three methods. The first is an outline where the controller would compare the outline to the outline of the master image stored by the user. The second option is 'Area', where it calculates a percentage matching of the target area of the instant image to the master image.

The last option is edge pixels which would judge the number of pixels in the instant image to the one in the master file. The three-options selection window is shown in Figure (3-29).

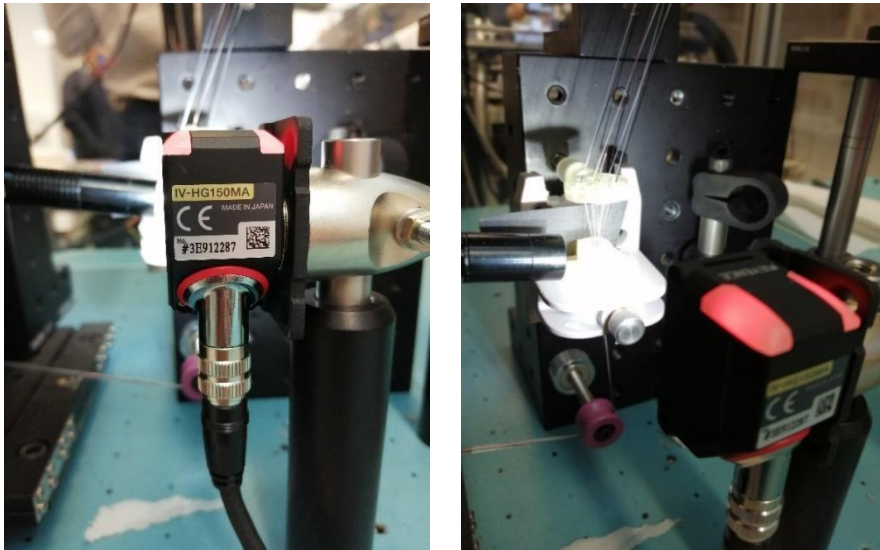


Figure 3-27 the digital camera that monitor the mould for detection prior entering the encapsulation area. The image above shows the sensor for two sides.

Since the detection is outside the mould, there is a need to move the soldered component to the encapsulation area. However, the camera can monitor the detection area closer to the mould, which minimised the number of steps between the detection area and the encapsulation area. Figure (3-28) shows an instant image of the system running.

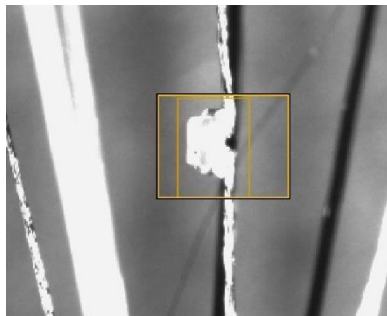


Figure 3-28 The camera sensor monitors the area prior to entering the mould of encapsulation.

Practically, the sensor was affected by the ambient light. Thus, there is a need to isolate the encapsulation cabinet from the ambient light for future development. However, the detectability of this system was sufficient, subject to calibration and no change in the ambient light.

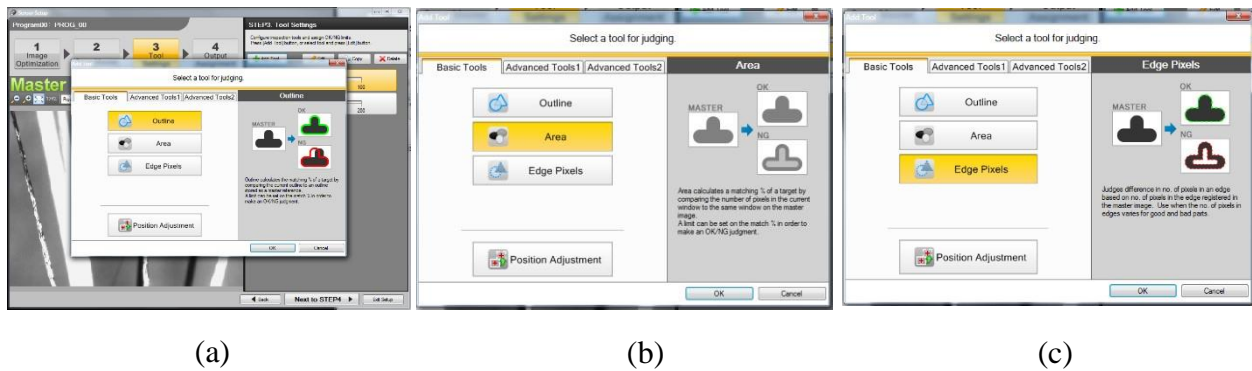


Figure 3-29 The judgment options for the camera (a) Outline (b) Area (c) Edge Pixels.

3.7.5 Detection system discussion

Several techniques have been evaluated in this research for detecting the soldered semiconductor for encapsulation. Photo micro-sensor has the advantages of small footprint and simplicity. However, the detection rate was low due to the lack of control of the semiconductor location between the transmitter and receiver photodiode. The vibration of the wire and twisting of the component led to positioning the component out of the detection range of the sensor.

The alternative solution evaluated was a laser micrometre, which has a wide range of detection allowing the wire to move within those limits. The laser micrometre showed high detectability. However, the size of the sensor made its integration into the system complicated. The sensor was positioned far from the encapsulation area. The challenge, in this case, was to move the detected component from the detection area to the encapsulation area precisely. Moreover, it was sensitive to nuds and faults in the wire adding a false detection signal.

The idea of on-site detection was necessary to improve the reliability of the system. Fibre optics integrated with analogue output combined the advantages of laser micrometre precision and the size of the photo micro-sensor. The fibre optics were integrated into the rubber of the mould allowing on-site detection where the encapsulation area and detection area are integrated. Despite the high detection rate, it should be noted that the sensor was sensitive to the colour of the semiconductor itself. Reflection of the light and orientation of the semiconductor inside the tube was a challenging task for this sensor. One suggestion that was not

tested in this project was to use a capacitive sensor that detects the change of mass inside the tube. The capacitive sensor shares the advantages of the optical fibres and avoids the limitations of colour absorbance or semi-conductor orientation.

The final version of the encapsulation unit used a vision sensor that monitors the detection area and compares the image to a pre-programmed reference image. The system showed good integration as it is a non-contact detection system. It showed a need to use the light controlled cabinet to avoid the effect of ambient light on the detection process. The sensor can be upgraded to a coloured vision sensor with AI built in.

To sum up, several detection systems have been assessed and each one has its advantages and limitations. Further investigation can be done for better performance and detection reliability of the system.

3.8 Winding mechanism

A storage and winding mechanism are needed as an essential step to maintain the tension of the copper wire and the carrier yarns steady during the encapsulation and to ensure proper packaging of the yarn before the next stage of the manufacturing process.

This part of the study will discuss the requirements of the winding unit, where the primary purpose is storing the core structure of the Electronically Functional yarns with their micro-pods before the next stage of the production. Thus, the designed mechanism must not damage the micro-pods and must avoid entangling the yarns.

Winding principles were considered to select the suitable mechanism and design for this application. Driving the winding mechanism can be frictional using surface contact driving or direct driving (Durur, 2000). The frictional method has been avoided in this design to prevent any micro-pod wound damage to the package; thus, direct driving was selected for the winding mechanism in this project.

Similarly, the traverse method is selected to use a reciprocating yarn guide to reduce the friction in the grooved drum method. This part of the chapter will introduce the technique used and the theoretical advantage of the selected method of winding.

The quality of the package is determined by several variables (Hebberling, 1969). The wind angle is an essential parameter in the winding process. As a general rule, the higher the winding angle, the better the package (Hebberling, 1969). The maximum angle can be found by a trial-and-error process.

To maintain a steady tension on the EFY core structure after the encapsulation, a (TS44/100, BTSR) tension sensor was used. The controlling program monitors the tension in the sensing area, which is located before the winding unit. Once the tension at the sensing point reduces below a pre-set tension [T], the winding unit starts winding the excess length of the yarn.

The designed winding, illustrated in Figure (3-30), unit consists of the following components: the stepper motor: ISM 9411, a rubber driving roller (diameter 22mm), and a timing belt (T5- 650 length 650mm and 130 teeth) that transfer the power from the motor shaft to the transverse mechanism. The tension sensor (TS44, BTSR) is mounted between the take-off roller and the winding mechanism.

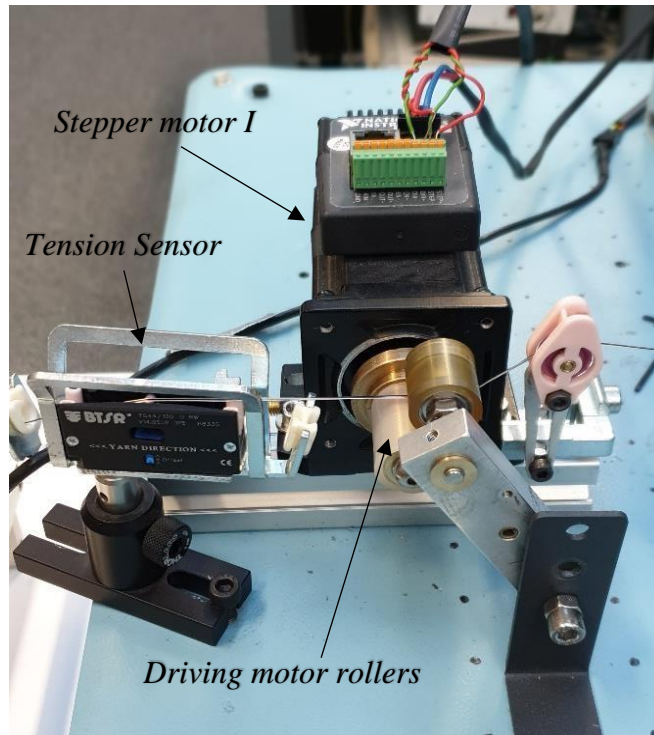


Figure 3-30. Tension sensing area between the winding mechanism and the driving motor. The sensor is located following the driving rollers to sense any excess length of filaments that need to be wound and ensure steady tension.

The ‘winding cycle’ shown in Figure (3-31) is defined as the cycle where the control system will check the tension at the beginning of each cycle and responds accordingly to maintain steady tension. For each ‘winding cycle’, the motor will rotate the package a predetermined number of steps $[n]$, and a synchronised belt will move the winding guide to distribute the yarn over the width of the package.

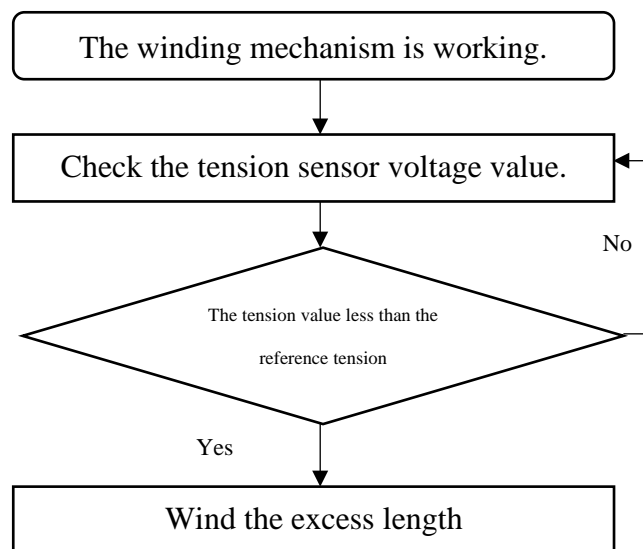


Figure 3-31 The winding cycle algorithm that is used in programming the controller system.

The diagram in Figure (3-32) shows a schematic design of the winding unit. The trans-

mission ratio r between the driving motor and the traverse shaft is calculated by dividing the number of teeth in the pulley fitted on the motor shaft by the number of teeth in the pulley on the traversing mechanism. $r = T_1$

T_2

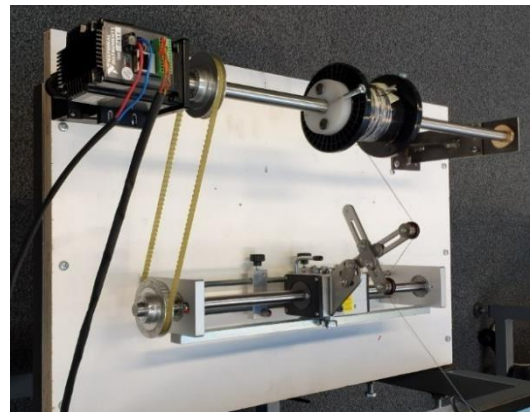
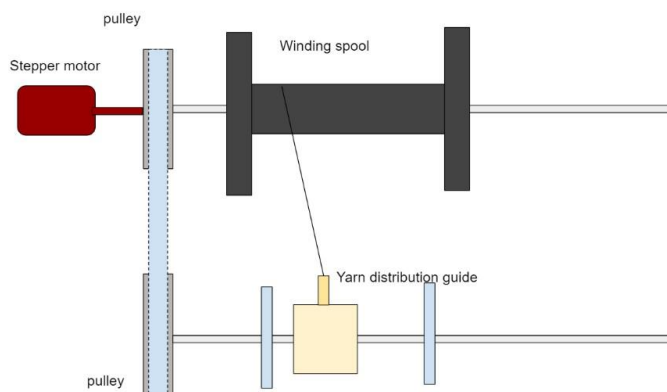


Figure 3-32 Schematic of the winding mechanism where the motor drives the winding spool and belt transfer the power needed to the linear yarn distributor.

The moving parts of the winding mechanism have a precise relationship with each other. During the design stage of this unit, the turns per mm in one layer needed in the final package need to be defined. Here is a definition of the main parameters needed in the design of this mechanism.

d : Wire diameter [mm]

d_m : Micro – pod diameter [mm]

d_p : Package Diameter [mm]

α : Winding angle [degree]

B : The traversing distance for full rotation of the motor driving shaft for transmission ration equal to 1 [mm]

n : Number of steps that the driving motor rotates for each winding cycle.

N : Number of steps for one full rotation of the driving motor shaft.

Following each winding cycle, the winding mechanism will draw a length L_w to be wound, which can be calculated by the following equation.

$$L_w = \sqrt{\Delta D^2 + \Delta T^2} \quad (3.8.1)$$

Where:

ΔT : The traversing length for each winding cycle [mm]

ΔD : The linear distance that the package rotate for each winding cycle [mm]

The winding angle α is defined as the angle between the thread layer on the package and the package axis and is illustrated in Figure (3-33). It can be calculated from the parameters of the design and the setting of the motor steps.

$$\tan \alpha = \frac{\Delta D}{\Delta T} \quad (3.8.2)$$

Where;

$$\Delta D = \pi \cdot d_p \cdot \frac{n}{N}$$

$$\Delta T = r \cdot \frac{n}{N} \cdot B$$

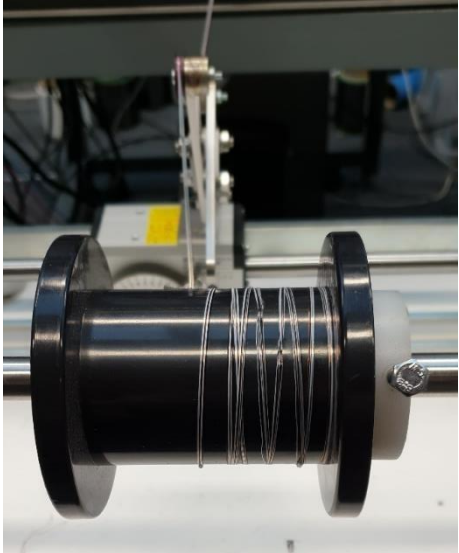
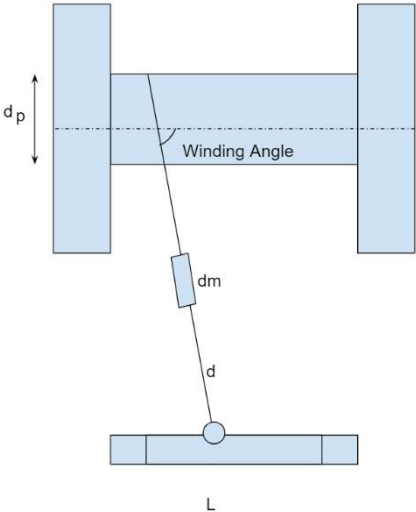


Figure 3-33 The winding angle between the package axis and the yarn.

Thus, the winding angle can be calculated according to the following formula:

$$\tan \alpha = \frac{\pi \cdot d_p}{r \cdot B} \quad (3.8.3)$$

Another critical parameter in the winding process is the wind ratio w which expresses the number of revolutions made by the package while the yarn guide makes a double traverse from one end of the package to another (Koranne and Mhedu, 2016).

$$w = 2 \frac{r \cdot L}{B} \quad (3.8.4)$$

Traverse length L is defined as the distance between extreme positions of a reciprocating thread-guide in one cycle of its movement, and it could be equivalent to the length of the package.

Ribbon is a known phenomenon in the winding of textile yarns in which the yarn wound on the winding package passes through the same yarn path during a certain period of winding. Entanglement of the yarn wound on the package that has ribbon occurred during the winding is more likely. The physical structure of the soldered components and the carrier yarn is sensitive to entanglement, and thus, ribboning needs to be prevented. This condition occurs when the winding ratio becomes an integer value (Durur, 2000). Gain is the angular displacement of the yarn at the beginning of a double traverse with respect to the corresponding position for the previous double traverse. To avoid the ribboning, the new yarn coil should fall slightly to one side or the other of the first coil. The minimum gain is dependent on the diameter of the yarn and the diameter of the bobbin used (Durur, 2000). Figure (3-34) shows a ready package wound by the designed system and has micro-pods encapsulated by the system.



Figure 3-34 Core structure of the EFY wound on the final package and ready for the next stage.

The accuracy of the driving and winding mechanism has been verified to ensure that the take-off roller and the winding mechanism would lead to a repetitive distance that can be used to control the distance between micro-pods. The mechanism was programmed using LabVIEW code to create a dummy micro-pod, each 20 mm. One hundred and fifty micro-pods were created with a cycle step of one hundred steps/cycle. Later the distance between each adjacent micro-pod was measured, and the histogram was plotted as shown in Figure (3-35).

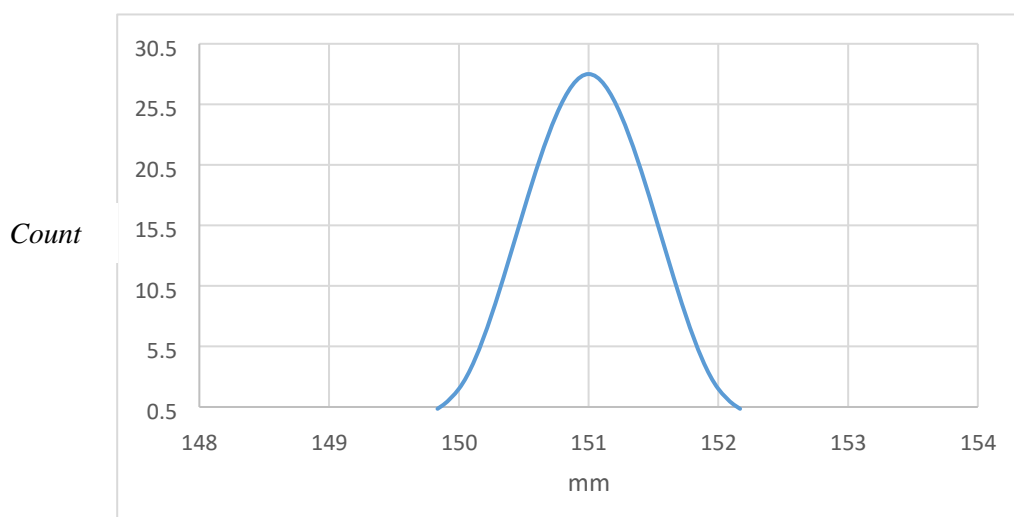


Figure 3-35 Histogram of the distance between the micro-pods when the program created equally spaces samples in 20mm.

3.9 Conclusion

This chapter detailed a novel method to encapsulate electronic components on flexible wire. This chapter shows an automated encapsulation mechanism design where copper wire

and a carrier yarn were fed through a sensor into a mould, and encapsulation was conducted at the point. The requirements for each component of the system are detailed in this chapter. The System design has been evaluated and assessed on different electronic components, such as package LEDs, resistors, and thermistors.

The designed mechanism did show the automation of the encapsulation process where repetitive micro-pods are created with no bubbles or cracks. Although many technologies have been tested for the detection process, further investigation is needed to improve the detection system's reliability and accuracy.

Chapter .4 Stress distribution analysis in the core structure of the Electronically Functional Yarn (EFY)

4.1 Introduction

The proposed approach to creating the core structure of electronically functional yarn (EFY) protects the soldered electronic component against mechanical stresses by applying a resin micro-pod covering the component and the solder joints. Tensile tests and wash trials have shown that debonding and peeling off LEDs, soldered onto a thin copper wire, tends to be the primary failure mode of the EFY, as shown in Figure (4-1). Moreover, copper wire breakage at the micro-pod and copper wire interface was observed where the copper wire had broken at the end of a micro-pod. Thus, stresses applied to solder joints need to be studied to understand this failure mechanism and minimise this breakage.

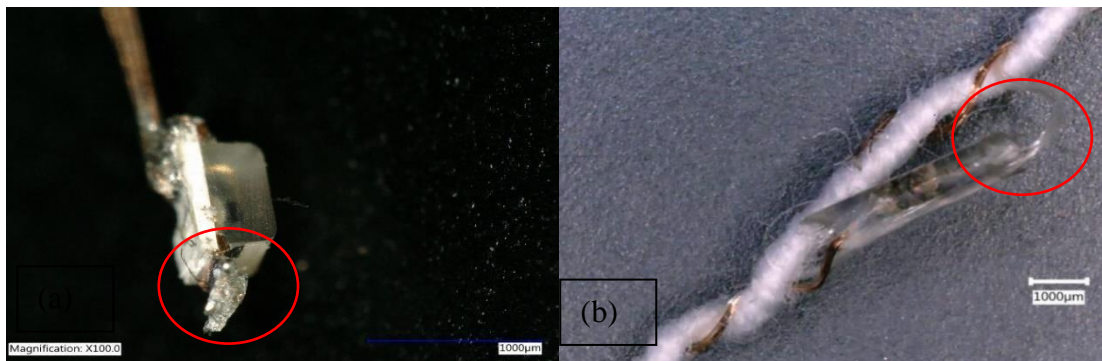


Figure 4-1 Failure mode of soldered LED under tension. (a) The debonding of solder pads on a component under axial loads of bare soldered components. (b) The copper wire is broken at the interface between the micro-pod and the wire from a complete EFY.

The soldered electronic component is the element that needs to be protected to ensure the final wearable electronics reliability. Soldered element encapsulation will add mechanical strength to the weak solder joints. The strengthened structures must be designed appropriately to avoid any premature failures and obtain sufficient strengthening effects after the encapsulation. A model capable of predicting the mechanical stress on the system and how the micropod affects mechanical stresses' transmission has yet to be developed.

Static analysis is a helpful tool to understand the mechanical properties of physical models. Stress, strain, and deformation of the core structure of the EFY can be investigated for different micro-pod designs to avoid failures at the design stage.

This chapter will discuss *the effect of adding a resin micro-pod around a component soldered onto a thin copper wire on the mechanical stress transferred to the component and the micro-pod influence on the failure mechanisms*. The study will help to understand how the micro-pod will support the solder joints and increase their durability. It will evaluate the influence of both the micro-pod resin material and the length of the micro-pod. Finally, the work will discuss the influence of adding carrier yarn and introduce the concept of a multicarrier yarn structure developed in the encapsulation unit.

4.2 Stresses transferred to the solder joints of the electronic components before encapsulation

Different designs of E-yarn will use components with different geometries. The number and positioning of copper wires used in the core structure of the E-yarn will also vary depending on the soldered component (Hughes-Riley & Dias, 2018; Lugoda et al., 2018; Satharasinghe et al., 2018, 2020). A different layout would lead to a different distribution of mechanical stresses. However, in this project, all samples assessed had the same geometry (relevant to commonly used components such as LEDs and thermistors) where the bonding structure is similar to the one known as a 'Single-Lap Joint' (Han et al., 2014), as shown in Figure (4-2).

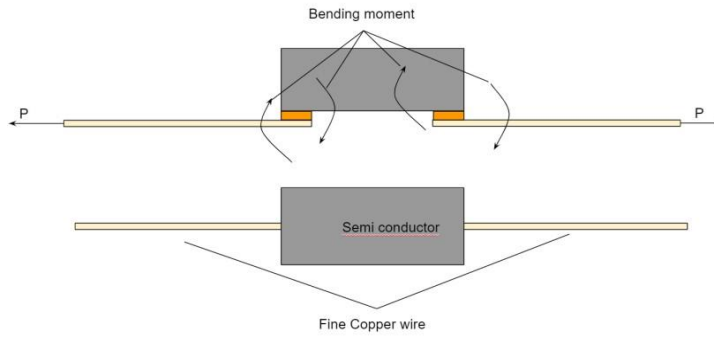


Figure 4-2 The geometry of the soldered semi-conductor before encapsulation, known as single-lap joint under axial loads P and the resulting bending moments.

The single-lap joint structure is used for assessing the shear strength of adhesives (Harris & Adams, 1984). There have been many studies to evaluate stress transfer in the layer of both the adhesive and adherend materials (Cheng & Taheri, 2006).

The analytical models for adhesively bonded lap joints are widely used for single and double-lap Joints (da Silva et al., 2008, 2009). The two-dimensional model is sufficient because stresses in the width direction are significantly lower than in the direction of the loading.

The inclusion of material non-linearity makes the solution too complex. Thus, a linear elastic for both adherence and adhesive is used to simplify the model. Theoretically, The adhesive shear stress (τ) is constant over the overlap length and is given by equation (4.1)

$$\tau = \frac{T}{b \cdot l} \quad (4.1)$$

Where T is the applied load, b is the joint width, and l is the overlap length.

One of the earliest analyses of a single-lap joint was Goland and Reissner's analysis which considered the effect of bending moment resulting from the eccentric load path of a single-lap joint. The joint will rotate, altering the direction of the load line with the tendency of the applied tensile forces to come into line, as shown in Figure (4-2) and Figure (4-3). As the joint rotates, the bending moment will decrease, giving rise to a non-linear geometric problem where the effects of the large deflections of the adherence must be accounted for (Changt & Muki, 1974; da Silva et al., 2008). The bending moment considered in this analysis may

analytically explain the solder pads debonding during axial loading of the core structure before encapsulation.

The mechanical loads transferred into the solder joints due to axial loads would result in shear stresses and bending moments that would lead to debonding of the solder pads of the component (Gustafsson, 2008).

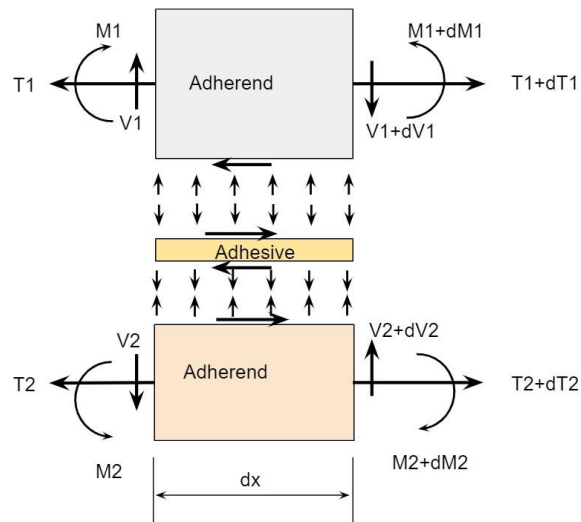


Figure 4-3 Stresses distribution between the adherend and the adhesive layer in single-lap joints and the resulted shear and bending stresses due to axial force inspired by (Gustafsson 2008).

Previous research, such as Chen and Cheng (Chen & Cheng, 1983), shows that the peak shear stresses occur near the joint ends. While others like Allman (Allman, 1977) showed that the distance at which the peak adhesive shear stress occurs from the joint ends would depend on the relative flexibility between the adherence and the adhesive. Chen and Cheng (Chen & Cheng, 1983) confirmed that the peak shear stress in the adhesive is at a distance of 20% of the adherend thickness.

Empirical results were obtained using Zwick Z2.5 Tensile tester (Zwick Roell Group, Ulm, Germany) to evaluate the physical properties of the core structure. The test was conducted on soldered LEDs (50mm copper wire length, test speed 200mm/min) to get the mechanical properties. Results showed a failure of the soldered LEDs at 3 N. Test results are presented in appendixes (7).

Stresses distribution in the single-lap joint; can be obtained by a finite element analysis (FEA) or a closed-form model (da Silva et al., 2009). The analysis setup in FEA objectives re to apply appropriate loads and boundary conditions under suitable assumptions. The analysis setup will result in a close representation of the physics of the system of interest. A simplified geometry model was designed using 3D CAD software 'Autodesk Inventor (Autodesk, Mill Valley, California, USA). The 3D model shown in Figure (4-4) presents a soldered component (0.5x0.5x1.0mm) soldered onto a copper wire has a diameter of 0.2mm. These dimensions were selected to stand for soldered LED on a thin copper wire.

This model was then used for finite element static analysis using 'Ansys workbench 19' and 'Ansys workbench 2021R1' (Ansys, Inc, Canonsburg, Pennsylvania, USA). Static analysis was conducted to analyse the stress distribution in the single-lap joint of the electronic component soldered onto thin copper wires.

The following assumption was considered for the simplified 3D model.

- The thickness of the soldering joints was neglectable compared to the size of the components and the wire.
- The copper wire is uniform, and the physical properties of both the electronic component and the wire are homogenous.
- The load applied in the modelling is axial to the copper wire, and boundaries restrict the deformation in the other direction.

The meshing of the model was selected to be program-controlled, and the transition is to be slow. The load was applied as [3] N on one side of the copper, while the other end was fixed using the 'fix support' option. Cylindrical support is added to the copper wire to prevent the bending resulting from the bending moment. The cylindrical support would fix the radial and tangential direction deformation and allow the deformation in an axial direction.

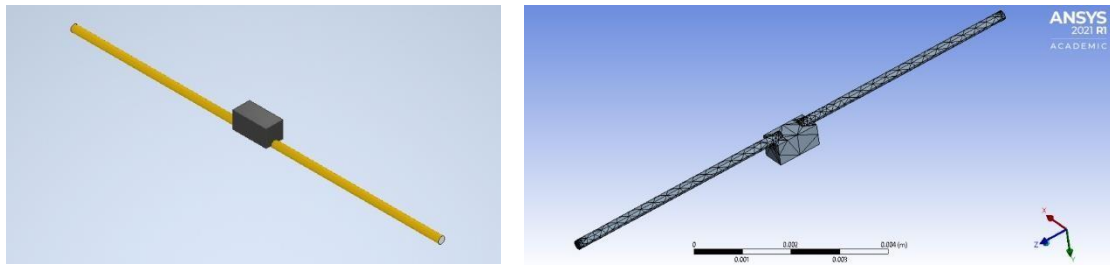


Figure 4-4 The 3D model of the soldered components in Autodesk Inventor to the left and in Ansys after meshing to the right.

The conducted static analysis calculated the overall stresses at each element based on the von-mises criterion, shear stresses in an XZ direction, the highest stress in one of the principal directions at each element, and the highest shear stress at each element by plotting Mohr's circles at each element, using the principal stresses.

Looking at the analysis results, the maximum shear stress was near the solder joint ends. The stresses at that point will be evaluated in this study by changing the parameters of the micro-pod and will investigate how adding the resin would affect the stress at the solder joints area. The analysis results are shown in Figure (4-5), where a section was made in the core structure to show the distribution of stresses. The analysis shows the point of interest where there is the maximum equivalent stress and maximum shear stress.

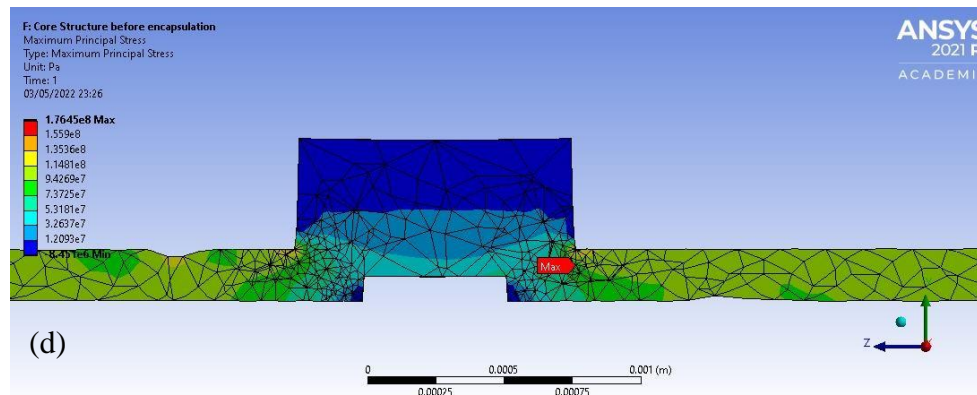
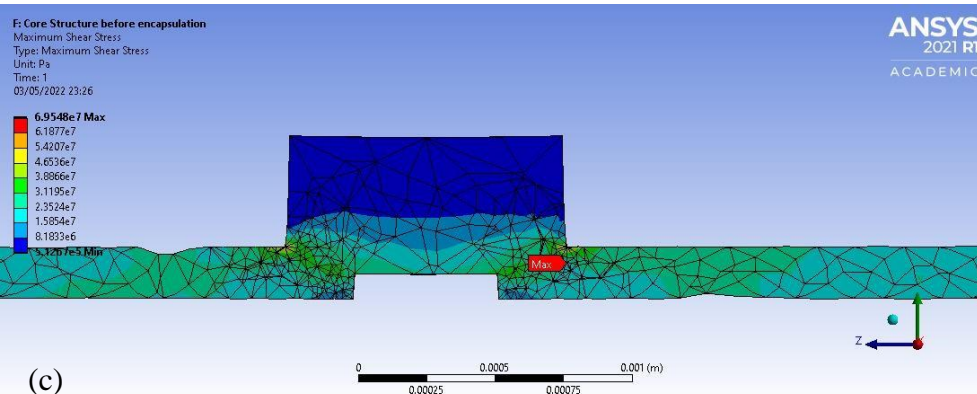
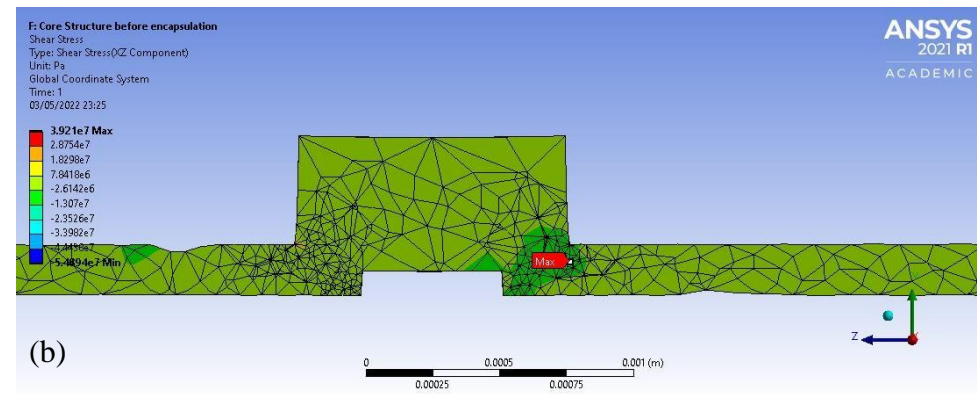
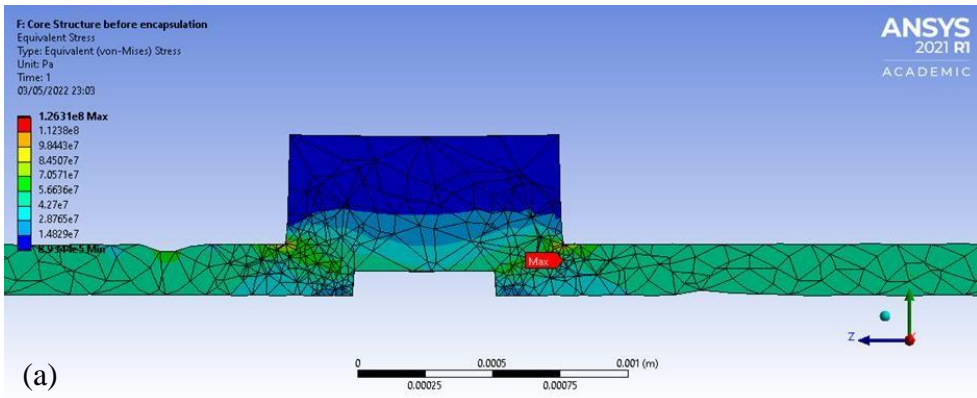


Figure 4-5 The resulting finite element analysis for the core structure of the electronically functional yarn before the encapsulation (a) equivalent stresses, (b) shear stresses in the direction of XZ, (c) maximum shear stress, (d) maximum principal stresses

4.3 Stress distribution following the encapsulation process.

Adding the resin micro-pod to the single-lap joint structure resulting from the soldering process will change the distribution of stresses in the matrix. Resistance to debonding is theoretically a function of the fibre-matrix interfacial bond, the strength of the bonding materials, and the interfacial bond area (Gray, 1984; Hutchinson & Jensen, 1990). In the case of soldering electronic components onto a wire, failure of the interfacial bonds occurs when the shear strength of the structure is reached (DiFrancia et al., 1996).

In this modelling, we assume the bonding between the material and the adhesive is perfect, and no separation occurs under loading. Thus, the contact was selected to be 'bonded' in the setting of Ansys.

Tensile tests have been conducted on an encapsulated semi-conductor to evaluate the strength added to the core structure after adding the resin without a carrier yarn. Previous work was carried out to evaluate the micro-pods impact on the core structure strength (S. Rathnayake, 2015); however, the encapsulation was assessed with a carrier yarn of polyester with no mention in that work of the pre-tension setting or the boundary conditions at the ends of the core structure. The previous experiment shows an improvement in the strength of manually soldered components with 7strands copper wire from 0.23 [N] to around 1[N] after the encapsulation (S.Rathnayake, 2015).

The test was conducted in this study without a carrier yarn to evaluate the micro-pods added value regardless of the carrier yarn's influence on the structure, as shown in Figure (46). The results of these tests were added to appendixes (7). These results showed that failure occurred after encapsulation at 3.5 N when encapsulated by a 3mm length of resin micro-pod using Dymax 9001v3.5. The results show an increase in core structure strength of the EFY by 16% compared to the tenacity before the encapsulation.

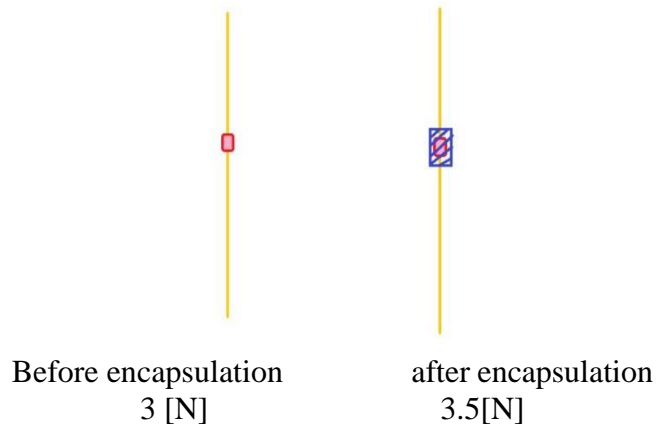


Figure4-6 A schematic illustration of the tensile test conducted to evaluate the tenacity of the core structure before and after the encapsulation without carrier yarn.

Static finite element analysis was conducted using 'Ansys workbench 2021R'. The 3D model used in this modelling after encapsulation is presented in Figure (4-7). The settings tree is shown in Figure (4-8). This analysis would understand the stress's distribution and concentration inside and outside the micro-pod.

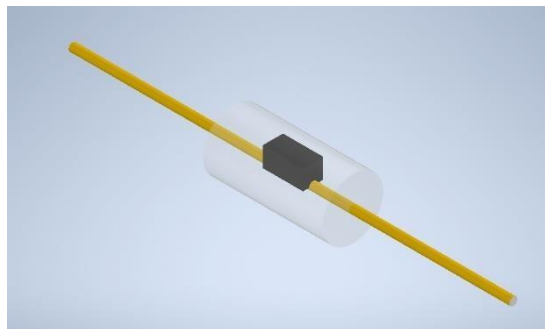


Figure 4-7 The 3D model prepared using Autodesk Inventor for the core structure after encapsulation without carrier yarn.

While the Materials used in this study for the soldered components and the wire were the same as in the earlier model, the micro-pod resin (Dymax 9001 v3.5) mechanical properties were selected from the manufacturer datasheet and presented in Table (4-2). Meshing settings were chosen to be program-controlled with a soft transition. The setting of the meshing is shown in Appendix (8)

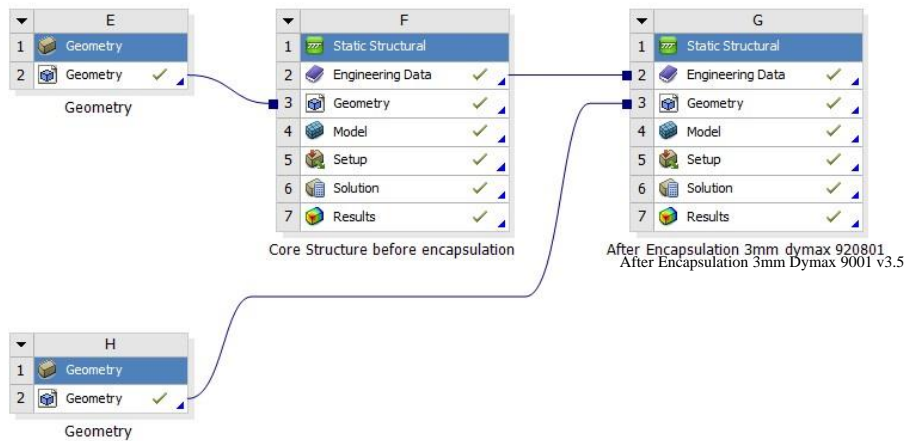


Figure 4-8 The analysis tree in Ansys for the core structure before and after the encapsulation.

The model showed that adding the resin reduced the maximum stress that the solder joints of the structure were subjected to, as shown in Figure (4-9). Moreover, It can be seen from Table (4-1) that the simulation showed that adding the resin would lead to a reduction in the equivalent stresses transferred to the solder joints by 6.85%, in comparison to the stresses before encapsulation, while the maximum shear stresses were similarly reduced by 6.7%. These results are in-line with the imperial tests that showed an increase in the total strength due to adding the resin micro-pod.

Table 4-1 Comparison between modelling results before and after encapsulation with Dymax 9001 v3.5 for a 3mm long resin micro-pod.

	Core structure Before encapsulation	After encapsulation by Dymax 9001v3.5 for 3mm length	Reduction percentage
Equivalent stresses	1.2631 X10 ⁸ [Pa]	1.176 X10 ⁸ [Pa]	6.85%
XZ shear stresses	3.921 X10 ⁷ [Pa]	3.943X10 ⁷ [Pa]	-0.5%
Maximum shear stresses	6.954X10 ⁷ [Pa]	6.483X10 ⁷ [Pa]	6.7%
Maximum principal stresses	1.764 X10 ⁸ [Pa]	1.748X10 ⁸ [Pa]	0.89%

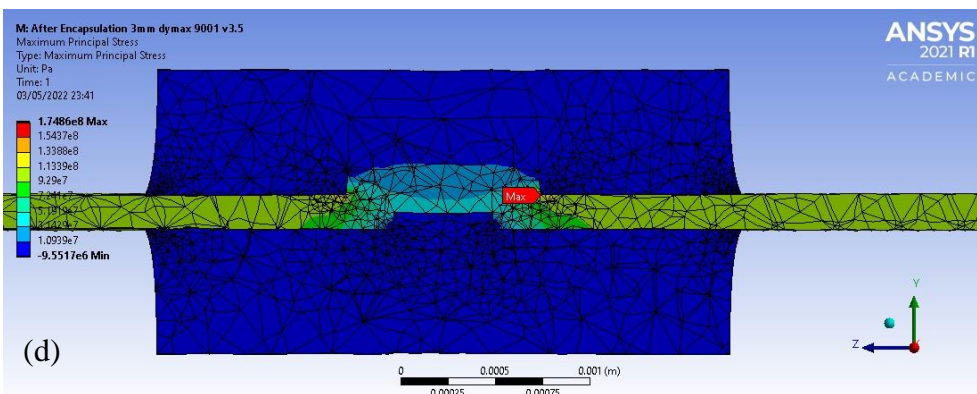
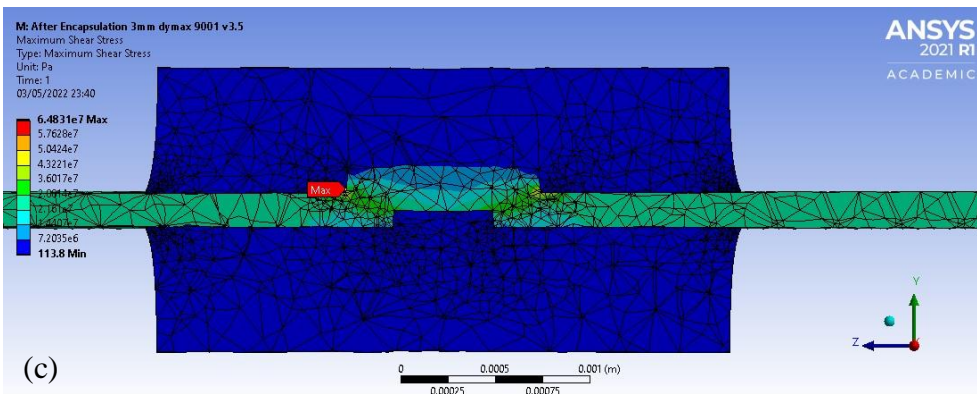
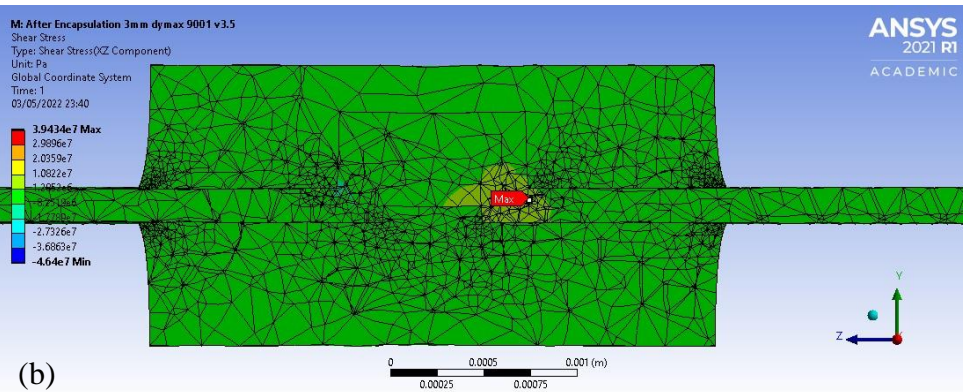
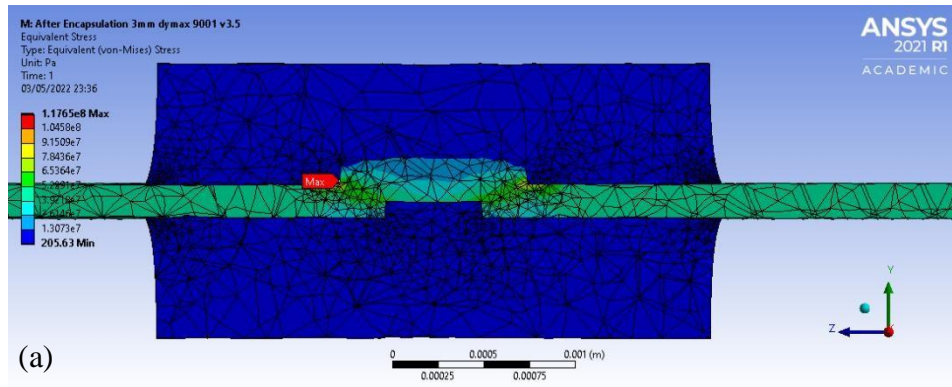


Figure4-9 The finite element analysis of the core structure after encapsulation by Dymax 9001 v3.5 for 3mm long micro-pod (a) equivalent stresses, (b) shear stresses in the XZ direction, (c) maximum shear stress for each element, (d) maximum principal stresses for each element.

4.4 The influence of resin characteristics on the mechanical properties

The mechanical properties of the resin used to create the micro-pod are a potential parameter that influences the mechanical properties of the core structure. UV curable resins have a wide range of mechanical properties that might affect the final micro-pod reliability and how it would protect the soldered electronic component. The modulus elasticity influence on the stresses transferred into the solder joints is investigated in this part of the thesis.

The material used in the model to evaluate the micro-pod influence has been changed in this study. The mechanical properties of different commercially available resins have been used to change the micro-pod material in the model and evaluate the stress distribution inside the micro-pod and the interface between the copper wire and the semi-conductor. Table (4-2) below shows the properties of the resin used in this analysis as reported in the manufacturer datasheets. The resin selected is UV curable Acrylated urethane and supplied by Dymax (Torrington, Connecticut, USA).

Table 4-2 The mechanical properties of commercial Dymax resins as stated in their datasheet.

Commercial Label	Tensile Strength	Modulus of Elasticity	Elongation at break
9001 v3.5	5 MPa	17 MPa	150%
920801	14MPa	760MPa	150%
9037	5.8MPa	6.2MPa	110%
OP-29 Gel	24MPa	200MPa	80%
429	21.6MPa	67MPa	120%
3094-T-rev-A	698MPa	14MPa	184%
3069-VT	17MPa	170MPa	175%

The model used had the same geometry and boundary conditions as Figure (4-7). The length of the micro-pod selected for this part of the study was [3] mm, while the boundary conditions restricted non-axial deflections. The load applied in this model was [3] N. Results

shown in Table (4-3), and Table (4-4) are for selected resins and the corresponding reduction in the stresses. The entire model results for each resin type are presented in Appendix (8).

Table 4-3 The changes in the mechanical stress transferred into the solder joints for different resin types.

Commercial Label	Equivalent Stresses X10⁸	XZ shear stresses X10⁷	Maximum Shear stresses X10⁷	Maximum principal shear stress X10⁸
9001 v3.5	1.1765	3.943	6.483	1.748
920801	0.998	3.348	5.493	1.490
9037	1.179	3.953	6.499	1.752
OP-29 Gel	1.127	3.781	6.212	1.678
429	1.163	3.898	6.407	1.728
3094-T-rev-A	1.177	3.946	6.487	1.749
3069-VT	1.135	3.807	6.255	1.689

The results presented in Table (4-4) of this finite element static analysis showed that the modulus of elasticity impacted the stresses transferred to the soldered joints. The higher the modulus of elasticity, the higher the reduction in the mechanical stress. However, it is essential to note that the bonding properties of the resin have not been discussed in this chapter.

Table 4-4 The reduction in the stresses transferred into the soldered joints after encapsulation for each resin.

Commercial Label	Equivalent Stresses	XZ shear stresses	Maximum Shear stresses	Maximum principal shear stresses
9001 v3.5	6.8%	-0.5%	6.7%	8.9%
920801	21%	14.6%	21%	15.5%
9037	6.6%	-0.8%	6.5%	-0.6%
OP-29 Gel	10.7%	3.5%	10.7%	4.8%
429	7.9%	-0.58%	7.88%	3.5%
3094-T-rev-A	6.7%	-0.6%	6.7%	-0.8%
3069-VT	10%	2.8%	10%	4.2%

4.5 Influence of the Length of the micro-pod on the stress distribution

One major factor of encapsulation is the length of the micro-pod. From a design point of view, the length of the micro-pod should be more than the length of the soldered components. Thus, the solder joints will be protected by the layer of the resin. However, the influence of the length on the mechanical properties of the micro-pod has not been investigated. In this part of this chapter, a brief static finite element analysis to investigate the change in the stress distribution inside the micro-pod for different lengths of micro-pods has been investigated. A 3D model was prepared using Autodesk inventor for different lengths of micro-pod to investigate the length of the micro-pod. The length selected for this model is [3mm, 5mm, and 7mm]. The material selected for this analysis is Dymax 920801, which showed the highest modulus of elasticity shown in Table (4-2).

The setting of the analysis in Ansys is shown in Figure (4-10). Mesh setting and boundaries condition are kept to the exact details presented in Appendix (8).

The analysis showed that the wire and resin contact length impact the maximum shear stresses in the soldered joints. The longer the micro-pod, the more protection is introduced to the solder joints, as shown in Table (4-5). Full modelling results are presented in Appendix (8).

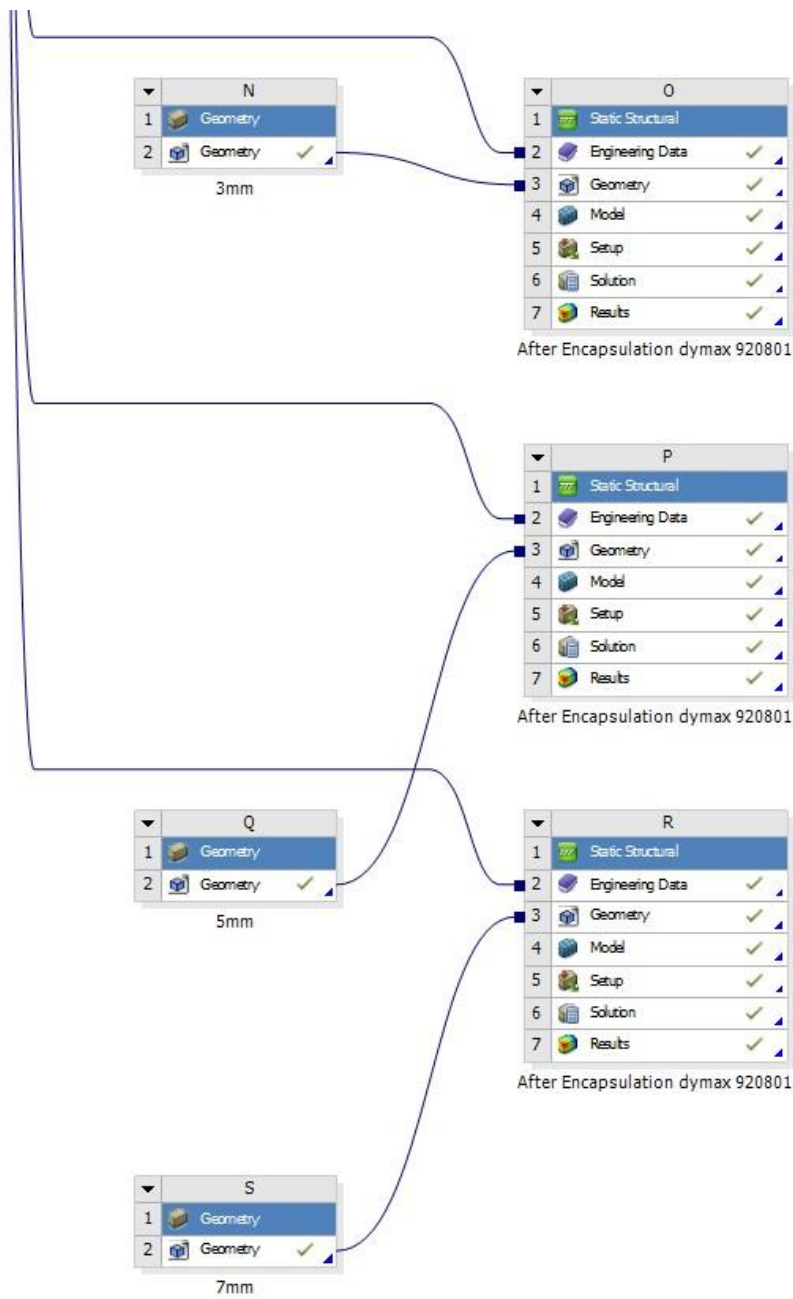


Figure 4-10 The setting tree in Ansys used for static analysis modelling the different lengths of micro-pod

Table 4-5 the mechanical stress simulated for different lengths of micro-pod for resin Dymax 920801

	Equivalent Stresses	YZ shear stresses	Maximum Shear stresses	Maximum principal shear stresses
Before encapsulation	1.2631X10 ⁸	3.921 X10 ⁷	6.954X10 ⁷	1.764 X10 ⁸
3[mm] micro-pod	0.978 X10 ⁸	4.13 X10 ⁷	5.38 X10 ⁷	1.47 X10 ⁸
Reduction in stresses	22.6%	-5.3%	22.6%	16.6%
5[mm] micro-pod	0.88X10 ⁸	3.38 X10 ⁷	4.89X 10 ⁷	1.32 X10 ⁸
Reduction in stresses	30.3%	13.8%	29.7%	25.2%
7[mm] micro-pod	0.823 X10 ⁸	3.45 X10 ⁷	4.532 X10 ⁷	1.2 X10 ⁸
Reduction in stresses	34.8%	12%	34.8%	31.9%

4.6 Carrier yarn influences on stress inside the micro-pod

The multi-carrier yarn was proposed to avoid the sudden change in the cross-section of the core structure. The multi-carrier yarns were introduced to give the micro-pod homogenous structure and avoid the rapid change in the side section of the core structure when using one carrier yarn.

The advantage of the multi-carrier method is that we can get rid of the packing yarns needed in the warp knitting stage, where the multi-carrier yarn used in this method fills the space inside the sleeve and replaces the packing yarns. Moreover, the core structure is more homogenous and consistent as the rapid change in the cross-section of the core structure is avoided. Figure (4-11) shows the schematic of the single carrier yarn and multi-carrier yarn methods.

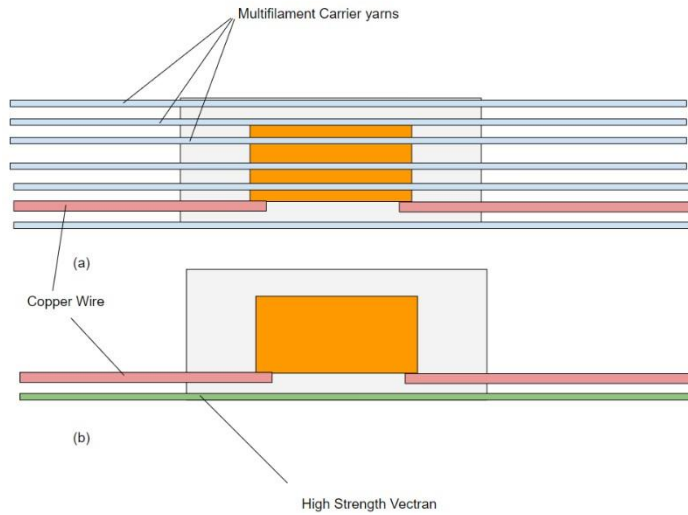


Figure 4-11 (a) multi carrier yarn core structure that have textile filament distributed inside the micro-pod. (b) single carrier yarn shows a rapid change in the cross section of the core structure.

Another advantage is bridging crack surfaces with strong, intact fibres in a zone behind the crack. That would improve the strength of the composite structure (Hsueh & Lu, 1989) and increase the bonding between the cured resin and the filaments.

Static Finite Element Analysis is conducted using Ansys 2021R to evaluate the influence of adding a carrier yarn to the micro-pod. The 3D model of the micro-pod with a carrier yarn is shown in Figure (4-12).

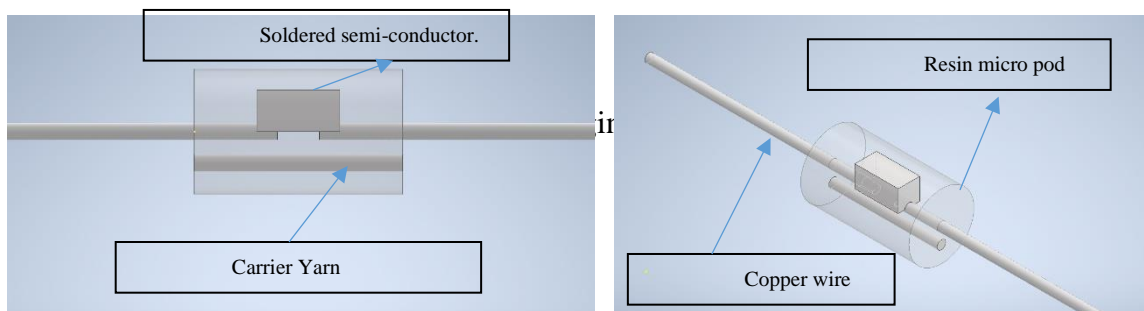


Figure 4-12 Side view and isometric view of the 3D model prepared for the Finite element analysis.

Figure (4-13) shows stresses transferred to the solder joints from axial loads 3 [N] for a 3mm micro-pod with one polyester carrier yarn embedded in the micro-pod at 0.375mm from the centre of the cross-section. The analysis could not be applied to the multi-carrier model as the number of nodes needed for meshing exceeds the student account limits. Results in Table

(4-6) shows that adding a carrier yarn would support the matrix and reduces the mechanical stress transferred into the solder joints.

Table 4-6 The mechanical stress simulated for with and without carrier for micropod of Dymax 920801 resin

	Equivalent Stresses	Maximum Shear stresses	Maximum principal shear stresses
Encapsulated without Carrier	1.01 X10 ⁸	5.59 X10 ⁷	1.5X10 ⁸
Encapsulated with one polyester carrier	0.82 X10 ⁸	4.5 X10 ⁷	1.23 X10 ⁸
Change	18.8%	19.5%	18%

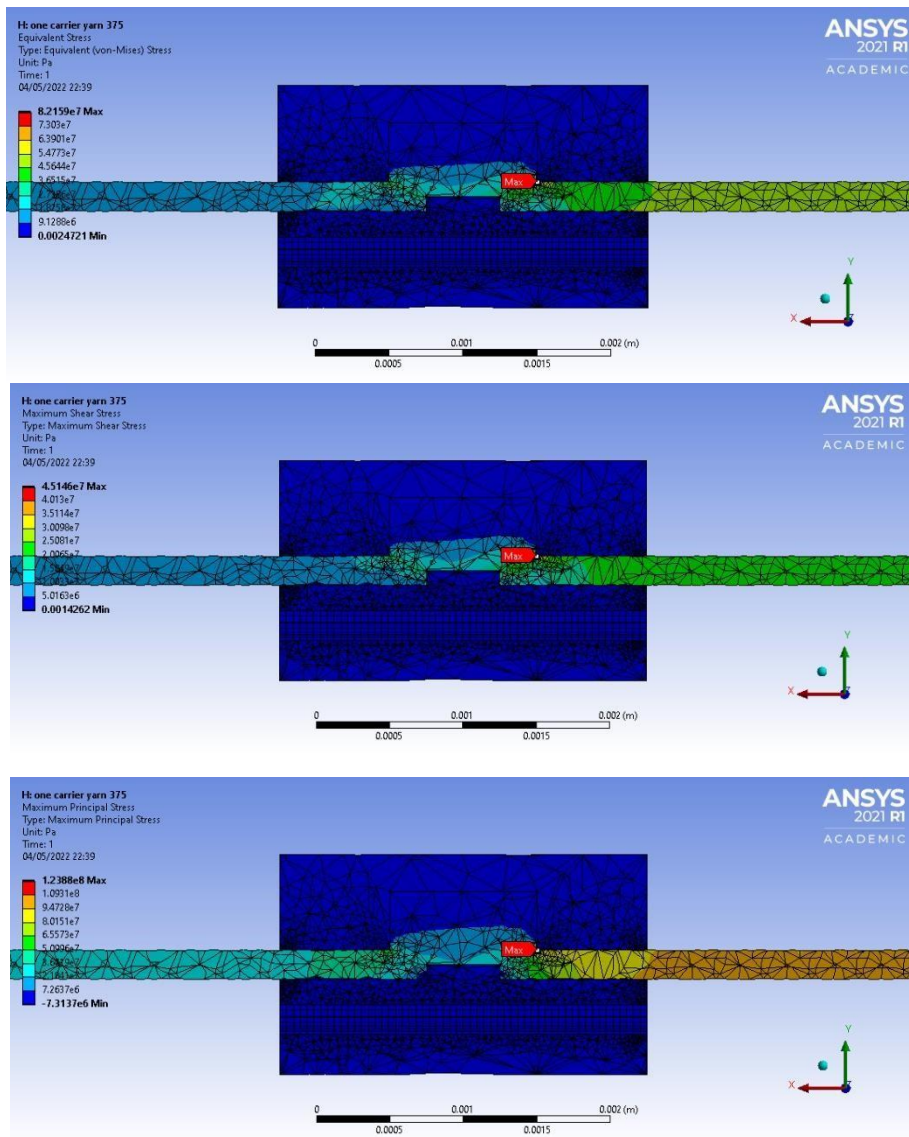


Figure 4-13 The finite element analysis of the core structure after encapsulation by Dymax 920801 for 3mm long micro-pod with a carrier yarn (a) equivalent stress, (b) maximum shear stress for each element, (d) the maximum principal stresses for each element.

A few alterations were made to the design of the encapsulation unit to apply the multicarrier yarn method. The new alteration is shown in Figure (4-14). The new design included a guide for eight textile yarns that are fed into the mould. Simultaneously, the copper wire with the soldered semi-conductor is fed from the centre of the guide ring. Thus, the carrier textile yarns are surrounding the electronic component and form a homogenous micro-pod. Figure (415) shows a semi-conductor encapsulated by the encapsulation unit with eight polyester carrier yarn.

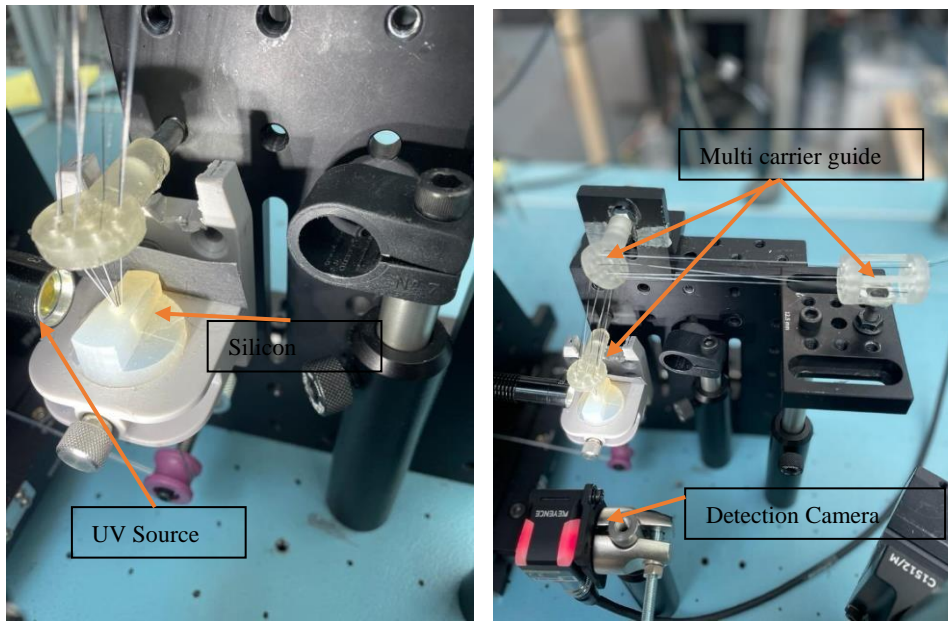


Figure 4-14 The alteration made to the design to add the multi-carrier method encapsulation to the design of the encapsulation unit.

4.7 Conclusion

The maximum shear stress distribution in the geometry of the soldered joints before and after the encapsulation by resin showed that adding the resin reduced the maximum stress transferred into the soldered joints. At the same time, the analysis showed that using a resin that had a higher modulus of elasticity would reduce the transferred mechanical stresses and that the length of the micro-pod would increase the durability of the resulting core structure.

The carrier yarn impacts the reliability of the solder joints and the multi-carrier yarn method introduced. The encapsulation unit was modified to reflect the advancement of this approach.

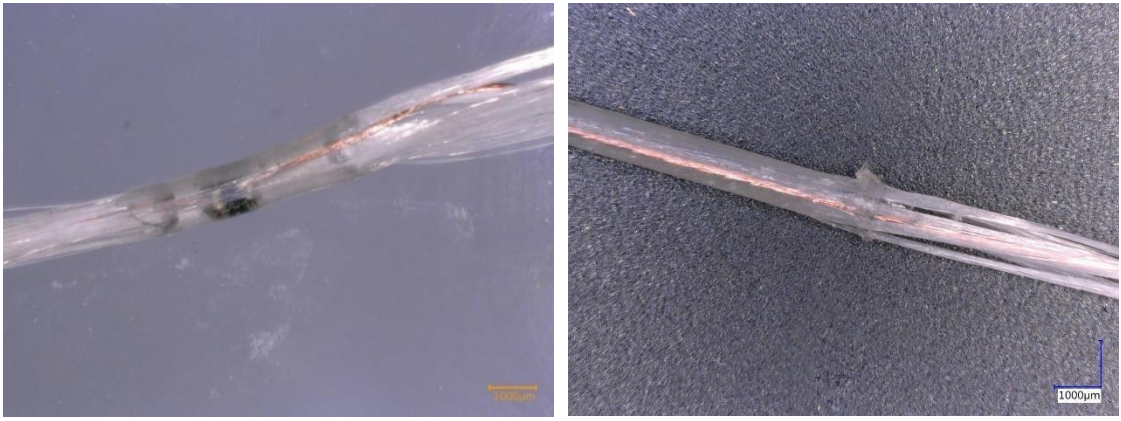


Figure 4-15 multi-carrier micro-pod encapsulated using the automated encapsulation unit.

Chapter .5 Conclusion and future work

5.1 Summary and Conclusion

A method for automating the encapsulating process of soldered electronic components was introduced and developed in this project. The automation of the E-yarn encapsulation process increased the speed of production of EFYs. The automated prototype encapsulation unit described in this work offered a substantial improvement over the manual process where the encapsulation process can be completed within previously used to produce EFY. Thus, it enabled fast, repeated encapsulation of electronics soldered to copper wire.

Silicon and PTFE tube moulds were selected to form the cylindrical resin micro-pods. The mould material was then evaluated for its suitability for the intended application, and a study of the resistance of the mould to de-mould the cured resin micro-pod and the UV absorbance of the rubber used in the mould design was conducted. The resin was selected based on the curing method and the time for curing, which was evaluated using FTIR. The resin dispenser and the curing method were evaluated as well. A winding mechanism to wind the copper wire firmaments populated with components and micro-pods was also developed, as this was needed to make the encapsulation unit standalone.

Finite element analysis was conducted using Ansys to understand the distribution of mechanical stresses inside the micro-pod and evaluate the micro-pod's influence on the transfer of stress into the soldered joints. The resulting model helped improve the encapsulation unit's design to create E-yarns with improved durability.

The encapsulation unit has subsequently been improved to avoid technical problems identified during testing and validated by trials to produce electronically functional yarns with different electronics.

Appendixes have been added after this chapter for more details regarding electrical wiring, LabView codes, calculations of the internal diameter of the warp-knitted sleeve, tension sensor calibration, buckling of the core structure phenomena, earlier designs used for the

encapsulation unit, an evaluation of the encapsulation unit on Kapton strips with electronic components, and the mechanical properties of some materials used in this project for completeness.

5.2 Contribution to knowledge

This thesis contributed to knowledge in the fields of E-textiles and manufacturing and filled the following gaps in knowledge:

- Introduced a critical analysis of the literature on protecting electronics embedded in E-textiles.
- A novel design for the automated encapsulation of components soldered onto copper wires has been constructed and tested.
- Parameters that influence the encapsulation components soldered onto copper wires were investigated.
- The stress distribution on a component soldered onto a copper wire before and after encapsulation was analysed and understood.
- Production of prototype yarns using the designed encapsulation unit was achieved.

5.3 Future Work

The encapsulation unit designed and constructed in this project is suitable for automated encapsulation of semiconductors that had been soldered onto the wire(s). Further improvement to the design can lead to an *improvement in the speed of manufacturing, reliability of the micropods*, increase in the *variety of electronic components that can be embedded*, and improve the *reliability of the process itself*.

The automated encapsulation unit was designed as a standalone unit where the manual transfer of the E-yarn from one stage of the process to the next was needed. Packages of partially completed E-yarn were passed between sets of machinery (soldering, encapsulating,

covering). The automation of the production process for each stage separately increased the speed of production of EFY compared to a manual process. The automated process can complete a micro-pod within less than 45 seconds, while the manual needs a lot more time than this. Automating the transfer of incomplete E-yarns from one to the next would further increase the speed of the manufacturing process of EFYs and would further remove the need for human intervention. Tensioners and feeders will be required for delivery regulation during the integration of the three stages to ensure optimal delivery at each stage of the production process.

A solution could be achieved by having the soldering and encapsulation applied at the same point to avoid the need for a detection system later. This would require an integration of the two-stage into one manufacturing process.

The encapsulation process had challenges in detecting the soldered semiconductor. In this research, we tested a variety of sensors and techniques for detection. Using a camera detector showed a promising error range and can be improved by isolating the ambient light and integrating a machine-learning algorithm to process the images and detect the existence of the electronic components with better reliability.

The design of the encapsulation unit was based on using one Vectran yarn embedded in the resin matrix to enhance the mechanical properties of the micro-pod and add protection to the semiconductors. However, this design was later improved to a set of Polyester yarn embedded on the circumference of the micro-pod. Further research must be conducted on the number of carrier yarns to be used and their physical properties to reduce the mechanical stress that can be transferred to the soldered joints of the electronic components.

Another development would be integrating electronics with a package size smaller than 0402, which was used in this research. Smaller electronics would lead to fine yarn with less change in the cross-section and less stress concentration on the solder joints. To achieve this improvement would be needed both the soldering and the encapsulation units.

Incorporating complex electronic circuits into a yarn can be achieved using flexible Kapton strips as a substrate. This would require longer micro-pods with a larger diameter. The outer surface of this micro-pod would lead to higher forces when removing it from the mould, which may exceed the strength of the carrier yarn, so further developments of the pulling-off method to reduce the force needed are required.

Possible developments in E-Textiles and garments containing EFYs can now take place in parallel with the developments in the production process. This is likely to lead to the need for new types of E-yarns, where different electronics are embedded for different applications. The thesis concentrated on a specific type of electronics that can be embedded by soldering two solder joints (like LEDs, resistors, Thermistors.) where the final structure is similar to a single lap joint's structure. Other electronics and solder-pad layouts would lead to different structures that need further investigations regarding tension control and stress distribution before and after encapsulation. RFIDs yarns required custom arrangements, and manual intervention to cut the antenna wire to a suitable length is required.

The wire driving and winding mechanism used in this project depended on Arduino UNO microcontrollers. This design was suitable for the prototype to prove the concept; however, it had limitations regarding the speed and the accuracy of positioning the semiconductor inside the mould. This needs to be improved with a more accurate wire feed system in the future.

The material of the mould used has limited the length of the micro-pod that can be created. This research used a commercial non-stick tube that was flexible and showed some resistance to removing the micro-pod from the mould. An idea to prepare the mould from coated transparent glass with PTFE would give the surface non-stick properties while keeping the mould rigid, allowing it to be mounted using traditional mechanical brackets.

The mechanical stress analysis conducted in the fourth chapter could be extended to validate various types of E-yarn (i.e., larger components etc.), and to be applicable to parallel soldering under development by ATRG where the components are soldered onto two separate wires.

The mechanical stress analysis shows that the rapid change in the cross-section of the core structure will lead to the concentration of mechanical stress. Tapered ends could be used to reduce stress concentration. That would increase the reliability of the core structure. Achieving tapered ends needs to be considered from a design point of view regarding the mould design and the encapsulation procedure. Achieving tapered ends on the micro-pod needs redesign of the encapsulation mould and system by using the split mould concept.

Twisting textile yarn around the core structure was proposed in the thesis's appendix to overcome the copper wire's buckling phenomena. The settings and parameters used to accomplish this can be investigated for better covering the final yarn and avoiding the buckling occurrence. This would improve the reliability of the resulting EFY.

The suggested improvements and recommendations for future investigation would increase the speed and the quality of production of EFY and lay the foundations for greater adoption of the technology in various E-Textiles garments.

References

Afroj, S. Et al. (2019) 'Engineering graphene flakes for wearable textile sensors via highly scalable and ultrafast yarn dyeing technique', ACS Nano. American Chemical Society, 13(4), pp. 3847–3857. Doi: 10.1021/acsnano.9b00319.

Arene et al. (2017) 'A method of inserting a wire into a groove of a semi-conductor chip, and equipment for the implementation of such a method.' Available at: <https://patentimages.storage.googleapis.com/af/89/51/8243c23b71ec7a/FR3062515A1.pdf> (Accessed: 17 August 2019).

Allman, D. J. (1977). A Theory for elastic stresses in adhesive-bonded lap joints. *The Quarterly Journal of Mechanics and Applied Mathematics*, 30(4), 415–436. <https://doi.org/10.1093/qjmam/30.4.415>

Amazon.co.uk (n.d) ‘Kingsons Beam Backpack - The most Advanced Solar Power Backpack - Waterproof, Anti- Theft Laptop Bag’. Available at: https://www.amazon.co.uk/Kingsons-Beam-Backpack-Waterproof-Anti-theft/dp/B07L9R76W3/ref=sr_1_fkmr0_1?Creativeasin=B06XWX335C&dchild=1&imprToken=qmctpk4kn0y1kajkenntzq&keywords=Lifepack+Solar+Powered+and+Anti-Theft+Backpack+with+laptop+storage&linkcode=g13. (Accesses 2nd May 2022).

Andia Vera Gianfranco, & Emmanuel, A. (2017). Device for reception emission radiofrequency (Patent No.FR3065579A1).<https://patentimages.storage.googleapis.com/6f/c6/0e/8e1daae149818aFR3065579A1.pdf>

Bernard Bancal (2018) E-thread technology: a revolutionary toolkit to embed electronics at the heart of everyday objects Leti Innovation Days. Available at: www.primo1d.com (Accessed: 14 August 2019).

Boyd, R. H. And Phillips, P. J. (1993) *The Science of Polymer Molecules*. Cambridge: Cambridge University Press (Cambridge Solid State Science Series). Doi: 10.1017/CBO9780511600326.

Bretterbauer, K. Et al. (2013) ‘UV-curable coatings of highly crosslinked trimethylmelamine based acrylates and methacrylates’, *European Polymer Journal*. Elsevier Ltd, 49(12), pp. 4141–4148. Doi: 10.1016/j.eurpolymj.2013.09.020.

Cao, Y., Smith; P. And Heeger, A. J. (1993) ‘processable form of electrically conductive polyaniline (19)’. The USA.

Chan, M. Et al. (2012) ‘Smart wearable systems: Current status and future challenges’, *Artificial Intelligence in Medicine*. Elsevier, 56(3), pp. 137–156. Doi: 10.1016/J.ARTMED.2012.09.003.

Changt, D. 1, & Muki, R. (1974). Stress distribution in a lap Joint under tension-shear. In *International Journal of Solids and Structures* (Vol. 10). Pergamon Press. [https://doi.org/10.1016/0020-7683\(74\)90055-9](https://doi.org/10.1016/0020-7683(74)90055-9)

Chen, D., & Cheng, S. (1983). An analysis of adhesive-bonded single-lap joints. *Journal of*

- Applied Mechanics, Transactions ASME, 50(1), 109–115. <https://doi.org/10.1115/1.3166976>
- Cheng, J., & Taheri, F. (2006). A smart single-lap adhesive joint integrated with partially distributed piezoelectric patches. *International Journal of Solids and Structures*, 43(5), 1079–1092. <https://doi.org/10.1016/j.ijsolstr.2005.04.020>
- Chiang, C. K. Et al. (1977) ‘Electrical conductivity in doped polyacetylene’, *Physical Review letters*, 24(12), pp. 7380–7382. Doi: 10.1103/physrevb.24.7380.
- Cho, G., Lee, S. And Cho, J. (2009) ‘Review and reappraisal of smart clothing’, *International Journal of Human-Computer Interaction*. Taylor & Francis Group, 25(6), pp. 582–617. Doi: 10.1080/10447310902997744.
- Costa, J. C. Et al. (2019) ‘Flexible Sensors From Materials to Applications’, *Technologies*, 7(35), pp. 1–83. Doi: 10.3390/technologies7020035.
- Curone, D. Et al. (2007) ‘Smart garments for safety improvement of emergency/disaster operators’, *Annual International Conference of the IEEE Engineering in Medicine and Biology - Proceedings*, pp. 3962–3965. Doi: 10.1109/IEMBS.2007.4353201.
- Cutecircuit (2020) Galaxy dresss. Available at: <https://cutecircuit.com/> (Accessed: 13 April 2020).
- Da Silva, et al. (2008). Closed-form solutions for adhesively bonded joints Two-dimensional linear elastic analyses. 1938, 1–32.
- Da Silva, et al. (2009). Analytical models of adhesively bonded joints-Part I: Literature survey. *International Journal of Adhesion and Adhesives*, 29, 319-33-. <https://doi.org/10.1016/j.ijadhadh.2008.06.005>
- Decker, C. (2001) ‘Contributed papers UV-radiation curing chemistry’, *Pigment and Resin Technology*, 30(5), pp. 278–286. Doi: 10.1108/03699420110404593.
- De Vries, H. And Peerlings, R. (2014) ‘Predicting conducting yarn failure in woven electronic textiles’, *Microelectronics Reliability*, 54(12), pp. 2956–2960.
- Dias, T., & S. Rathnayake, A. (2016). Patent WO2016/038342 A1 Electronically functional yarns (Patent No. WO2016/038342 A1; GB2529900B1).
- Dias, T., & Fernando, A. (2010). Operative devices installed in yarns (Patent No. WO 2006/123133).

Dias, et al. (2006). Switches in textile structures (Patent No. US 2009/0026056A1).

Diffrancia, et al. (1996). The single-fibre pull-out test. 1: Review and interpretation. *Composites Part A: Applied Science and Manufacturing*, 27 (8 PART A), 597–612. [https://doi.org/10.1016/1359-835X\(95\)00069-E](https://doi.org/10.1016/1359-835X(95)00069-E)

Diz, E. L., & Spragg, R. (2011). Analysis of UV- Curable Resins by FT-IR.

Domskienė, J. And Strazdienė, E. (2005) ‘Investigation of fabric shear behaviour’, *Fibres & Textiles In Eastern Europe*, 13(2), p. 50. Available at: http://www.fibtex.lodz.pl/50_08_26.pdf (Accessed: 13 May 2019).

Durur, G. (2000). Cross Winding of Yarn Packages (Issue July). University of Leeds.

Dymax Corporation. (2009). Multi-Cure® 9001-E-V3.5 Resilient, Clear Encapsulant. [Www.dymax.com](http://www.dymax.com)

Ericsson, A. And niketech. (n.d.). Pasta Platform for advanced smart textile applications. [online] Available at: <https://www.youtube.com/watch?V=v14tfm4fgi8> [Accessed 3 May 2022].

Fink, Y. And Rein, M. (2018) ‘Thermally Drawn fibre including devices’, US Patent 10,509,186. Available at: <https://patentimages.storage.googleapis.com/40/d0/29/92c0c66552f22a/WO2018022856A1.pdf> (Accessed: 31 July 2019).

Fuloon (2020) Fuloon 16 LED Light Up Safety visibility vest with reflective stripes. Available at: <https://www.amazon.co.uk/Fuloon-Safety-Visibility-Reflective-Stripes/dp/B00BMLAB7S> (Accessed: 20 June 2020).

Gianfranco Andia Vera (2018) ‘Patch antenna for coupling a transmitting/receiving terminal to a RFID device’. Available at: <https://patentimages.storage.googleapis.com/a8/0f/09/374c726afbb7ec/WO2019025683A1.pdf> (Accessed: 17 August 2019).

Google (2015) Jacquard by Google. Available at: <https://atap.google.com/jacquard/> (Accessed: 28 April 2021).

- Gopalsamy, C. Et al. (1999) 'The wearable motherboard: The first generation of adaptive and responsive textile structures (ARTS) for medical applications', *Virtual Reality*, 4(3), pp. 152–168. Doi: 10.1007/BF01418152.
- Gray, R. J. (1984). Analysis of the effect of embedded fibre length on fibre debonding and pullout from an elastic matrix - Part 1 Review of theories. In *Journal of Materials Science* (Vol. 19, Issue 3, pp. 861–870). Kluwer Academic Publishers. <https://doi.org/10.1007/BF00540456>
- Gustafsson, J. (2008). Stress equations for 2D lap Joints with a compliant elastic bond layer. [Http://www.byggmek.lth.se](http://www.byggmek.lth.se)
- Hardy, D. Et al. (2018) 'An automated process for inclusion of package dies and circuitry within a textile yarn', in *Symposium on Design, Test, Integration and Packaging of MEMS/MOEMS, DTIP 2018*. Doi: 10.1109/DTIP.2018.8394189.
- Hardy, D. Et al. (2018) 'Engineering a costume for performance using illuminated LED-yarns', *Fibers*, 6(2), p. 35. Doi: 10.3390/fib6020035.
- Hardy, D. A. Et al. (2019) 'Automated insertion of package dies onto wire and into a textile yarn sheath', *Microsystem Technologies*. Doi: 10.1007/s00542-019-04361-y.
- Harris, J. A., & Adams, R. A. (1984). Strength prediction of bonded single lap joints by nonlinear finite element methods. *International Journal of Adhesion and Adhesives*, 4(2), 65–78. [https://doi.org/10.1016/0143-7496\(84\)90103-9](https://doi.org/10.1016/0143-7496(84)90103-9)
- Harms, H. Et a. (2008) 'SMASH: A Distributed Sensing and Processing Garment for the Classification of Upper Body Postures', in *ICST 3rd international conference on Body area networks*, p. Article No. 22. Available at: <https://pdfs.semanticscholar.org/db8a/13d6156a19f7a501cd4df58fea249f39a0ff.pdf> (Accessed: 19 January 2019).
- Han, X., et al (2014). The strength prediction of adhesive single lap joints exposed to long term loading in a hostile environment. *International Journal of Adhesion and Adhesives*, 55, 1–11. <https://doi.org/10.1016/J.IJADHADH.2014.06.013>
- Hayward, J. (2019) *E-Textiles 2019-2029: Technologies, Markets and Players A comprehensive review of materials, processes, components, products and markets*. Available at: <https://www.idtechex.com/en/research-report/e-textiles-2019-2029-technologies-marketsand-players/671>.

- Hebberling, F. (1969) 'The Maximum Wind Angle in Winding of Textile Packages', *Textile Research Journal*, 39(9), pp. 799–808. Doi: 10.1177/004051756903900901.
- Heeger, A. J. (2010) 'Semiconducting polymers: The Third Generation', *Chemical Society Reviews*, 39(7), pp. 2354–2371. Doi: 10.1039/b914956m.
- Hefter, M. (1910) 'Knitted electric heating body.' Available at: <https://patents.google.com/patent/US975359A/en> (Accessed: 16 February 2019).
- Henkel. (2019). Printed Circuit Board Protection. [Henkel-adhesives.com/electronicstechnomelt-simply3.com](https://www.henkel-adhesives.com/electronicstechnomelt-simply3.com)
- Hideki Shirakawa et al. (1977) Synthesis of Electrically Conducting Organic Polymers: Halogen Derivatives of Polyacetylene, (CH). Available at: <https://pubs.rsc.org/en/content/articlepdf/1977/c3/c39770000578> (Accessed: 16 February 2019).
- Higgins, M. (2016) Understanding Ultraviolet LED Wavelength. Available at: <https://uvebtech.com/articles/2016/understanding-ultraviolet-led-wavelength/> (Accessed: 20 January 2020).
- Hsueh, C. H., & Lu, M. C. (1989). Elastic stress transfer from fiber to coating in a fiber-coating system. *Materials Science and Engineering A*, 117(C), 115–123. [https://doi.org/10.1016/0921-5093\(89\)90092-0](https://doi.org/10.1016/0921-5093(89)90092-0)
- Hutchinson, J. W., & Jensen, H. M. (1990). Models of fiber debonding and pullout in brittle composites with friction. *Mechanics of Materials*, 9(2), 139–163. [https://doi.org/10.1016/0167-6636\(90\)90037-G](https://doi.org/10.1016/0167-6636(90)90037-G)
- Hughes-Riley, T. Et al. (2017) 'A Study of Thermistor Performance within a Textile Structure', *Sensors*, 17(8), p. 1804. Doi: 10.3390/s17081804.
- Hughes-Riley, T. And Dias, T. (2018) 'Developing an Acoustic Sensing Yarn for Health Surveillance in a Military Setting', *Sensors*. Multidisciplinary Digital Publishing Institute, 18(5), p. 1590. Doi: 10.3390/s18051590.
- Ilanchezhiyan, P. Et al. (2015) 'Highly efficient CNT functionalised cotton fabrics for flexible/wearable heating applications', *RSC Advances*, 5(14), pp. 10697–10702. Doi: 10.1039/c4ra10667a.
- Jeon, J. W. Et al. (2018) 'Pyroprotein-based electronic textiles with high thermal durability', *Materials Today*. Elsevier Ltd, 21(9), pp. 944–950. Doi: 10.1016/j.mattod.2018.03.038.

- De Jonckneere, J. Et al. (2007) 'OFSETH: Optical fibre embedded into technical textile for healthcare, an efficient way to monitor patient under magnetic resonance imaging', Annual International Conference of the IEEE Engineering in Medicine and Biology - Proceedings, pp. 3950–3953. Doi: 10.1109/IEMBS.2007.4353198.
- Jutila, M. Et al. (2014) 'Implementation of a wearable sensor vest for the safety and well-being of children', *Procedia Computer Science*, 32, pp. 888–893. Doi: 10.1016/j.procs.2014.05.507.
- Karim, N. Et al. (2017) 'Scalable Production of Graphene-Based Wearable E-Textiles', *ACS Nano*. American Chemical Society, 11(12), pp. 12266–12275. Doi: 10.1021/acsnano.7b05921.
- Kim, D.-H. Et al. (2008) 'Materials and noncoplanar mesh designs for integrated circuits with linear elastic responses to extreme mechanical deformations.', *Proceedings of the National Academy of Sciences of the United States of America*. National Academy of Sciences, 105(48), pp. 18675–80. Doi: 10.1073/pnas.0807476105.
- Klaassen, B. Et al. (2015) 'A full body sensing system for monitoring stroke patients in a home environment', *Communications in Computer and Information Science*, 511(January), pp. 378–393. Doi: 10.1007/978-3-319-26129-4_25.
- Köhler, A. R., Hilty, L. M. And Bakker, C. (2011) 'Prospective Impacts of Electronic Textiles on Recycling and Disposal', *Journal of Industrial Ecology*, 15(4), pp. 496–511. Doi: 10.1111/j.1530-9290.2011.00358.x.
- De Kok, M. Et al. (2015) 'Failure modes of conducting yarns in electronic-textile applications', *Textile Research Journal*, 85(16). Doi: 10.1177/0040517515573405.
- Komolafe, A. Et al. (2019) 'Integrating Flexible Filament Circuits for E-Textile Applications', *Advanced Materials Technologies*, 4(7). Doi: 10.1002/admt.201900176.
- Koranne, M. V. And Mhedu, K. (2016) 'Suitable traverse ratios for step precision winding', *Fashion and Textiles*. Springer Singapore, 3(1), pp. 1–8. Doi: 10.1186/s40691-016-0062-0.
- Kwong, D., Sumanochitraporn, N. And Kaewpirom, S. (2011a) 'Curing behavior of a UVcurable coating based on urethane acrylate oligomer: the influence of reactive monomers', 33(2), pp. 201–207.
- Kunwong, D., Sumanochitraporn, N. And Kaewpirom, S. (2011b) 'Curing behavior of a UVcurable coating based on urethane acrylate oligomer: The influence of reactive monomers', *Songklanakarin Journal of Science and Technology*, 33(2), pp. 201–207.

- Langenhove, L. Van (2007) 'Types of smart medical textile', in Langenhove, L. Van (ed.) *Smart Textiles for Medicine and Healthcare: Materials, Systems and Applications*, pp. 1–25. Available at: <http://scholar.google.com/scholar?hl=en&btnq=Search&q=intitle:No+Title#0>.
- Leaders, M. (2020) LED-T-Shirts. Available at: <https://www.led-t-shirts.eu/> (Accessed: 20 June 2020).
- Levi's (2019) jacquardtm By Google | Levi's® GB Gb. Available at: https://www.levi.com/GB/en_GB/jacquard-by-google/c/levi_collections_google_jacquard (Accessed: 28 April 2021).
- Li, M. (2018) *Electronic Packaging for Functional Electronic Textiles*. Southampton University. Doi: 10.1016/0041-2678(70)90288-5.
- Li, M., et al. (2018) 'Stress Analysis and Optimisation of a Flip Chip on Flex Electronic Packaging Method for Functional Electronic Textiles', *IEEE Transactions on Components, Packaging and Manufacturing Technology*, 8(2), pp. 186–194. Doi: 10.1109/TCPMT.2017.2780626.
- Li, M., et al. (2018) 'The thickness and material optimisation of flexible electronic packaging for functional electronic textile', in 2018 Symposium on Design, Test, Integration & Packaging of MEMS and MOEMS (DTIP). IEEE, pp. 1–6. Doi: 10.1109/DTIP.2018.8394186.
- Li, M. Et al. (2019) 'Novel electronic packaging method for functional electronic textiles', *IEEE Transactions on Components, Packaging and Manufacturing Technology*, 9(2), pp. 216–225. Doi: 10.1109/TCPMT.2019.2892404.
- Lifeshirt -Vivonoetics (2019). Available at: <https://www.vivosense.com/portfolio/lifeshirt/> (Accessed: 13 May 2019).
- Linz, T. Et al. (2005) 'Embroidering electrical interconnects with conductive yarn for the integration of flexible electronic modules into fabric', *Proceedings - International Symposium on Wearable Computers, ISWC, 2005*, pp. 86–89. Doi: 10.1109/ISWC.2005.19.
- Linz, T. Et al. (2008) 'Embroidered Interconnections and Encapsulation for Electronics in Textiles for Wearable Electronics Applications'. Doi: 10.4028/www.scientific.net/AST.60.85.
- Loriga, G. Et al. (2005) 'A wearable health care system based on knitted integrated sensors', in 2005 IEEE Engineering in Medicine and Biology 27th Annual Conference. IEEE, pp. 7349–7352. Doi: 10.1109/IEMBS.2005.1616209.

- Loriga, G. Et al. (2006) 'Textile sensing interfaces for cardiopulmonary signs monitoring', (February), pp. 7349–7352. Doi: 10.1109/iembs.2005.1616209.
- Lugoda, P., et al. (2018) 'A wearable textile thermograph', *Sensors. Multidisciplinary Digital Publishing Institute*, 18(7), p. 2369. Doi: 10.3390/s18072369.
- Lugoda, P., et al. (2018) 'Developing novel temperature sensing garments for health monitoring applications', *Fibers. Multidisciplinary Digital Publishing Institute*, 6(3), p. 46. Doi: 10.3390/fib6030046.
- Lugoda, P. Et al. (2020) 'Flexible temperature sensor integration into E-Textiles using different industrial yarn fabrication processes', *Sensors (Basel, Switzerland)*, 20(73). Doi: 10.3390/s20010073.
- Lugoda, P., Dias, T. And Morris, R. (2015) 'Electronic Temperature sensing yarn', *Journal of Multidisciplinary Engineering Science Studies (JMESS)*, 1(1), pp. 2912–1309.
- Mattmann, C., Clemens, F. And Tröster, G. (2008) 'Sensor for measuring strain in textile', *Sensors*, 8(6), pp. 3719–3732. Doi: 10.3390/s8063719.
- Mccarthy, B. J. (2015) 'An overview of the technical textiles sector', in Anand, A. R. H. S. C. (ed.) *Handbook of Technical Textiles*. 2nd Editio. Woodhead Publishing.
- Memis, I. And Goh, Y. (2018) 'Electronic packaging materials: properties and selection', *Reference Module in Materials Science and Materials Engineering*, (October 2017), pp. 1–11. Doi: 10.1016/b978-0-12-803581-8.02020-8.
- Minges, M. L. (1989) *Electronic materials handbook: packaging (Vol. 1)*. Boca Raton, Florida: CRC Press.
- Ministryofsupply (2019) Men's mercury intelligent heated jacket. Available at: <https://www.ministryofsupply.com/products/mens-mercury-intelligent-heated-jacket> (Accessed: 20 January 2019).
- Novel manufacturing methods for functional electronic textiles manufacturing electronic Yarns (2020). Available at: <https://e-yarns.com/novel-manufacturing-methods-for-functional-electronic-textiles/> (Accessed: 29 April 2021).
- Ojuroye, O. O. Et al. (2019) 'Embedded capacitive proximity and touch sensing flexible circuit system for electronic textile and wearable systems', *IEEE Sensors Journal*. IEEE, 19(16), pp. 6975–6985. Doi: 10.1109/JSEN.2019.2911561.

Osaka, K. Et al. (2006) 'Cure monitoring of UV polymer by Raman spectroscopy', Proceedings of the 12th U.S.-Japan Conference on Composite Materials, pp. 497–506.

Paradiso, R., Loriga, G. And Taccini, N. (2005) 'A wearable health care system based on knitted integrated sensors', IEEE Transactions on Information Technology in Biomedicine, 9(3), pp. 337–344. Doi: 10.1109/TITB.2005.854512.

Park, S, & Jayaraman, S. (2003) 'Smart Textiles: Wearable electronic Systems', MRS Bulletin, 28(8) (May), pp. 585–591.

Pauline Vandongen (2020) Radius Available at: <http://www.paulinevandongen.nl/project/phototrope/> (Accessed: 20 June 2020).

Pola, T. And Vanhala, J. (2007) 'Textile electrodes in ECG measurement', in Proceedings of the 2007 International Conference on Intelligent Sensors, Sensor Networks and Information Processing, ISSNIP. IEEE, pp. 635–639. Doi: 10.1109/ISSNIP.2007.4496917.

Press, N. A. (1990) Materials for high-density electronic packaging and interconnection, national Materials advisory board commission on engineering and technical systems. Doi: 10.1016/0261-3069(91)90124-m.

Rajoo, R. Et al. (2010) 'Embedding of 15um thin chip and passives in thin flexible substrate', 2010 12th Electronics Packaging Technology Conference, EPTC 2010. IEEE, pp. 489–496. Doi: 10.1109/EPTC.2010.5702689.

Rein, M. Et al. (2018) 'Diode fibres for fabric-based optical communications', Nature. Springer US, 560(7717), pp. 214–218. Doi: 10.1038/s41586-018-0390-x.

Rolland, D. Et al. (2018) 'Method for joining a microelectronic chip to a wire element'. Available at: <https://patentimages.storage.googleapis.com/f1/02/3d/18a9a2456eb50a/WO2018193198A1.pdf> (Accessed: 17 August 2019).

Rothmaier, M., Luong, M. P. And Clemens, F. (2008) 'Textile pressure sensor made of flexible plastic optical fibers', Sensors, 8(7), pp. 4318–4329. Doi: 10.3390/s8074318.

S. Rathnayake, A. (2015) Development of the core technology for the creation of Electronically -Active, Smart Yarn. Nottingham Trent University.

- Satharasinghe, A., Hughes-Riley, T. And Dias, T. (2018) 'Photodiodes embedded within electronic textiles', *Scientific Reports*. Springer US, 8(1), p. 16205. Doi: 10.1038/s41598-01834483-8.
- Satharasinghe, A., Hughes-Riley, T. And Dias, T. (2020) 'An investigation of a wash-durable solar energy harvesting textile', *Progress in Photovoltaics: Research and Applications*. John Wiley and Sons Ltd, 28(6), pp. 578–592. Doi: 10.1002/pip.3229.
- Sholtes, K., Keliher, R. And Linden, K. G. (2019) 'Standardisation of a UV LED Peak Wavelength, Emission Spectrum, and Irradiance Measurement and Comparison Protocol', *Environmental science and technology*, 53, pp. 9755–9763. Doi: 10.1021/acs.est.9b02567.
- Simone, L. K. And Kamper, D. G. (2005) 'Design considerations for a wearable monitor to measure finger posture Finger flexion range of Motion sensors home monitoring'. Doi: 10.1186/1743-0003-2-5.
- Srivastava, A. Et al. (2008) 'UV curable polyurethane acrylate coatings for metal surfaces', *Pigment & Resin Technology*, 37(4), pp. 217–223. Doi: 10.1108/03699420810887843.
- Stoppa, M. Et al. (2014) 'Wearable Electronics and Smart Textiles: A Critical Review', *Sensors*. Multidisciplinary Digital Publishing Institute, 14(7), pp. 11957–11992. Doi: 10.3390/s140711957.
- Stylios, I. J. And G. K. (2013). *Joining Textiles; Principles and applications* (I. Jones & G. K. Stylios (eds.)). Woodhead Publishing Limited.
- Tao, X. Et al. (2017) 'How to make reliable, washable, and wearable textronic devices', *Sensors*. Multidisciplinary Digital Publishing Institute, 17(637). Doi: 10.3390/s17040673.
- Wang, H., Lin, J. And Shen, Z. X. (2016) 'Polyaniline (PANI) based electrode materials for energy storage and conversion', *Journal of Science: Advanced Materials and Devices*. Elsevier, 1(3), pp. 225–255. Doi: 10.1016/J.JSAMD.2016.08.001.
- Wang, Z., Volakis, J. L. And Kiourti, A. (2015) *Embroidered antennas for communication systems*, *Electronic Textiles: Smart Fabrics and Wearable Technology*. Elsevier Ltd. Doi: 10.1016/B978-0-08-100201-8.00011-4.
- Weng, W. Et al. (2016a) 'Smart electronic textiles', *Angewandte Chemie - International Edition*, 55(21), pp. 6140–6169. Doi: 10.1002/anie.201507333.

Weng, W. Et al. (2016b) 'Smart electronic textiles', *Angewandte Chemie - International Edition*, 55(21), pp. 6140–6169. Doi: 10.1002/anie.201507333.

Wudl, F., Kobayashi, M. And Heeger; Alan (1987) 'Polyisothianaphtene, A New Conducting Polymer'.

Xue, P. Et al. (2004) 'Electromechanical behaviour of fibres coated with an electrically conductive polymer', *Textile Research Journal*, 74(10), pp. 929–936. Doi: 10.1177/004051750407401013.

Zeng, W. Et al. (2014) 'Fiber-based wearable electronics: A review of materials, fabrication, devices, and applications', *Advanced Materials*, 26(31), pp. 5310–5336. Doi:10.1002/adma.201400633.

Zysset, C. Et al. (2013) 'Textile integrated sensors and actuators for nearinfrared spectroscopy', *Optical Society of America*, 21(3). Available at:
https://www.osapublishing.org/directpdfaccess/AF06937B-A195-C05F-DB5B99C58C082B55_248887/oe-21-33213.pdf?Da=1&id=248887&seq=0&mobile=no
(Accessed: 19 January 2019).

Appendixes

6.1 Appendix 1: Electrical Wiring of the Encapsulation Unit components

6.1.1 Introduction

The Encapsulation Unit designed and demonstrated earlier in Chapter.3 has many electrically wired components to a control unit. The analogue input, digital input, and digital output port from the Arduino UNO board were used to control all the elements required to achieve one working system that can be monitored and controlled from a PC through the LabVIEW program. LabVIEW code was developed, and each code will be demonstrated individually in Appendix 2.

6.1.2 Stepper motor

The stepper motor used in this project is ISM 7411, which can be controlled either by Ethernet or the pulse/Direction mode. Arduino UNO was used to generate a pulse train and direction signal to control the motor, where the pulse would make the motor rotate one step. The pulses direction determines the steering direction.

Since pulse mode is the traditional way to control steppers, the pulse train generation for the application requires a stepper interface module or PLC. However, Arduino UNO was suitable at this project stage because the design does not require high frequency.

The wiring diagram between the motor Drive and Arduino is shown in the following diagrams where the Step and DIR- are connected to the common point in the Board (GND). Step+ and DIR+ are connected to digital output pins to generate the required steps. It is worth noting that the motor (National instrument NI) supplier offers NI 9512 series C a stepper interface module that is compatible with ISM 7411 for real-time controlling in industrial applications.

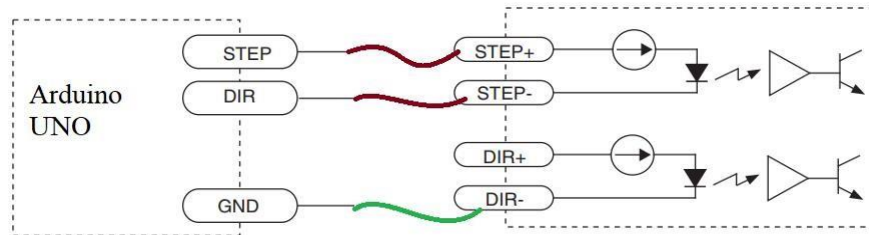
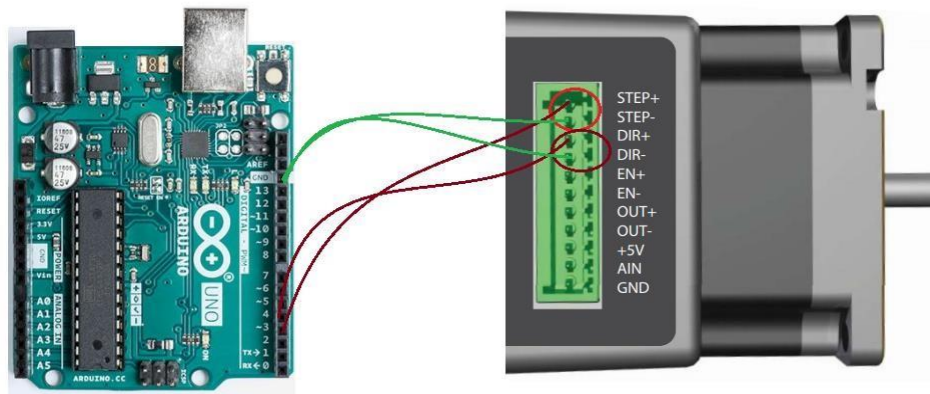


Figure 1 The stepping pin is connected to digital pin 3 in the control card. All negative pin is wired to the GND.

6.1.3 UV curing wiring

The UV source is Bluewave QX4 supplied by Dymax, a footswitch for manual activation with two wires. These two wires were connected to a 5VDC relay. The digital output from Arduino UNO will activate the 5VDC relay to latch and unlatch the footswitch pedal connection presented in Figure (2). It is worth noting that the Bluewave QX4 controller has a PLC output and input pins for external control for future development as shown in Figure (3).

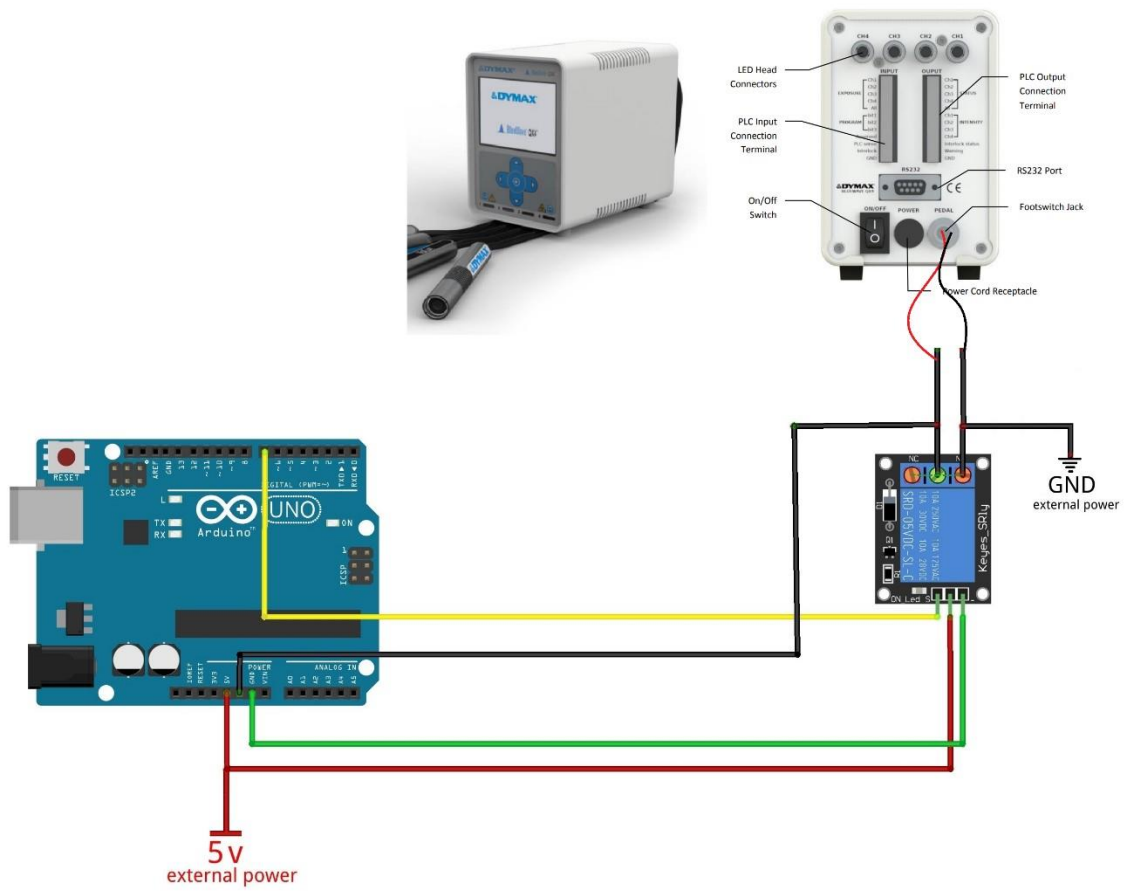


Figure 2 The footswitch connection is wired to digital output pin 7 in the control board.

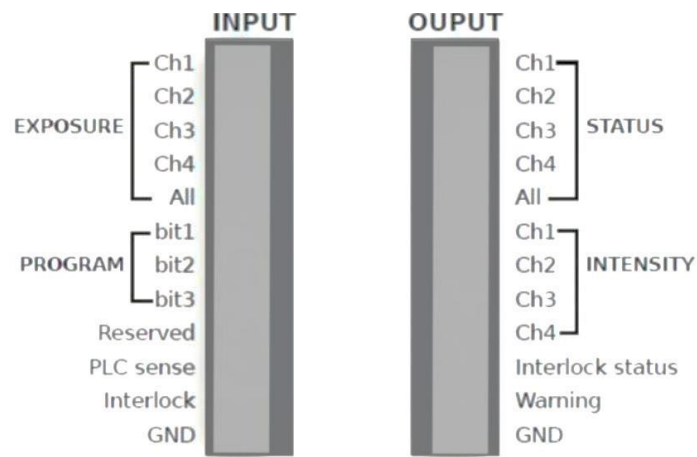


Figure 3 The input and output layout of the QX4 Dymax UV source.

6.1.4 The resin dispenser

There are many methods to control the eco-pen dispenser into Labview, depending on the level of integration needed. However, there is no specific driver for this from NI or Intertronics. There was a need to use either microcontroller or NI PCI cards for automation to generate the signal required. It all depends on the integration level needed. Instead of a footswitch, a relay was used to activate the program and switch it on and off through the microcontroller, as shown in Figure (4).

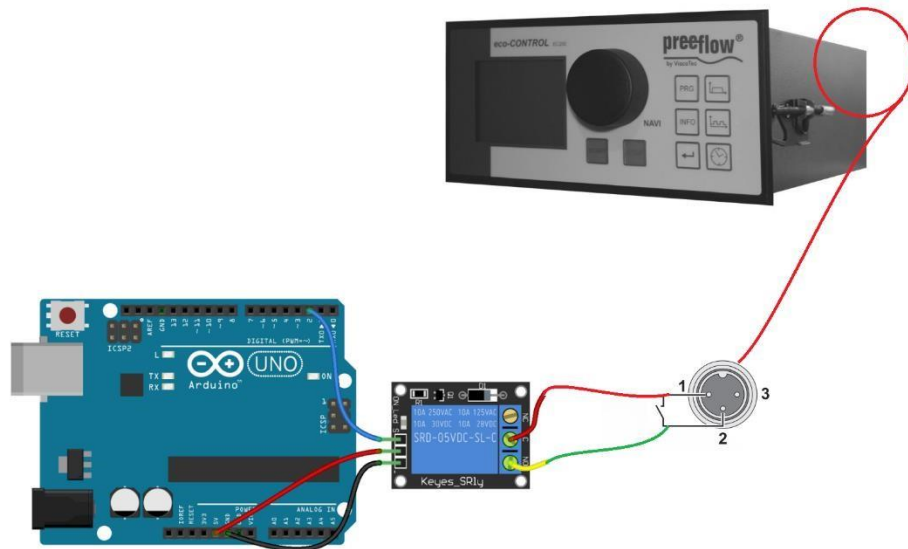


Figure 4 The wiring diagram of the Dispenser system to the microcontroller using a DC relay.

6.1.5 Tension Sensor

The tension sensor used for tension monitoring needs a separate power source (12V), and the analogue signal range generated by the sensor is between 0 and 10V. The analogue output signal needs to be lowered to 5VDC as Arduino Board cannot read a 10VDC analogue signal. Thus, a voltage divider circuit was used with two resistors, each 100 Ohm, to divide the voltage generated by the sensor to be in the range (0-5V). It is critical in this approach to have

a mutual ground for the differential analogue signal and the connected PIN in UNO, as shown in Figure (5).

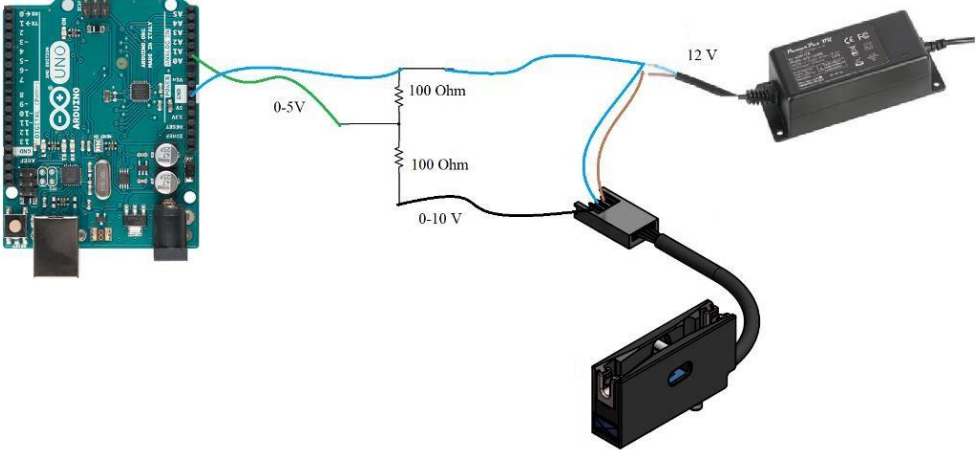


Figure 5 The wiring diagram of the tension sensor to the microcontroller.

6.2 Appendix 2: The LabVIEW Code used for controlling and monitoring the encapsulation unit.

6.2.1 Introduction

LabView is a graphical programming language used in this project to control and monitor the encapsulation system. This appendix will show and describe the LabVIEW codes that were used for controlling the encapsulation unit. The code will control the following components: The stepper motor, the linear stage, the dispenser, the UV curing LED, and the winding system. The encapsulation process is coded in flat sequence code that will operate the components according to the algorithm mentioned earlier in Chapter 3. The code is programmed according to the wiring layout described in Appendix 1.

6.2.2 Initialisation

The first step programmed in the code is initialising the system before running it. The initialisation includes initialising the relays to their normal state, homing the linear stage to the zero position, and defining the Arduino Board used for controlling both stepper motors. The code used for initialisation is grouped outside the while loop, as shown in Figure (6).

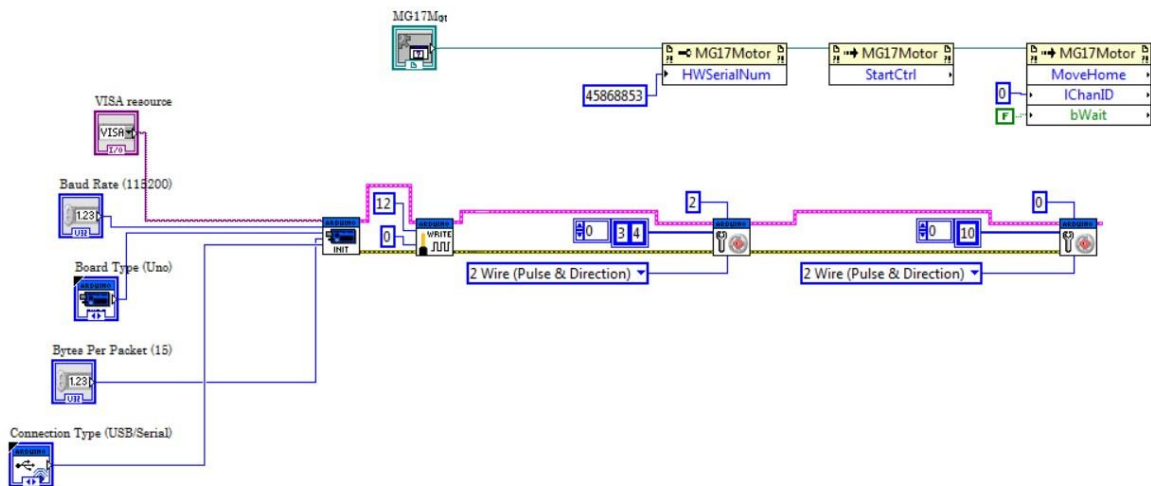


Figure 6 Initialisation Code for the relays and the linear stage in Labview.

6.2.3 The Linear stage

LabVIEW can be used to communicate with any APT-based controller. Active-X technology helped to build a user interface by LabVIEW to control the Linear stage LT-150. The supplier of the linear stage has offered a detailed guide on creating a user interface using LabVIEW for their controllers' which was much appreciated. The linear stage moves in two encapsulation steps, moving down to the encapsulation point to dispense the resin and homing to avoid curing the resin in the dispenser tip. Both codes are shown in the following Figure (7).

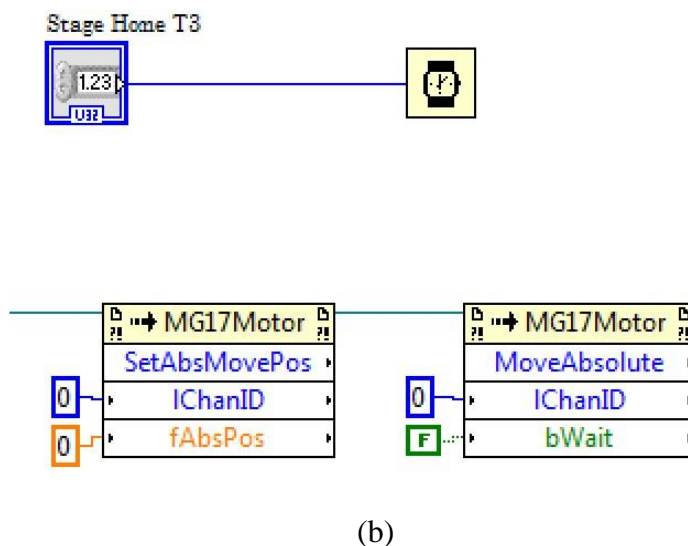
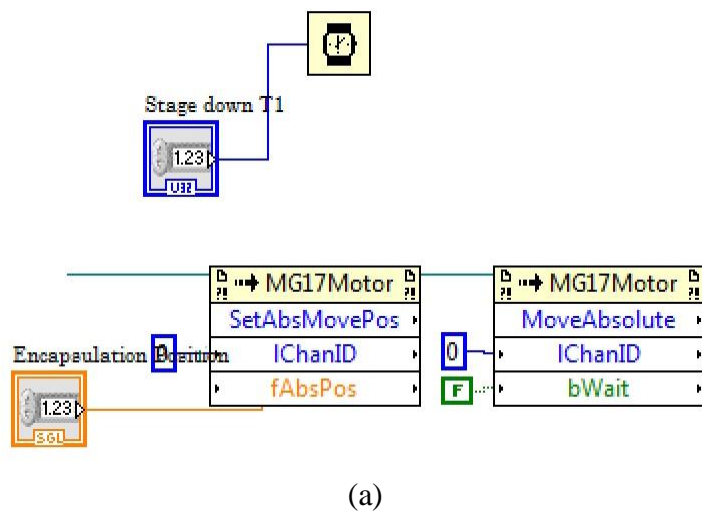


Figure 7 Moving the linear stage at two points in the flat sequence, (a) moving to the encapsulation point, (b) homing after dispensing.

6.2.4 Stepper motor

The stepper motor is controlled at two stages in this code, the encapsulation process and searching for components mode. The operator is required to specify the distance between the encapsulation point and the detection point and the distance required for each detection cycle. This distance is then interpreted into stepper steps or entered the system as several steps. The code shown in Figure (8) shows the control for the driving motor labelled no.2.

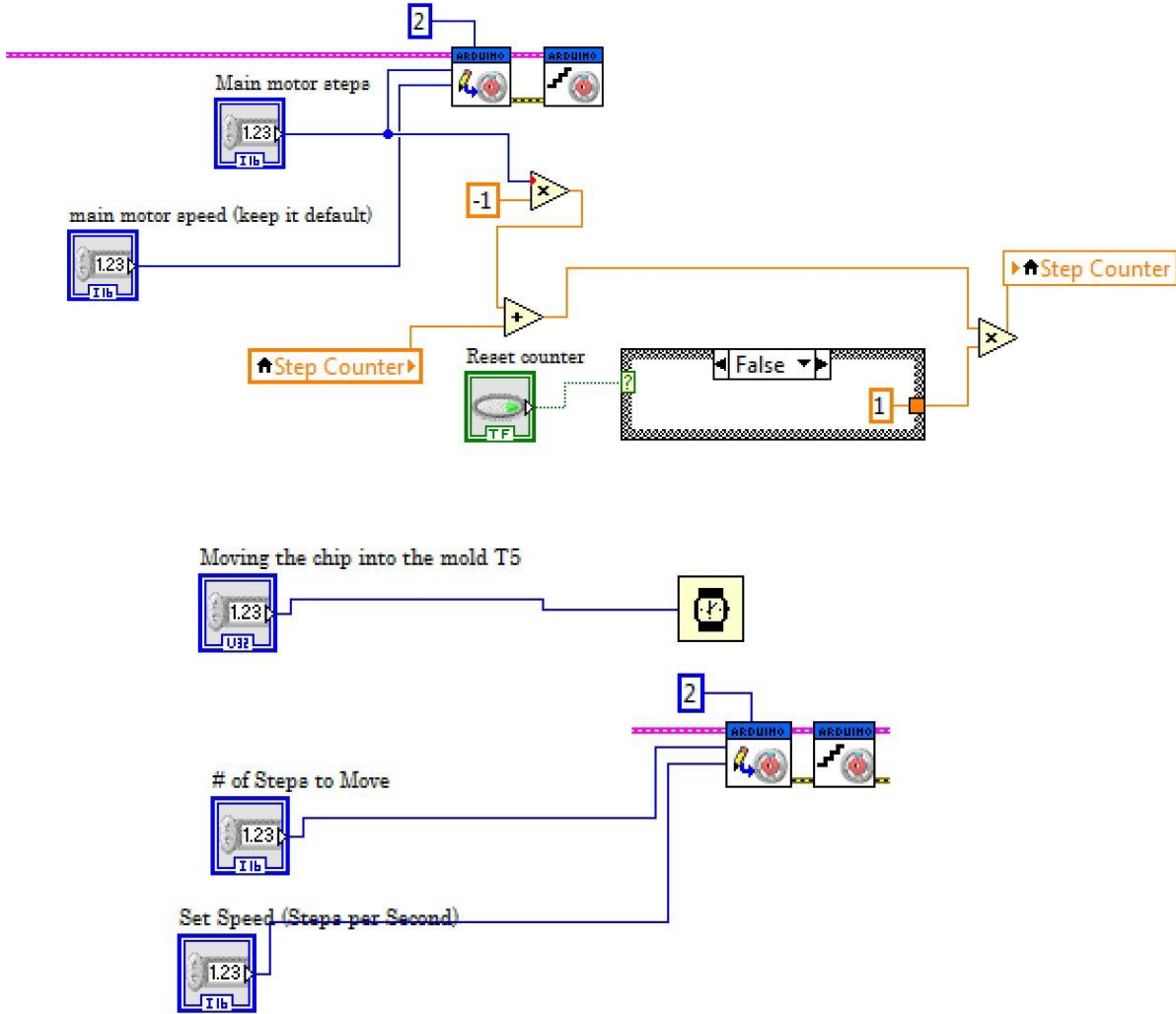


Figure 8 The code for running the stepper motor for both searching for component mode and moving the detected component to the encapsulation point mode.

6.2.5 Relay control

The relay control is used to activate the dispensing and curing. Both are activated by a digital output pin from Arduino Uno Card. Pin 7 and Pin 8, respectively. It is worth mentioning

that practically there was a need to give 50ms to activate the mechanical relays used in this project. The codes shown in Figure (9) are used for activating the UV and resin dispenser. The delay time is a user-defined time to allow system activation.

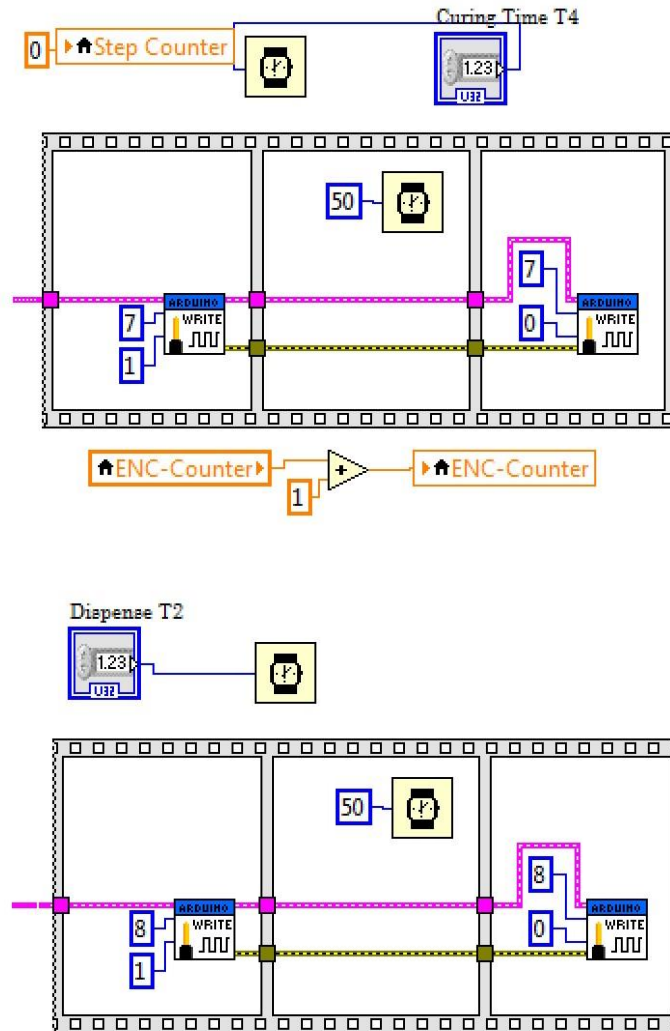


Figure 9 The LabView code for activating the relays controlling the dispenser and the UV source.

6.2.6 Winding mechanism

The winding mechanism is controlled by a stepper motor labelled no.0. A comparison logic is used to compare the signal from the tension sensor with a reference value. Once the tension drops below the reference value, the winding mechanism would activate the stepper motor inside the case code. The code used for the winding mechanism is running in parallel with the main code. The code is shown in Figure (10).

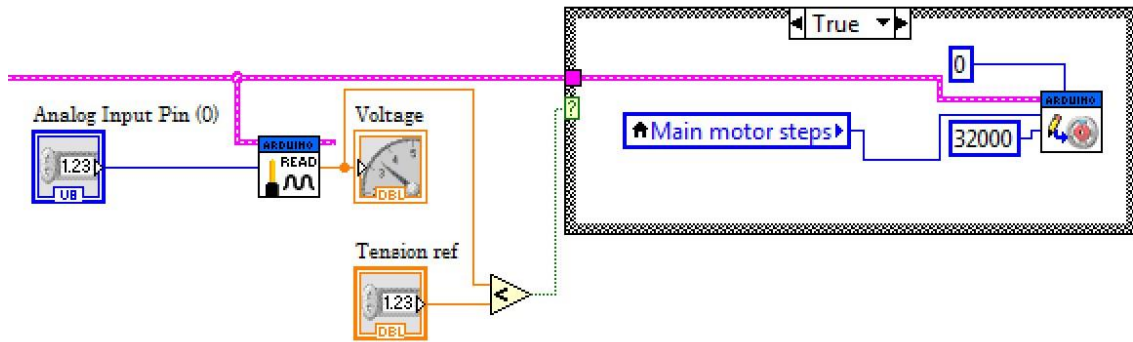


Figure 10 Labview Code used to control the winding mechanism.

6.3 Appendix 3: Calculation of the Internal diameter of circular warp knitted sleeve.

6.3.1 Introduction

Manufacturing an electronically functional yarn includes inserting resin micro-pods containing electronics into a small cylinder of tubular warp knitted structure. That gives the final yarn a structure that can be used in ordinary textile machinery. Since the soldered electronic components have different sizes, their micro pods would have different diameters after the encapsulation.

The space available in the cylindrical sleeve is restricted. The insertion process needs a geometry study of the space available before inserting different micro pod sizes. The space available inside the knitted tube varies depending on the knitting structure, yarn number, and the knitting cylinder diameter used.

In this part of the thesis, we present a method to determine the optimum packing conditions for electronic components into a small diameter circular warp knitted structure. This process needs to be investigated to achieve an electronically functional yarn with a consistent structure that holds the electronic component. Geometry analysis of the knitted structure and the space inside the sleeve has been performed. Thus, this section will specify *'What is the suitable diameter of the knitting cylinder for packing a micro pod with a specified size'*.

6.3.2 Analytical study of the cross-section of the sleeve

Circular warp knitting is different from flat knitting regarding the arrangements of the needles and their mechanism. Needles in warp knitting machines move jointly on the needle bar, and yarns are usually fed from bobbin creel and warp beam or without the latter. On the other hand, for circular warp knitting, the yarns will be fed through a patterning ring that makes the shogging motion, and needles are mounted on the cylindrical needle bed. The knitting is as follows:

1. Threads are swung from the back to the front of the needles.
2. Overlap stage: sideways shog.
3. Threads are swung to the back of the needle.
4. Needles start to move downwards.
5. Underlap stage (shogging).
6. Needles rise again, and the formation of new stitch starts.

The shogging movement of the patterning ring changes the warp-knitted structure by increasing/decreasing the needle number that the thread will skip during the shogging, as shown in Figure (11). The knitted sleeve structure influences the internal diameter of the space inside. The overlapping process and the overlapping number are essential in determining the warp-knitted structure. The knitting cylinder diameter and the number directly relate to the internal space size. Thus, choosing the appropriate knitting cylinder is essential to avoid the intersection between the yarn forming loops of the outer surface and the micro-pod fed into the sleeve. The hollow yarn structure is stuffed with a group of packing yarns inserted around the micro pod.

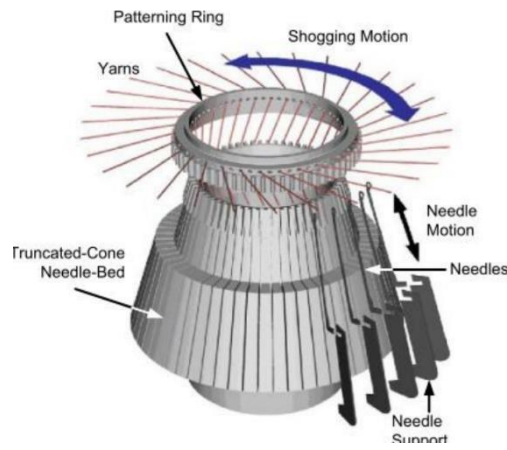


Figure 11 Warp knitting cylinder used in the manufacturing of the electronically functional yarn at ATRG.

To simplify the model, the stitch forming the sleeve thickness is considered neglectable, and the yarns' thickness is ignored. Based on these assumptions, the outer structure would be presented as a line that connects the needles according to the number of needles skipped after shogging, as presented in Figure (12).

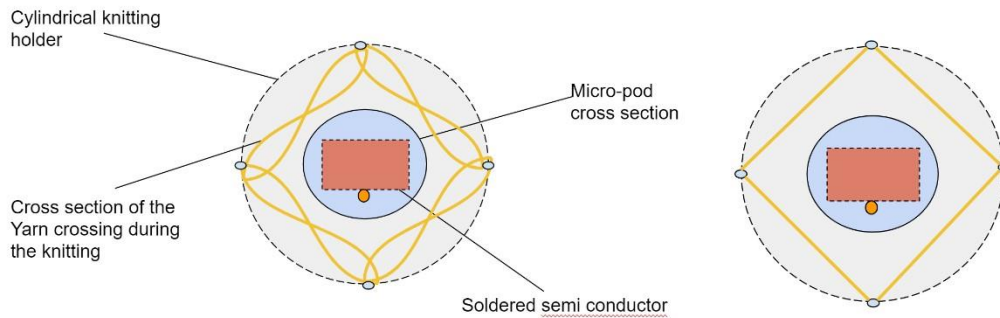


Figure 12 Simplification of the cross section of knitted sleeve.

A mathematical method has been used to determine the micro-pod d maximum diameter that can be inserted into a sleeve knitted by a cylindrical warp knitting machine with an internal diameter D and specific knitting structure, as shown in Figure (13).

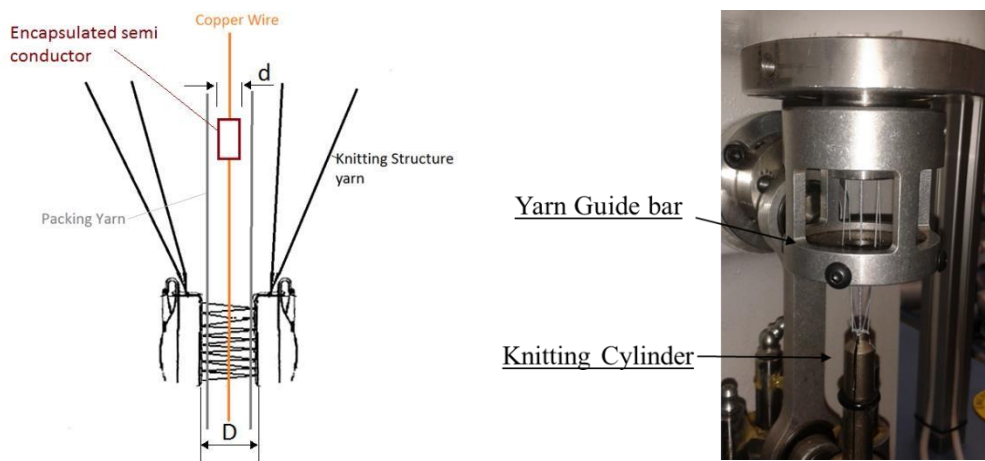


Figure 13 The insertion of the micro pod and the core structure of the electronically functional yarn into the cylindrical warp knitting machine.

The simplest structure can be knitted using the Ruis knitting machine, knitted with four needles (the minimum possible number) and two possible patterns. In the first pattern, the shogging motion moves the patterning ring where each yarn feeds the next adjacent needle. The other possible pattern will move the pattern ring, skipping one needle to form a structure, as shown in Fig (14). It can be seen from Figure (14) that the later structure does not have a tubular structure, and there is no space to fit a micro pod inside.

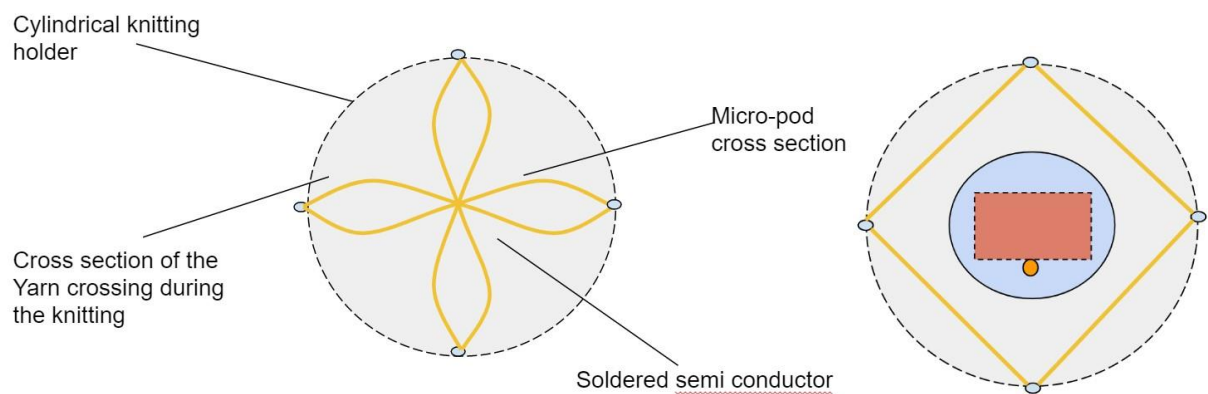


Figure14 The pattern that can be knitted using four needles in cylindrical warp knitting machine.

The more needle used, the more structure can be knitted by changing the patterns and shogging movements. However, a structure can be knitted with no space inside to fit a micropod for every even needle number. The structure would not have an internal diameter when the number of needles skipped during the shogging is half the number of needles, as shown in Figure (15).

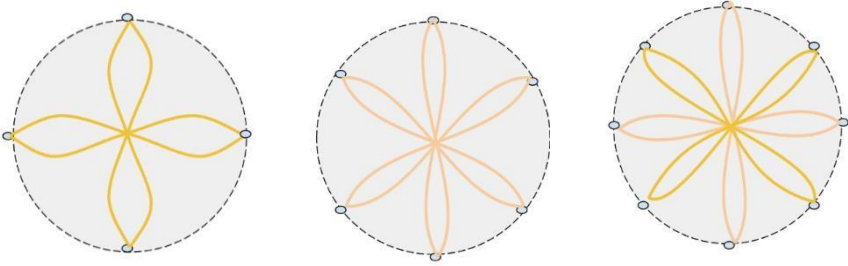
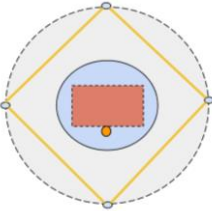
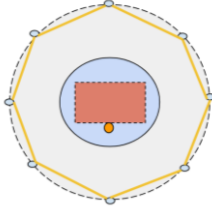
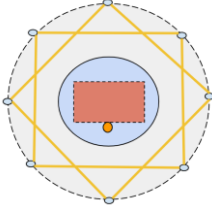
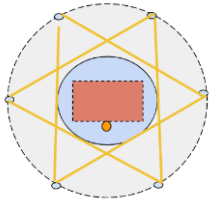
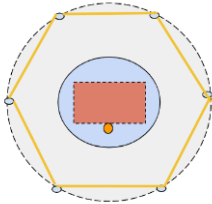


Figure 15 Possible knitted structure that has no internal space to accommodate the micro-pod.

The relationship between the maximum diameter of the micro-pod d and the internal diameter of the knitting cylinder D is illustrated in Table (1). The knitting pattern is also illustrated in Table (1) for some of the main knitting structures that can be done using the Ruis warp knitting machine for several needles.

Table 6 The relationship between the maximum diameter of the micro pod that can fit into warp knitted sleeve and the internal diameter of the needle bed cylinder for different arrangements and knitting structures.

Number of needles	Simplified cross-section of the yarn arrangement for different numbers of needles and knitting structure	Number of needles skipped after the shogging movement	The maximum micro-pod diameter d_{max}
4		1	$d_{max} = \frac{D}{\sqrt{2}}$
8		1	$d_{max} = \sqrt[4]{\frac{8}{11}} \cdot D$
8		2	$d_{max} = \frac{D}{\sqrt{2}}$
6		2	$d_{max} = \frac{D}{2}$

6		1	$d_{max} = \frac{\sqrt{3}}{2} D$
---	---	---	----------------------------------

6.4 Appendix 4: Tension Sensor Calibration

The tension sensor TS44/50 used in the winding mechanism has an analogue voltage signal. Applying higher tension on the wire would increase the signal value of the analogue signal generated by the sensor.

The microcontroller reads the analogue signal while LabVIEW compares the voltage to a reference value pre-determined by the system's user. Thus, there is a need to interpret this voltage signal into physical tension. Moreover, this will prevent exceeding the specified tension, which might lead to the core structure failure during the manufacturing process.

The calibration was conducted using a Vectran yarn and calibration weight up to sixty five grams. The analogue voltage was plotted against the calibration weight, as shown in Figure (16). This sensor can be used now in any future development of the system as the analogue output is interpreted into force tension.

The graph plotted using MATLAB, shown in Figure (17), is a polynomial in the third degree relationship between the weight and the analogue voltage from the sensor. The equation was derived using MATLAB curve fitting tools with goodness SSE:0.1059 and R square of 0.999.

The polynomial model is:

$$f(x) = -1.579e^{-5} x^3 + 0.8492e^{-3}x^2 + 0.1263x + 0.3124$$

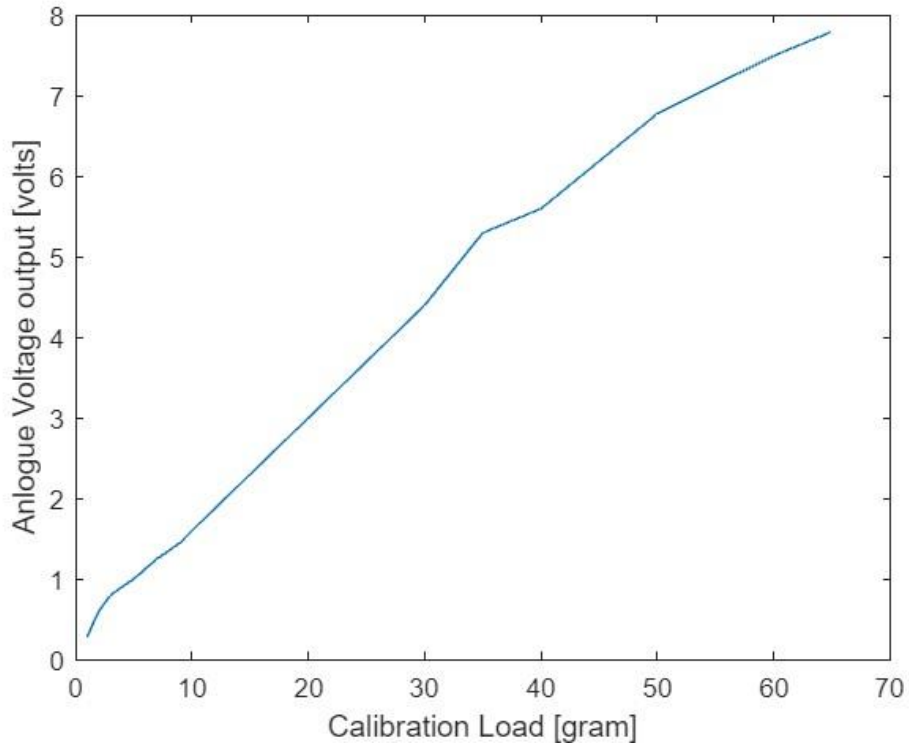


Figure 16 The calibration curve of the tension sensor.

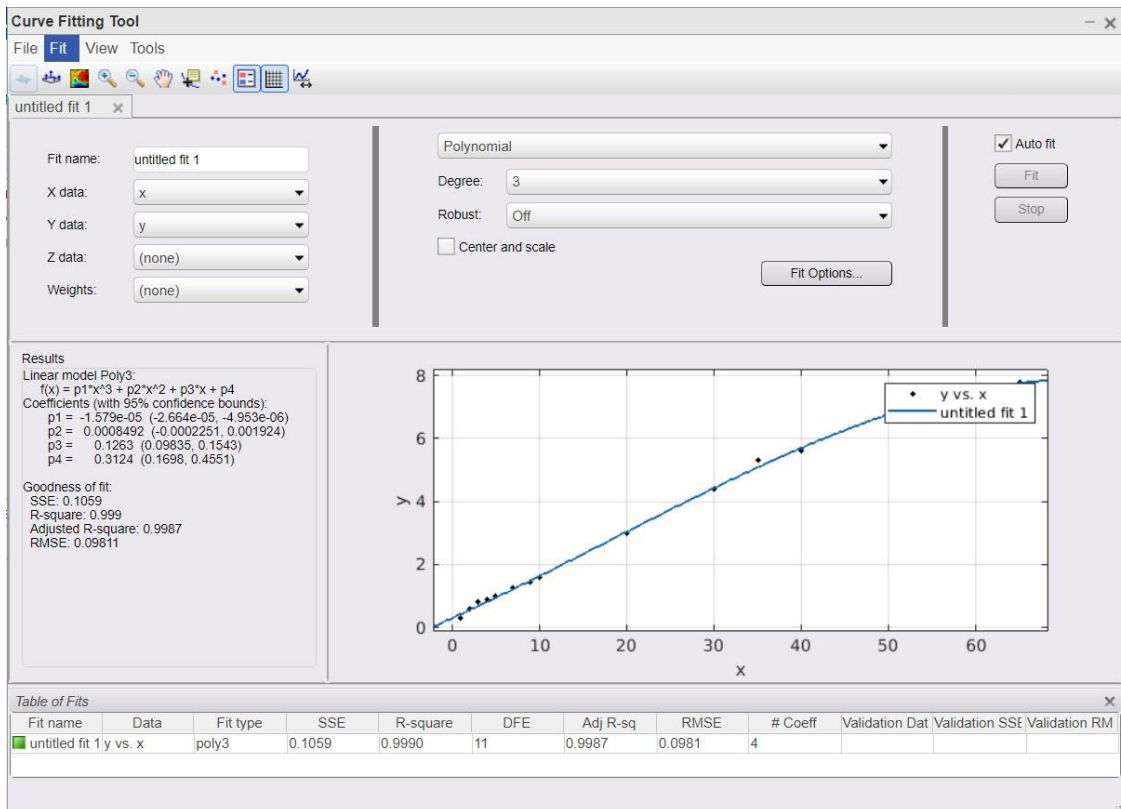


Figure 17 The fitting equation calculated by MATLAB.

6.5 Appendix 5: Early design of the encapsulation unit

The encapsulation design was initially proposed using a PTFE block that can be machined to create a small channel where the copper and the electronic component will pass through and encapsulate. Figure (18) shows the Unit design. The mould in the proposed design consists of two parts; one is stationary while the other is mounted into the linear stage.

Two stepper motors are planned to be used as delivery and pulling-off systems. Once the semiconductor is in the encapsulation point, the first linear stage will close the mould. At the same time, another linear stage that holds a dispenser will move down to dispense the resin at a specific position. The resin is then cured by UV. After that, the mould will open to enable micro-pod ejecting.

The disadvantage of this design is that the PTFE mould wall will block UV and make the curing process more complicated. Moreover, machining PTFE is not easy to make a precise mould that guarantees complete sealing between the mould parts. Thus, there was a need to modify the proposed design, and a new approach was evaluated.

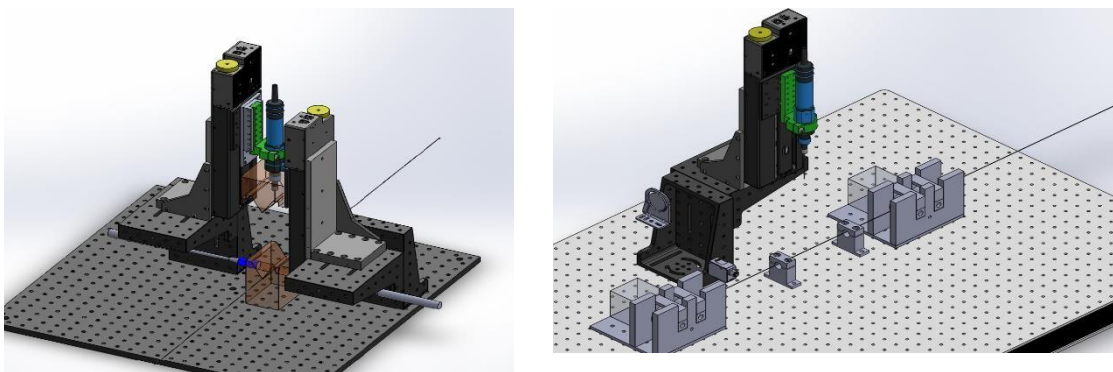


Figure 18 The proposed design of the encapsulation unit prepared in Solid works.

The new design used a PTFE tube as a mould instead of the two-part mould design. PTFE surfaces do not stick to adhesives. Thus, physical bonding was needed. This design aims to use a channel in the tube as a mould, as shown in Figure (19).

The advantage of this design is its need for just one linear stage to move the dispenser and much fewer mechanical components. The mould, which is the tube in this case, will remain stationary. Moreover, the channel in the mould would reduce the UV blocked for the curing process.

The resulting micro-pod from this design is illustrated in Figure (20). Experimental tests showed that there is a need to control the resin flow inside the channel. Uncontrolled flow resulted in a deformed micro-pod or unprotected component, as in Figure (20).

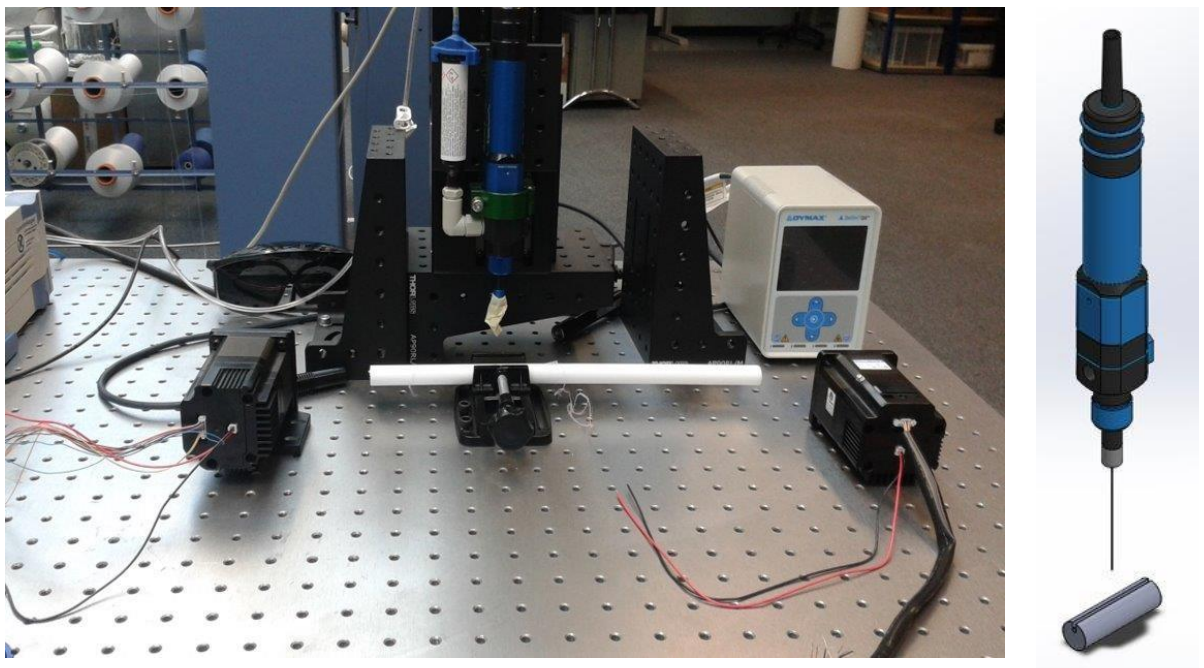


Figure 19 The Design of the encapsulation unit at the early stage.

The challenges in controlling the resin flow volume and the micro-pod shape led to a final approach using a transparent PTFE tube, as shown in Figure (21) and detailed in chapter 3 of this thesis.

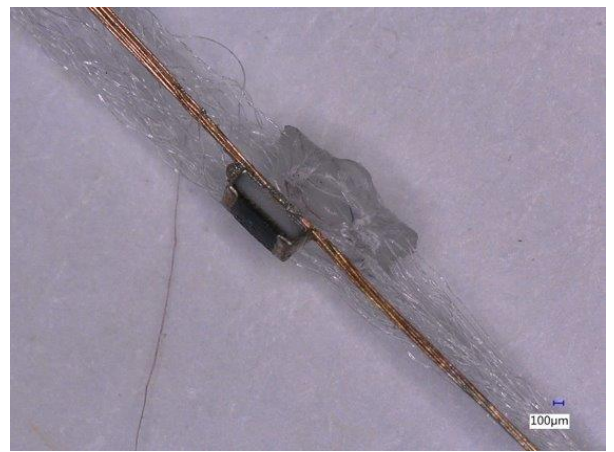


Figure 20. The early encapsulation made by the first concept of the encapsulation unit.

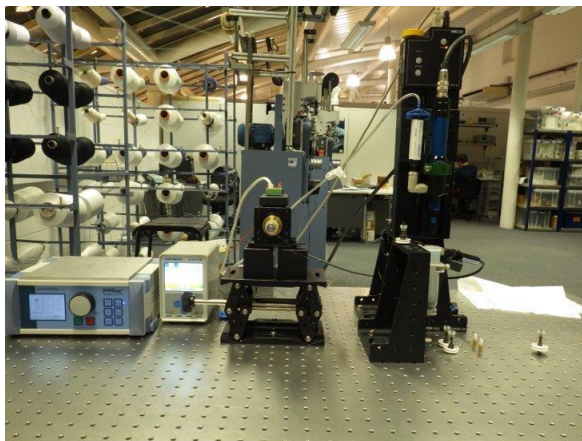


Figure 21 The Transparent PTFE tube mould added to the design of the encapsulation unit

6.6 Appendix 6: Buckling of the copper wire inside the knitted sleeve

Under certain circumstances, the core structure of the EFY is longer than the length of the knitted sleeve at relaxation. The longer filament will be in compression due to length imbalance. This phenomenon, illustrated in Figure (22), starts when the internal filaments are forced into compression while subject to different restraints of neighbouring filaments. A similar effect can be seen in ropes, hoses, and optical cables (Hobbs et al., 2000).



Figure 22 Copper wire buckling concept and an example of the phenomena in the EFY.

The outer structure of the electronically functional yarn consists of Warp knitted loops, while the internal core is a straight wire and textile yarns fill the space inside the hollow structure. Knitted fabrics have high stretchability. Due to the nature of the knitting process, the fabric is knitted under high stress and extension. This difference in elasticity between the outer surface and what is used inside leads to the buckling of elements. or kinking

During the outer surface knitting, the structure is subject to take-off rollers tension applied from one side, and the feeders' tension applied from the other side. This means that the knitted structure is produced under tension and will be released after the take-off rollers. Once the structure is in zero stress status, the yarns used as packing fibres are subject to a kind of pressure that cause the copper wire to buckle and forms a small deformation that comes out of the yarn's outer structure.

This increase is due to the knitting loop deformation in the warp knitted structure, loop reorientation, and the yarn elasticity used to form the loop. The loop deformation is due to the tension applied to the whole yarn between the yarn feeders and the take-off rollers. The deformation will maintain the circumference of the loop. This will increase the knitted structure length in the mentioned direction. At the same time, the elasticity and the mechanical properties of the yarn used in the knitting process are influenced by the tension applied during the knitting and will deform accordingly.

A wrapping technique was introduced to avoid this deformation effect on the knitted structure length and the resulting internal compression. Twisting the core structure with a textile yarn will add extra length to the copper wire and add physical control points that prevent the copper wire from protruding from the external sleeve structure, as shown in Figure (23)



Figure 23 Twisting the core structure of the EFY around textile yarns to overcome the buckling phenomena

6.7 Appendix 7: Mechanical Properties of the core structure and copper wire.

6.7.1 Soldered LED tensile test result sample

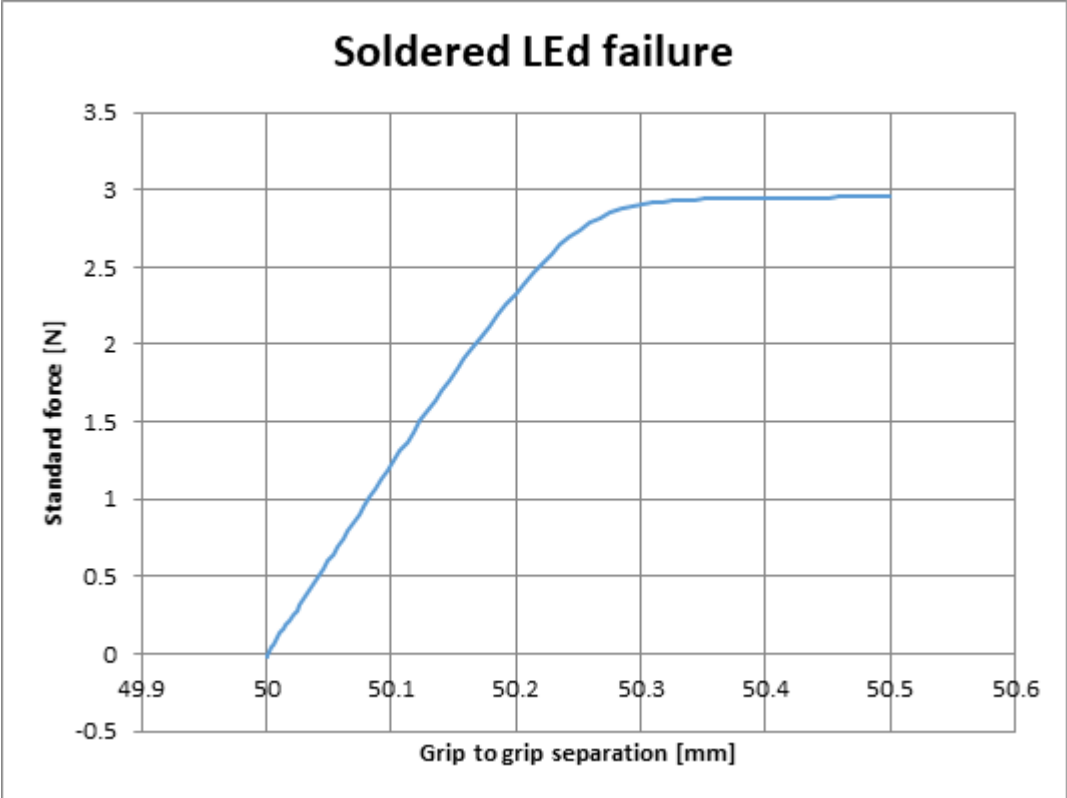


Figure 24 Tensile test of 50 mm copper wire with a soldered LED failed due to debonding of the solder pads of the component. Assessed by Zwick tensile tester

6.7.2 Tensile test results for Encapsulated Led sample

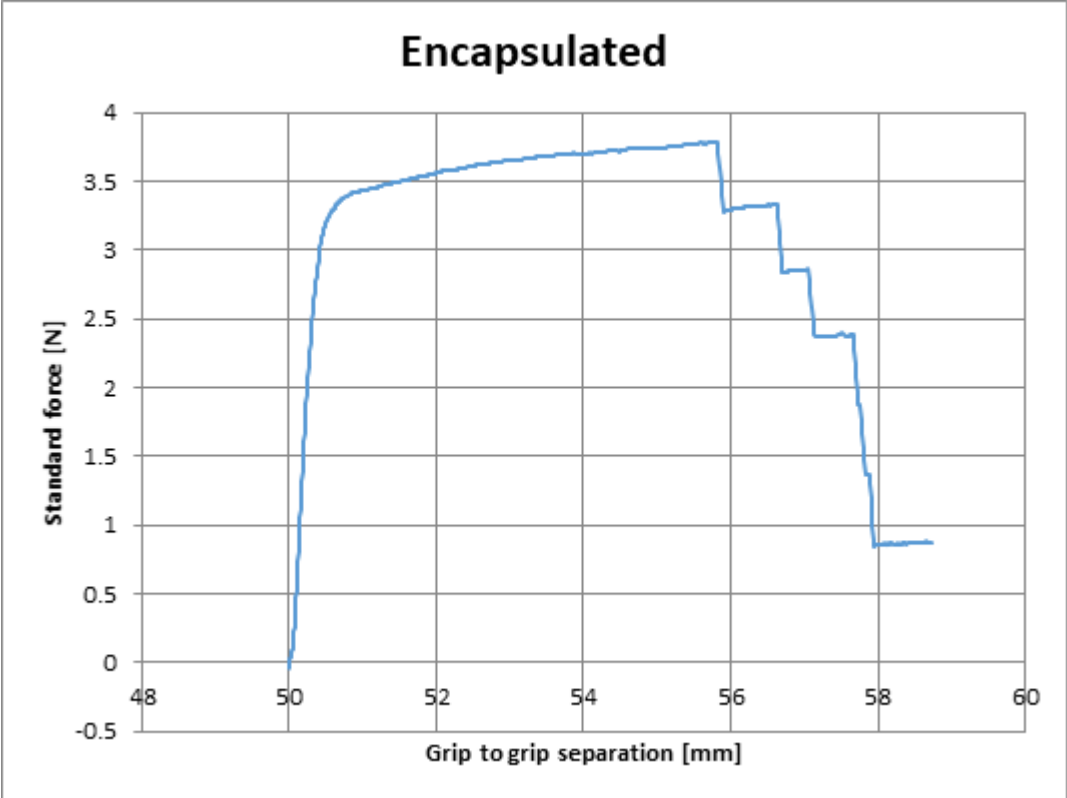


Figure 25 Tensile test of 50 mm copper wire with an encapsulated LED failed at the interface between the copper wire and the micro-pod. Tested by Zwick tensile tester

6.7.3 Tensile Test results for 7 stranded copper wire sample

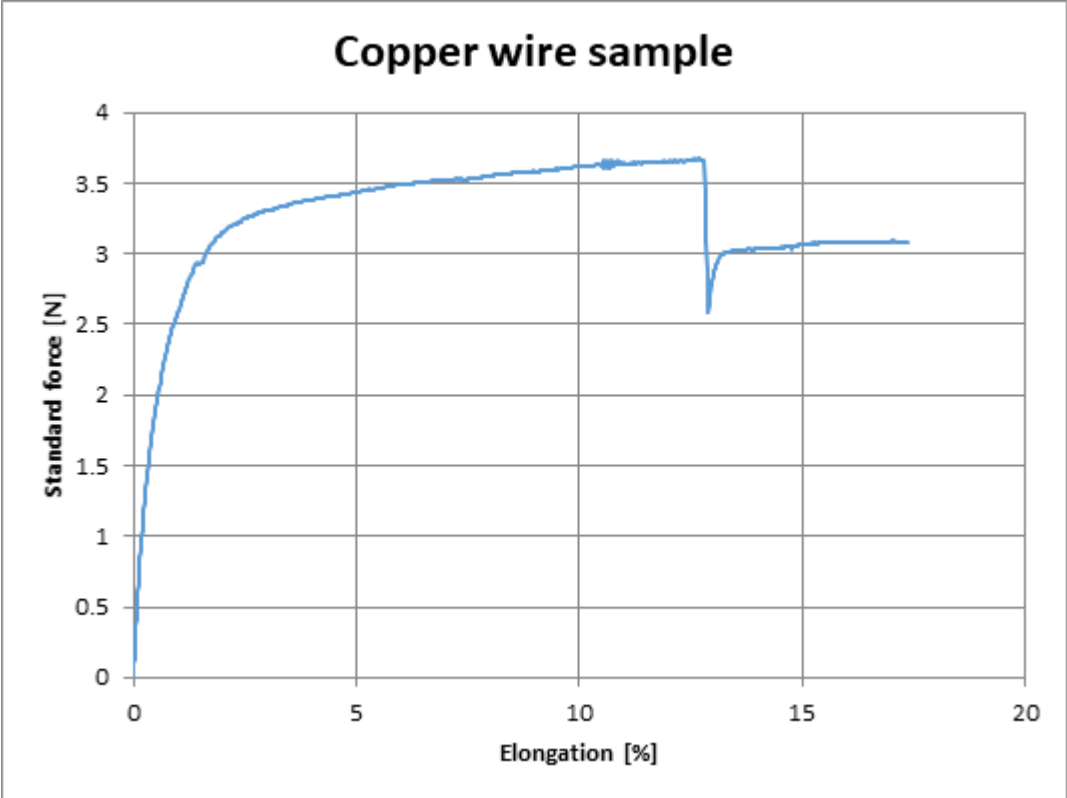
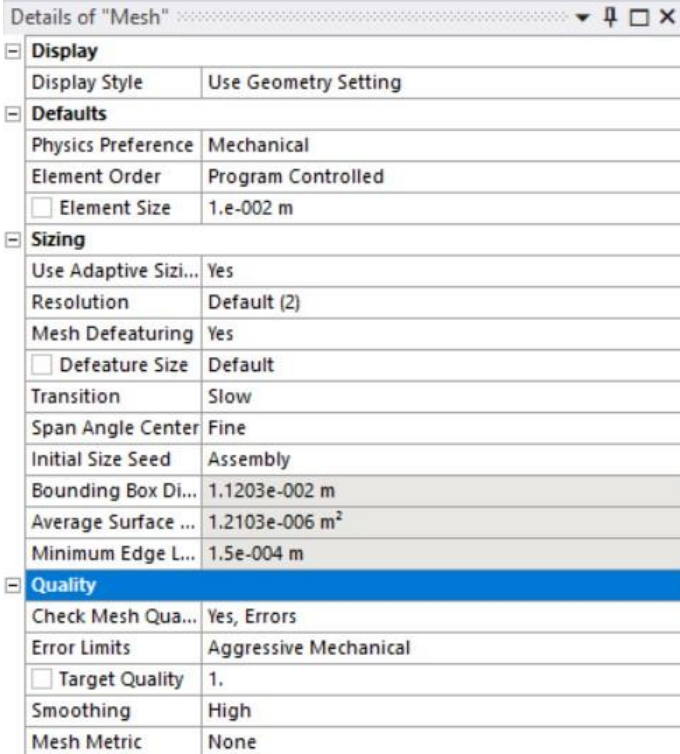


Figure 26 Tensile test of 50 mm copper wire Tested by Zwick tensile tester

6.8 Appendix 8: Ansys Modelling results

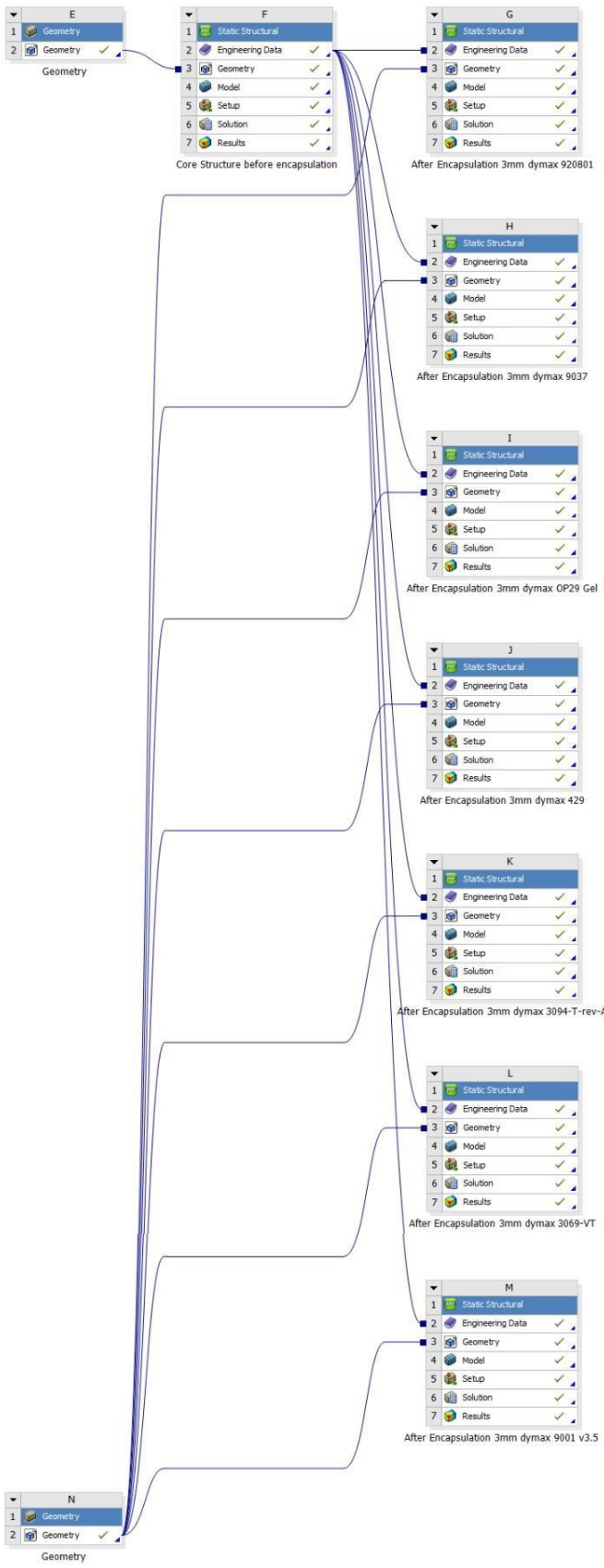
6.8.1 Meshing the system

Chapter 4 introduced a mechanical analysis of the mechanical stress in the core structure of the EFY. Meshing is a finite element analysis process that divides the CAD model into small components defined as elements. The settings of finite element analysis are sensitive, and a small change in meshing settings can lead to a massive change in the results. Thus, the settings are recorded in this appendix to maintain the results of the model consistent and repetitive. The meshing setting shown in Figure () is the setting used to analyse the core structure before encapsulation, after encapsulation, variant resin properties, and different lengths of micro-pod.

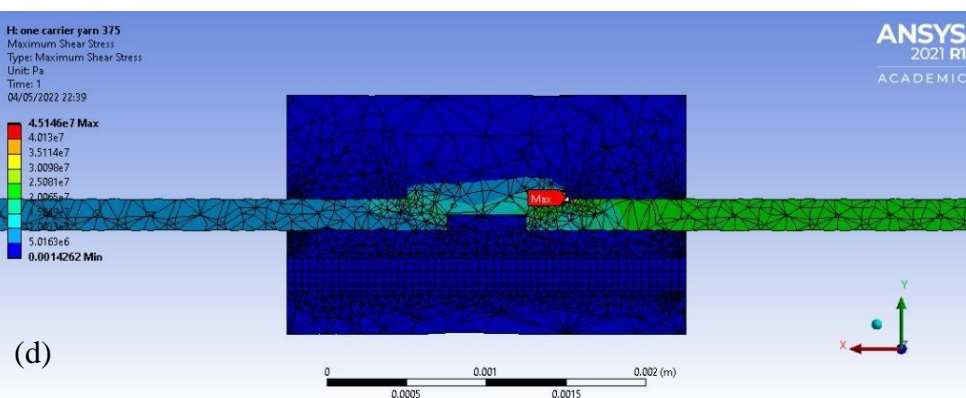
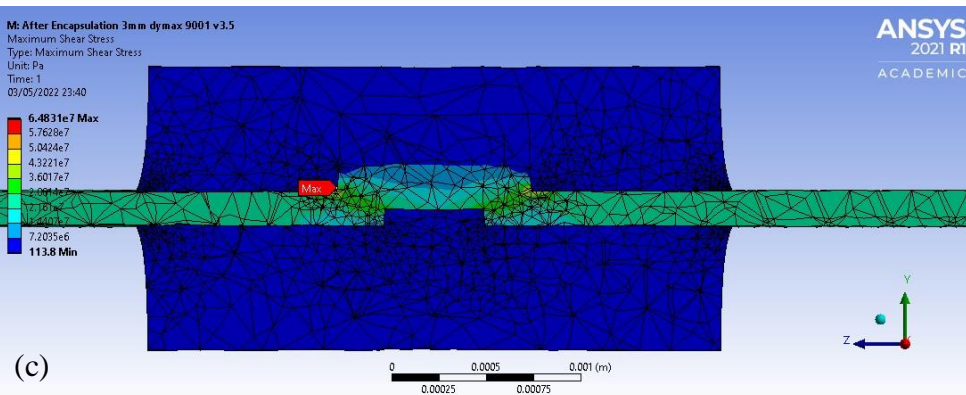
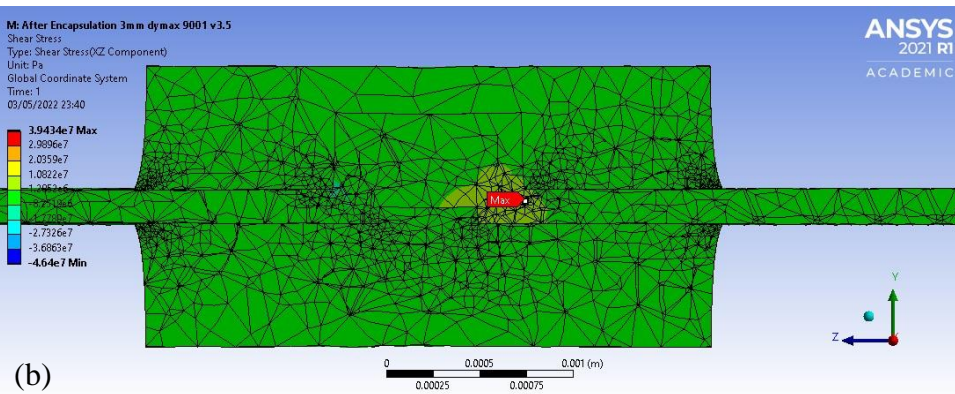
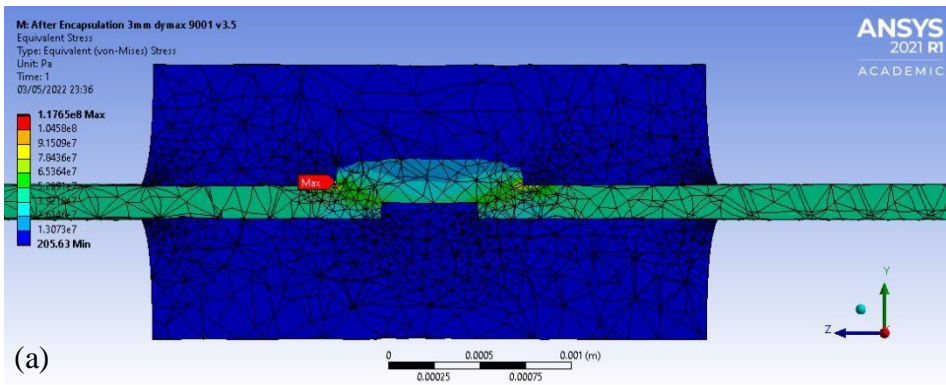


Details of "Mesh"	
Display	
Display Style	Use Geometry Setting
Defaults	
Physics Preference	Mechanical
Element Order	Program Controlled
<input type="checkbox"/> Element Size	1.e-002 m
Sizing	
Use Adaptive Sizi...	Yes
Resolution	Default (2)
Mesh Defeaturing	Yes
<input type="checkbox"/> Defeature Size	Default
Transition	Slow
Span Angle Center	Fine
Initial Size Seed	Assembly
Bounding Box Di...	1.1203e-002 m
Average Surface ...	1.2103e-006 m ²
Minimum Edge L...	1.5e-004 m
Quality	
Check Mesh Qua...	Yes, Errors
Error Limits	Aggressive Mechanical
<input type="checkbox"/> Target Quality	1.
Smoothing	High
Mesh Metric	None

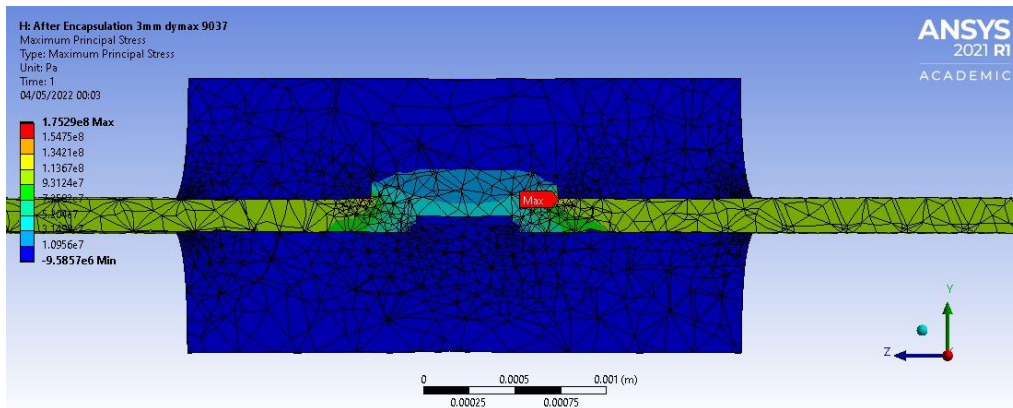
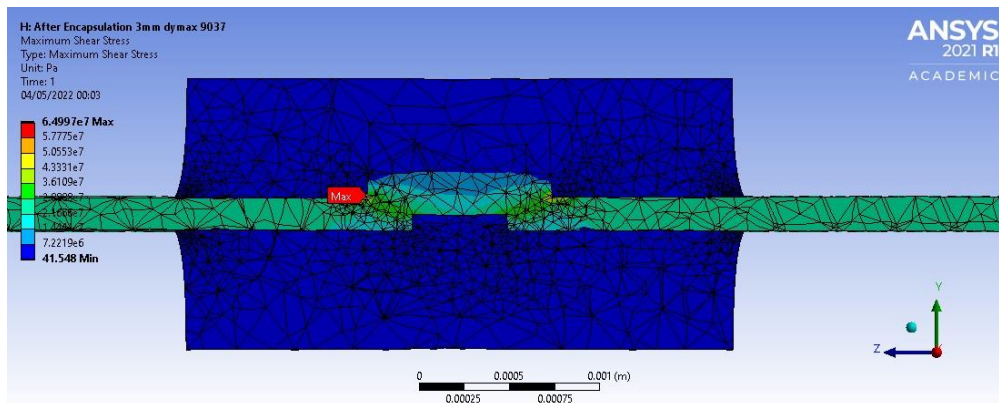
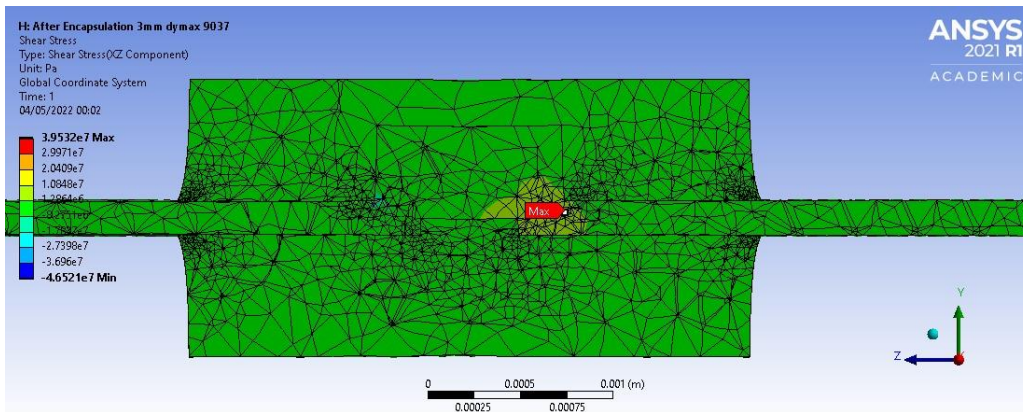
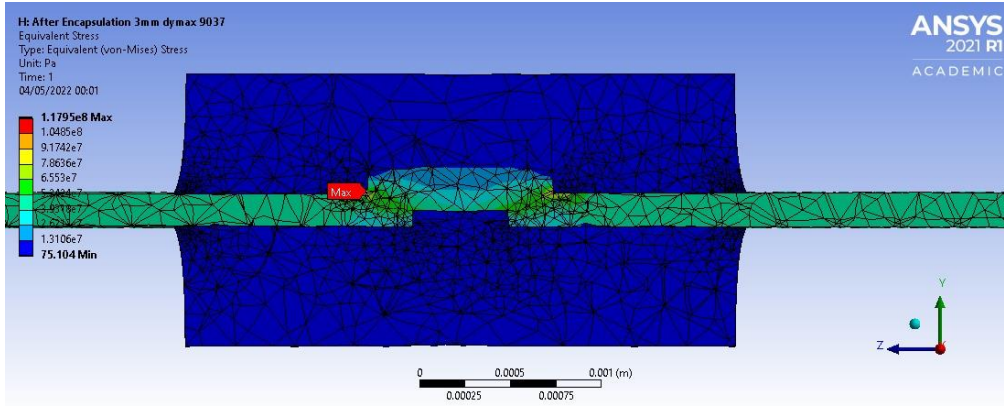
6.8.2 system arrangements in Ansys for modelling the core structure before and after encapsulation for different resin properties



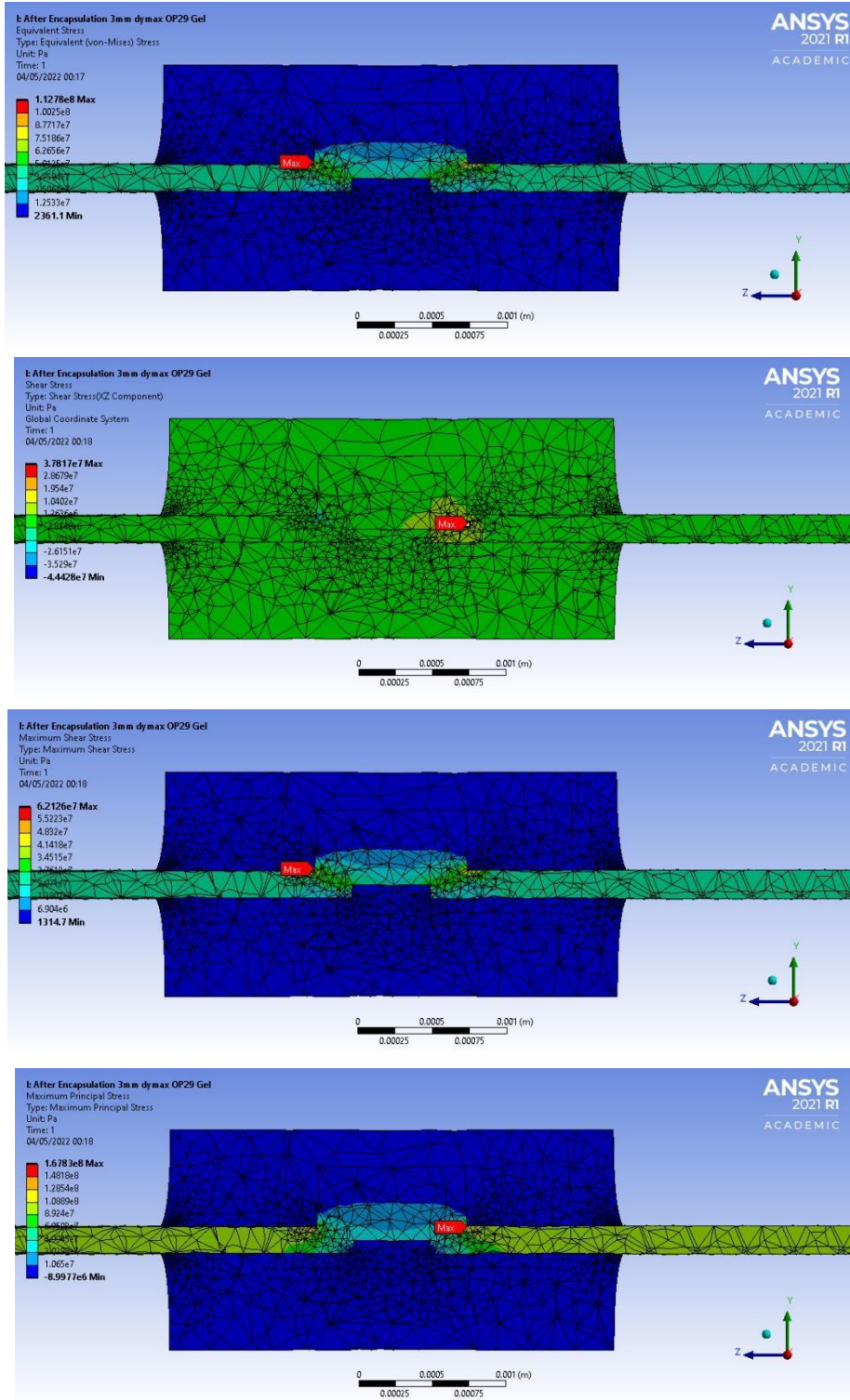
6.8.3 Analysis results for Dymax 9001 v3.5



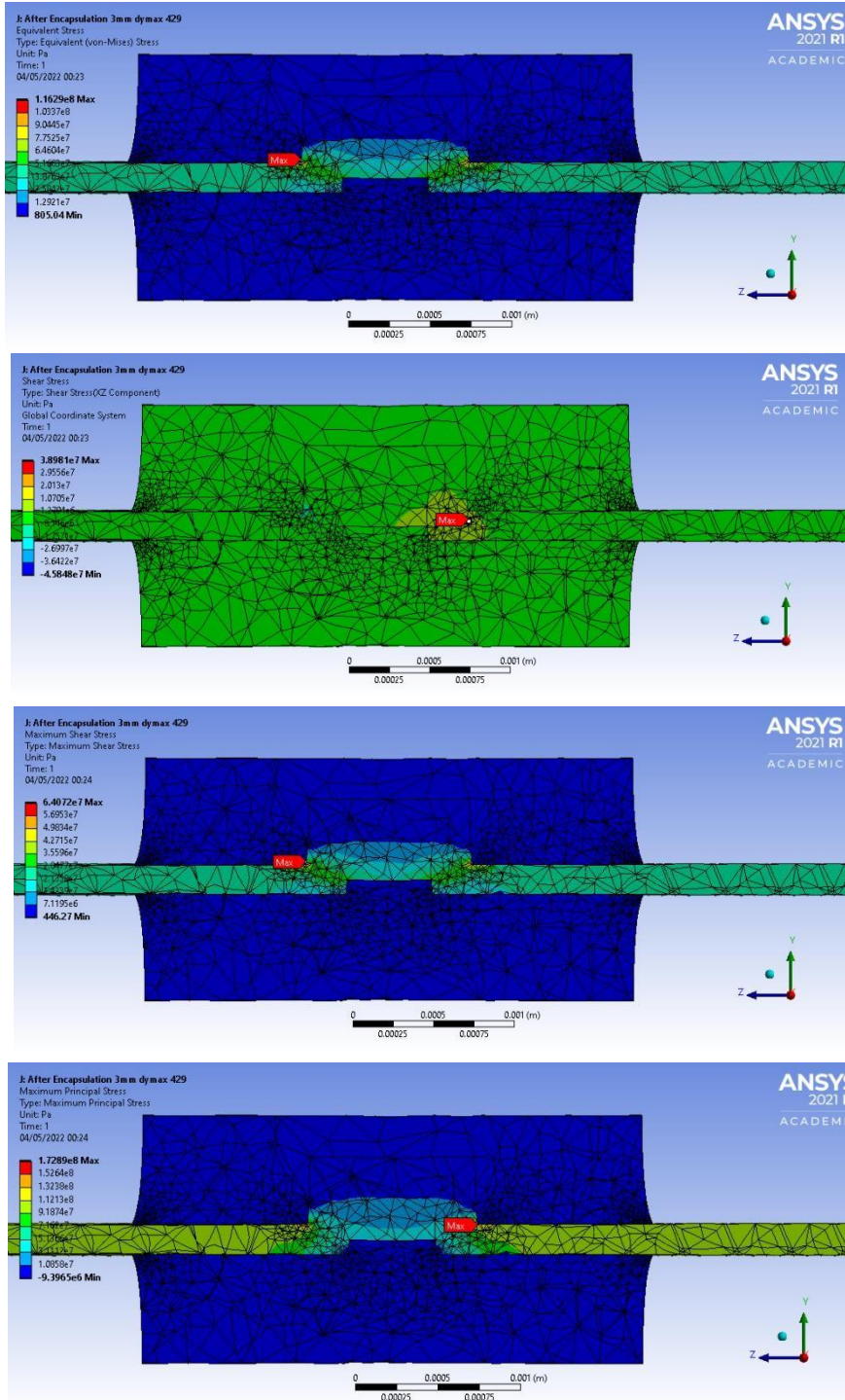
6.8.4 Analysis results for Dymax 9037



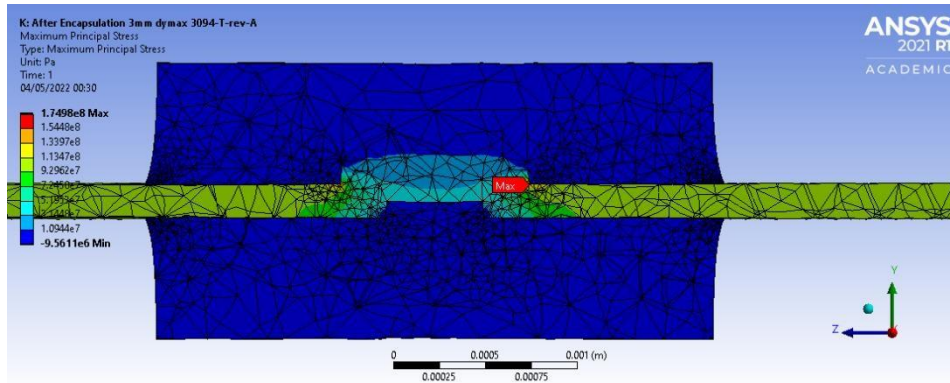
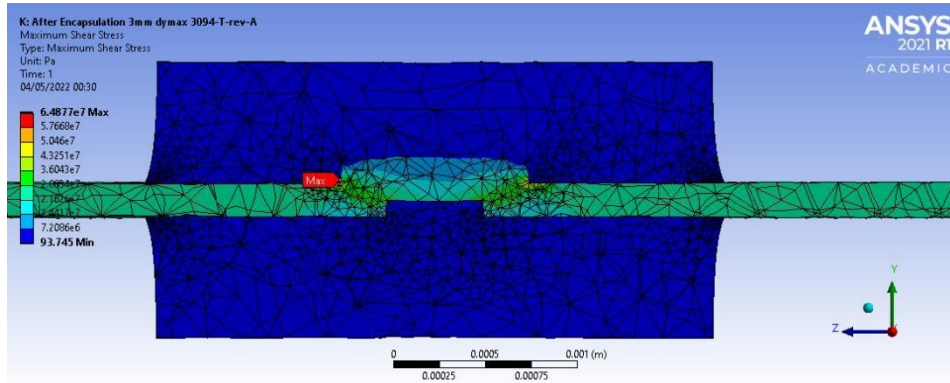
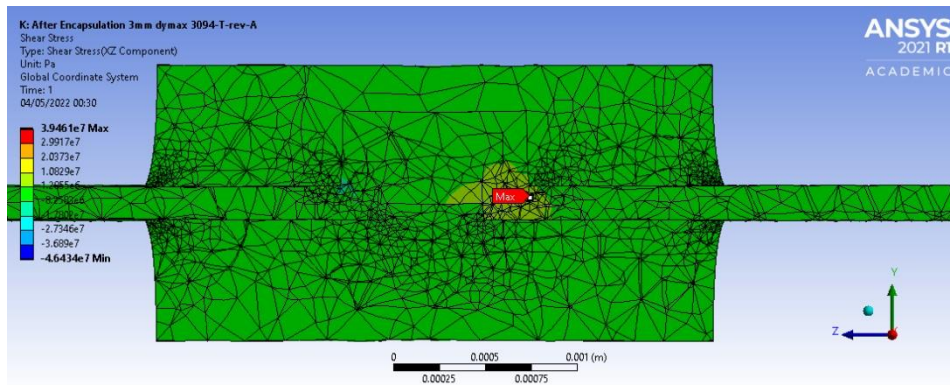
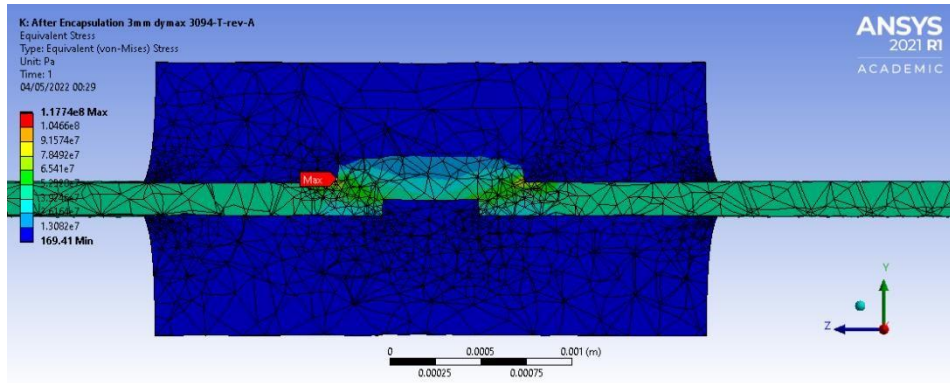
6.8.5 Analysis results for Dymax OP Gel



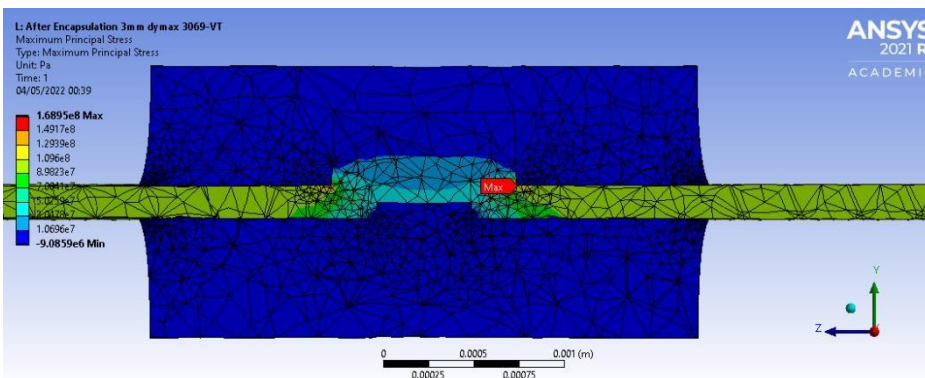
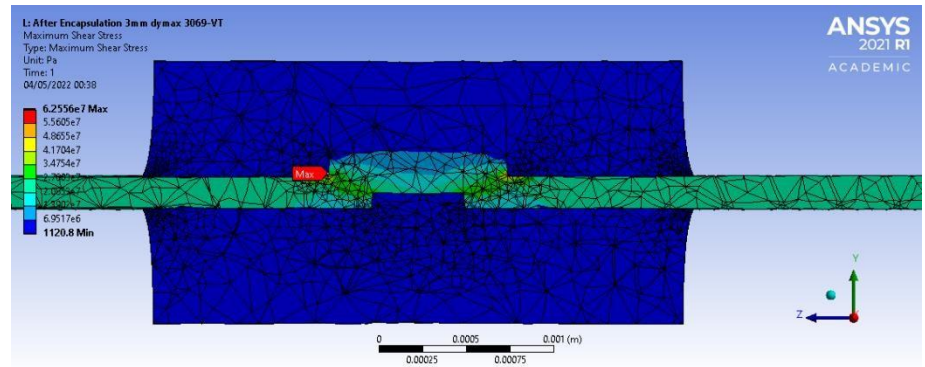
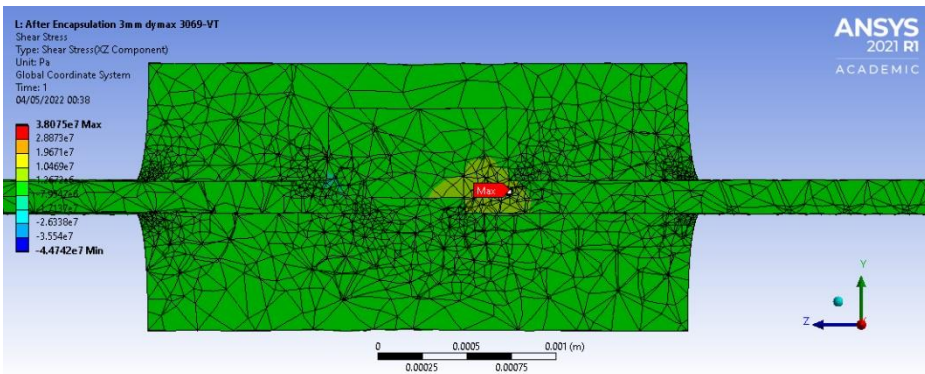
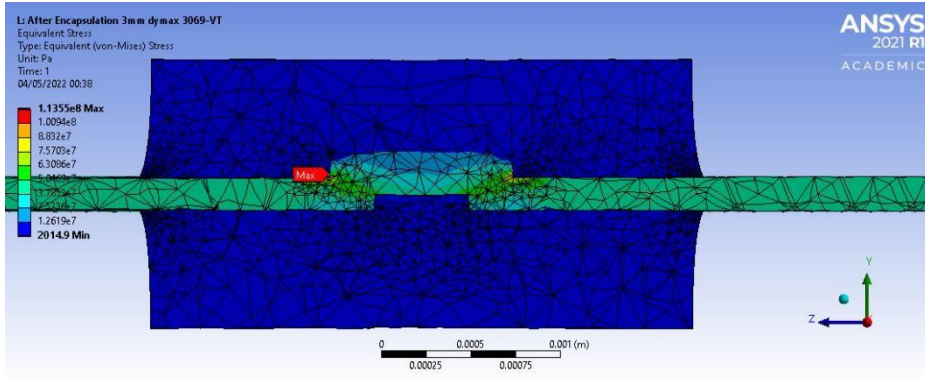
6.8.6 Analysis results for Dymax 429



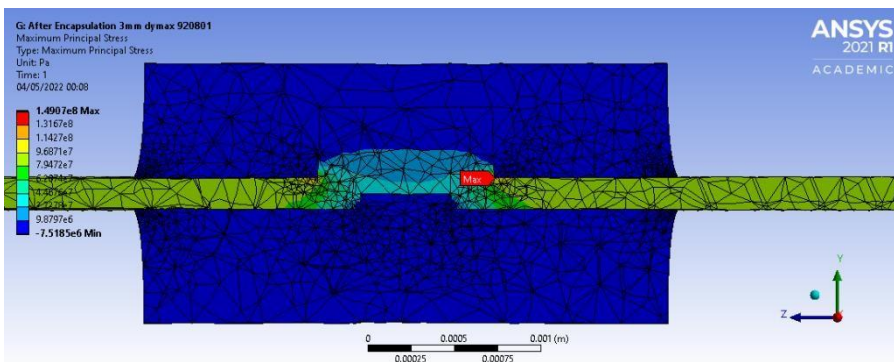
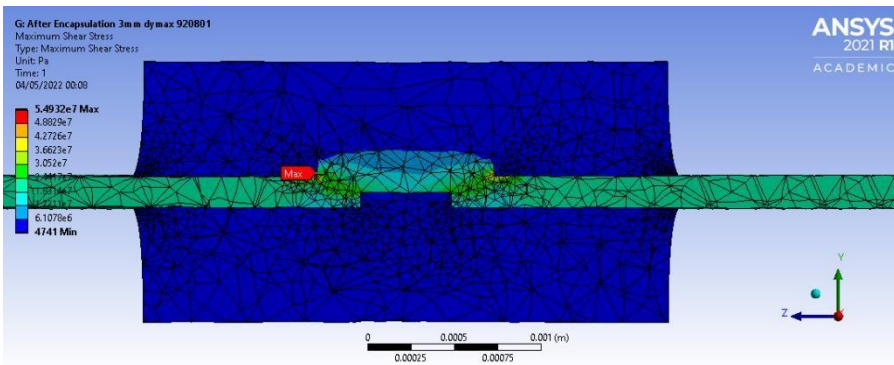
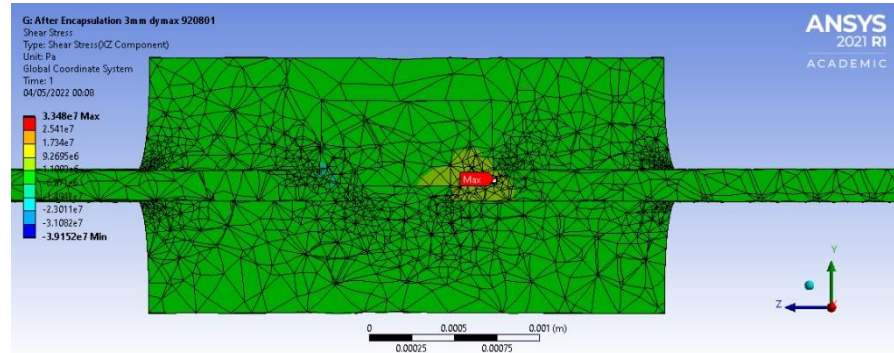
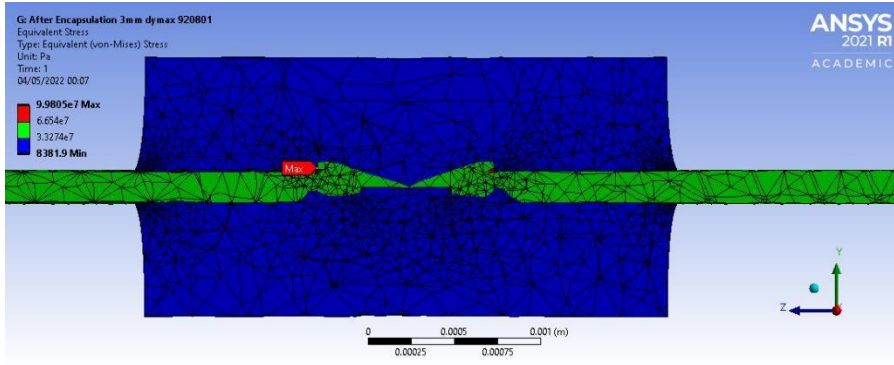
6.8.7 Analysis results for Dymax 3094 T-rev-A



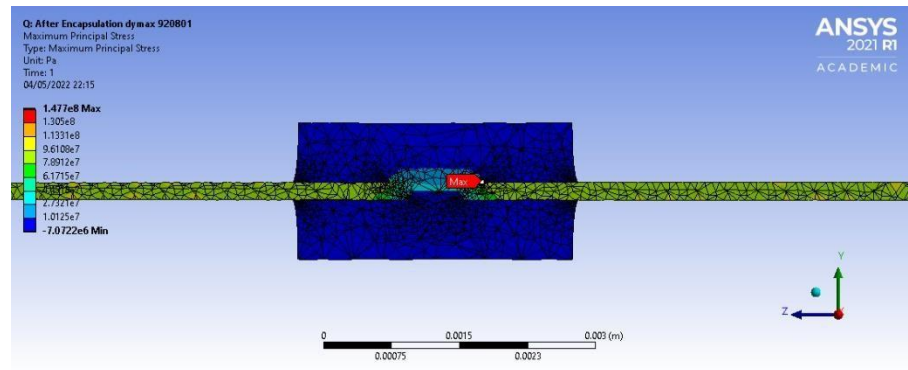
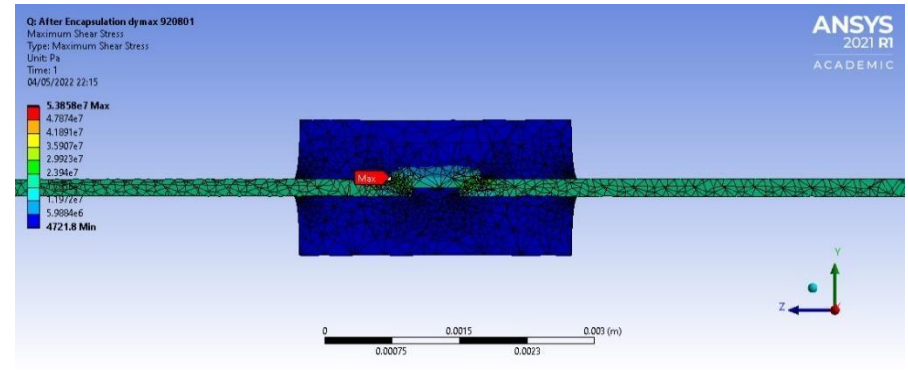
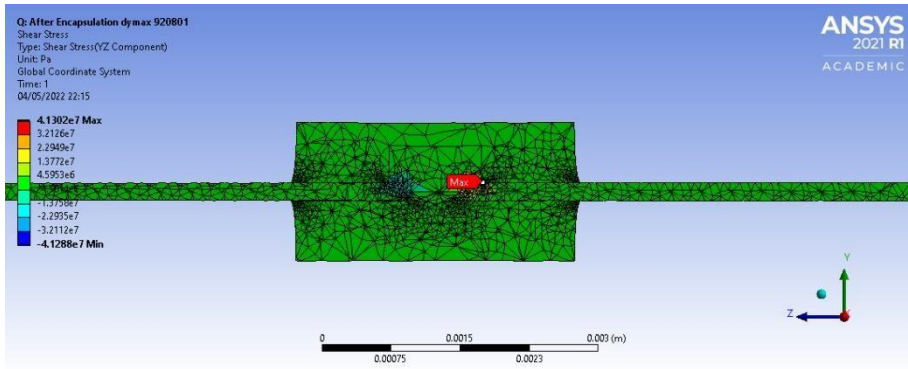
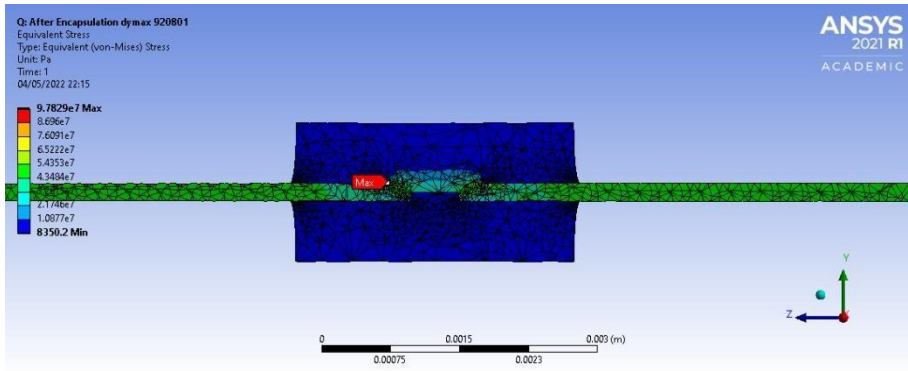
6.8.8 Analysis results for Dymax 3069-VT



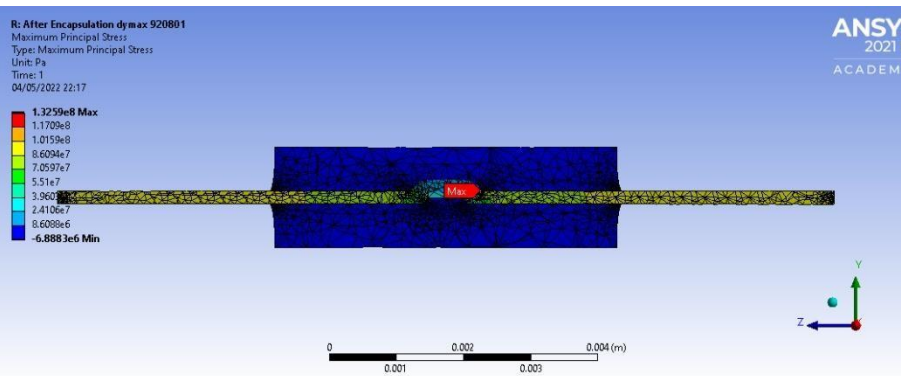
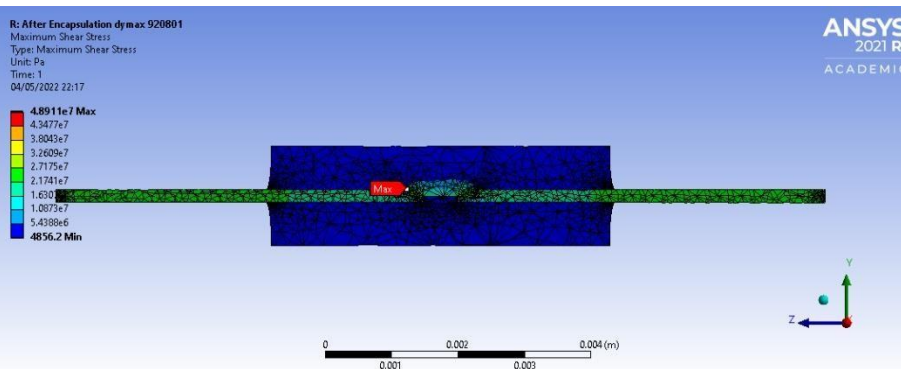
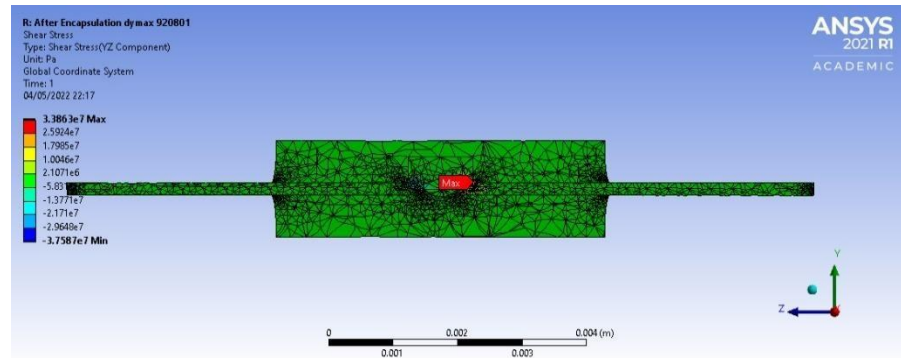
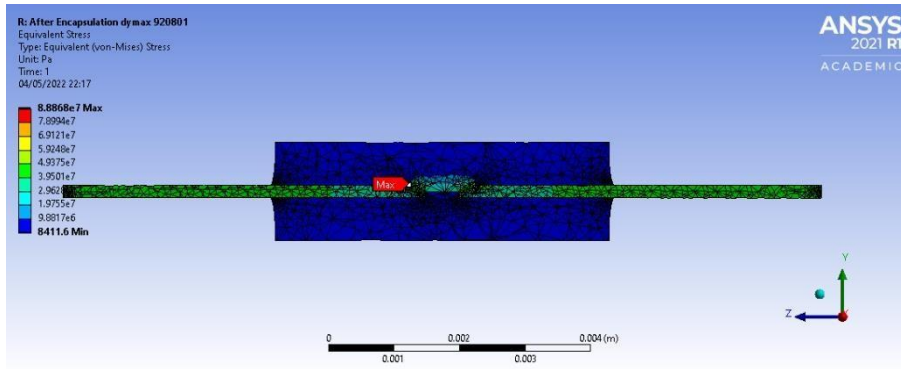
6.8.9 Analysis results for Dymax 920801



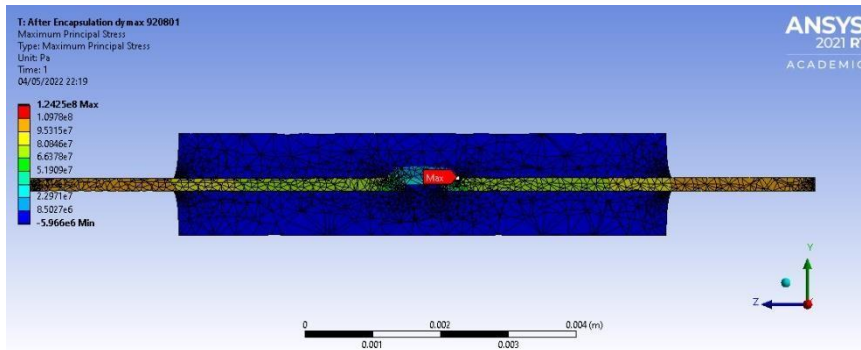
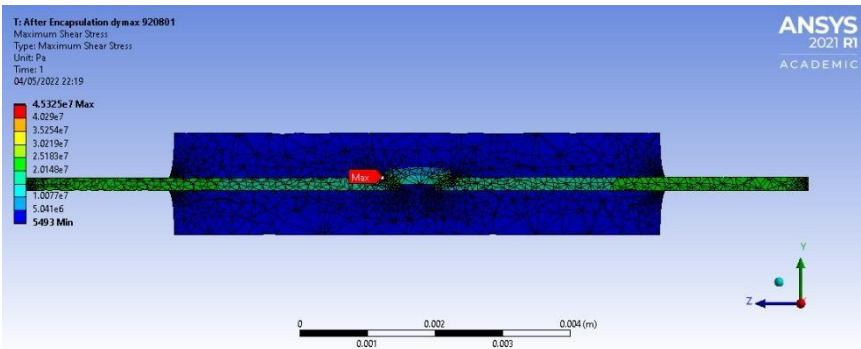
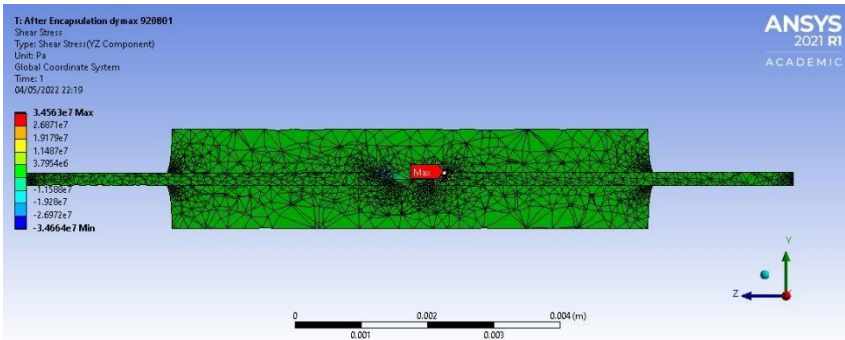
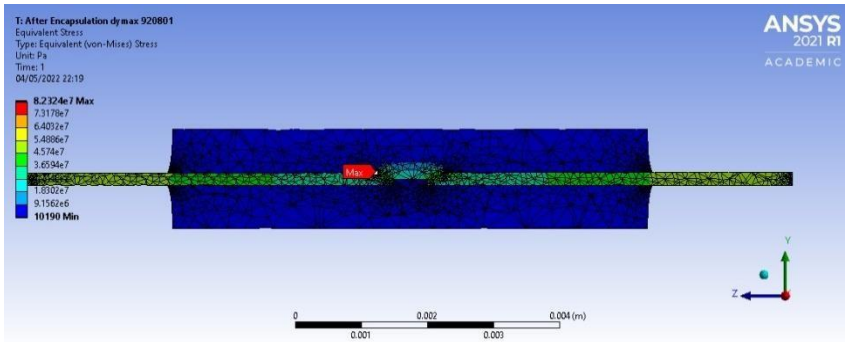
6.8.10 Analysis results for a micro-pod length of 3mm



6.8.11 Analysis results for a micro-pod length of 5mm



6.8.12 Analysis results for a micro-pod length of 7mm



6.9 Samples encapsulated by the Encapsulation unit

During the project, variant types of semiconductors were tested and encapsulated by the encapsulation unit. That included but was not limited to thermistors, resistors, and LEDs. The following images are microscopic images of some samples encapsulated by the unit during the development process.

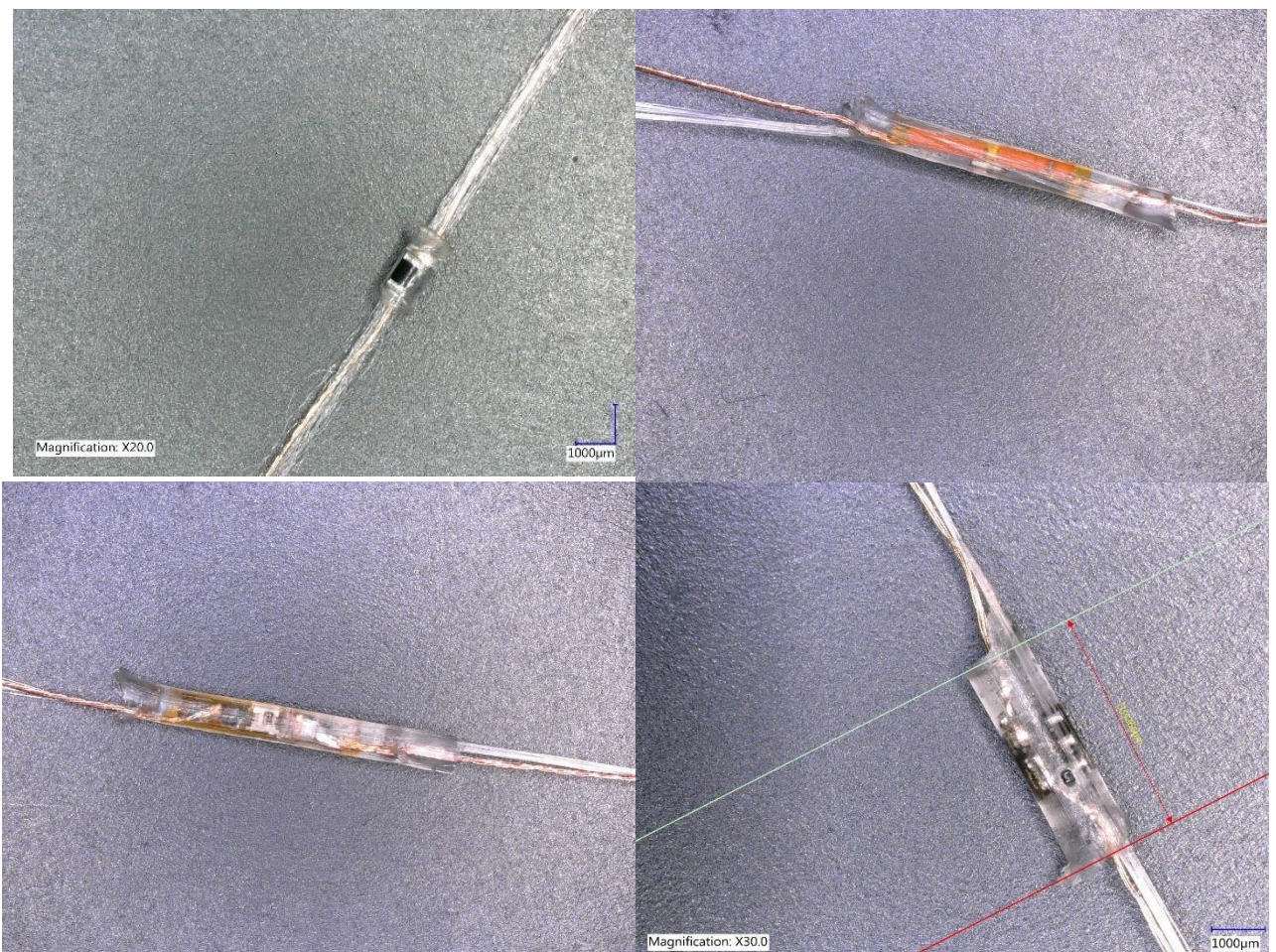


Figure 27 Samples encapsulated by the encapsulation unit. The image shows a resistor, Kapton strip, Kapton strip with LED, and RFID chip

